Next-generation neutron capture therapy

A study on the feasibility of NCT with Gd-PSMA tracer molecules as a new treatment modality for prostate cancer

ASTRID GARRETSEN, MSC., LL.M

Master thesis Biomedical Engineering

TU Delft

Student number: 1362879

14 May 2018

Technical supervisor: Dr. ir. Antonia Denkova (TU Delft)

Clinical supervisor: Dr. Wouter Vogel (NKI-AvL)

Abstract

Neutron capture therapy (NCT) is a binary form of radiotherapy that utilizes the high cross section of some nonradioactive elements, in particular boron-10 and gadolinium-157, for thermal neutron capture. The energetic charged particles (electrons and alpha particles) released in the capture reaction cause a high localized deposition. For almost a century, NCT has been regarded as the holy grail of targeted radiotherapy, but its superiority over other available treatments has not been demonstrated so far. Limitations included amongst others a poor and non-selective biodistribution of Boron carrier molecules, the limited availability of suitable neutron sources, a lack of tools for patient selection and individualized dosimetry, and a shortage of properly conducted clinical trials.

Recent developments in molecular imaging have resulted in a plethora of new tracers for cancer-specific targets, which can be labelled with a range of useful elements. This could potentially enable the distribution of typical NCT-isotopes with unprecedented tumour-to-background ratios, and consequently lead to more selective dose delivery to tumour cells. Prostate Specific Membrane Antigen (PSMA) is one of these new tracers, which binds specifically to prostate tumour cells. When labelled with gadolinium-157, NCT dose could be delivered selectively to this cellular target.

This research aims to investigate *in vitro* whether NCT with Gd-PSMA tracer molecules is feasible as a new treatment modality for prostate cancer. The labelling of gadolinium to PSMA has been realized. A ratio of Gd:PSMA of 1:1.25 for 15 minutes at 60˚C provides optimal labelling of Gd-PSMA with a 90% yield. PSMA-positive and PSMA-negative cell lines have been selected and validated as experimental models and have been used to determine the optimal concentration of Gd-PSMA in the cells. A concentration of 17 ± 11 (1σ) µg/g of PSMA could be achieved in PSMA-positive cells. Monte Carlo simulations, however, show that concentrations of PSMA (labelled with enriched Gd) of at least 114 µg/g will be required to achieve a significant dose enhancement induced by the presence of gadolinium. Preliminary irradiations with one of the currently most suitable neutron beams have indicated that the neutron background dose and the neutron activation level in these experiments were acceptable with regard to cell viability, and that transport of cells from the hospital-side to the reactor-side and back does not present a bottleneck for performing *in vitro* irradiation studies.

With at least an order of magnitude higher uptake of Gd-PSMA in cells, availability of a thermal neutron fluence rate > $4*10^{12}$ $m^{-2}s^{-1}$ (as e.g. offered by the former BNCT beam in Petten), and a still acceptable level of activation by neutrons after irradiation by this beam, meaningful *in vitro* studies of Gd-PSMA for NCT will become feasible. Further research requires multidisciplinary input from all partners involved.

Contents

1 Introduction

In oncology, three main treatment modalities are distinguished, chemotherapy (and related therapies), surgery, and radiotherapy. One of the subtypes of radiotherapy is neutron capture therapy (NCT). NCT is a binary form of radiotherapy that aims to selectively irradiate tumours using inter- and/or intracellular induction of ionizing particles [(Moss 2014, Nedunchezhian 2016)]. Classical NCT applies the stable isotope boron-10 as a target for the capturing of thermal neutrons, because of its high cross section for thermal neutron capture. This kind of NCT is generally referred to as BNCT. Boron is distributed using a tracer molecule that accumulates preferentially in tumour, typically the amino-acid Boron-phenylalanine (BPA) [(e.g. Moss 2014, Nedunchezhian 2016)]. After loading with boron, the tumour area is irradiated with (epi)thermal neutrons. Neutron capture by boron-10 induces emission of alpha particles (helium-4) and recoiling nuclei (lithium-7), both high-LET particles with short path lengths of 4.5-10 µm [(e.g. Sauerwein 2012)]. These emissions induce concentrated ionizations around the location of boron-10, in a range comparable to the diameter of a single human cell. Surrounding normal tissue cells will receive a limited dose, for example from neutron capture events in normal tissue components or physiological tracer distribution [(Hawthorne 1993)], or from gamma contamination of the neutron beam. Depending on the specificity of the tracer and the quality of the neutron beam, the net result is highly selective damage to tumour cells that accumulated the tracer with relative sparing of normal tissues.

BNCT provides several theoretical advantages over other treatment options like external beam radiotherapy, brachytherapy, and systemic radionuclide therapy. Biological tumour targeting followed by wide regional neutron irradiation ensures complete tumour coverage, and reduces reliance on observer-dependent manual target delineation. Undetected locoregional microscopic tumour spread is automatically included in the beam penumbra. This characteristic also reduces the effect of small setup errors and tissue motion or deformation. The highly selective dose to malignant cells may allow delivery in one fraction, and it permits re-irradiation in areas where the maximum tolerance for normal tissues has already been reached.

Despite these strong technical and radiobiological characteristics, the superiority of NCT relative to state of the art treatment options could not be demonstrated to date. The reasons for this include amongst others the poor and non-selective biodistribution of Boron carrier molecules, the limited availability of suitable neutron sources, a lack of tools for patient selection and individualized dosimetry, and a shortage of properly conducted clinical trials. These reasons will be discussed more extensively in Chapter 2, which provides a critical review on the current limitations of BNCT.

However, several recent developments indicate interesting new options for NCT. These developments include advances in the neutron energy transport modelling, which offer perspectives for modern treatment planning based on anatomy and tracer biodistribution. In addition, they include the availability of in-hospital accelerators for neutron production, which reduces the dependency on reactor-based neutron beams. Yet the largest development foreseen is related to the recent advances in molecular imaging which have resulted in a plethora of new tracers for cancer-specific targets. These targeting agents can be labelled with a range of useful elements. This could potentially enable the distribution of typical NCT-isotopes with unprecedented tumour-to-background ratios and, consequently, to more selective dose delivery to tumour cells. At the subcellular level, many ligands exhibit preferential accumulation in structures with radiobiological relevance like the cell membrane,

mitochondria, lysosomes or DNA. When applied with gadolinium-157, which has a much higher thermal neutron cross-section than boron-10 and induces Auger electrons with ultra-short path lengths, NCT dose can potentially be delivered selectively to such subcellular targets. The development of chemically parallel tracers for PET and MRI allows a theranostic approach with optimal patient selection and individualized dosing.

One of the targets for which new molecular imaging tracers have been developed is the membrane protein Prostate-Specific Membrane Antigen (PSMA) which is discovered to be overexpressed on the cells of > 90% of prostate tumours [(Lückerath 2018)]. When labelled with gadolinium-157, NCT dose could be delivered selectively to this cellular target. Potentially, the use of Gd-PSMA tracers for NCT could become a new, personalized treatment modality for prostate tumours.

The main goal of this research is to investigate *in vitro* whether NCT with Gd-PSMA tracer molecules is feasible as a new treatment modality for prostate cancer. Specific research objectives to examine this feasibility include:

- To establish and optimise the labelling of gadolinium to PSMA (paragraph 3.1);
- To select and verify the experimental model, i.e. PSMA-positive and PSMA-negative cell lines (paragraph 3.2);
- To estimate the minimum Gd-PSMA concentration in PSMA-positive cells required for Gd-NCT and to study *in vitro* whether this concentration can be achieved in PSMA-positive cells (paragraph 3.3);
- To determine if *in vitro* studies of the radiation response to thermal neutrons are feasible using neutron beams available in the Netherlands (paragraph 3.4).

The thesis will finish with a discussion and some concluding remarks and future perspectives with respect to the feasibility of using Gd-PSMA for NCT.

2 Critical review on the current limitations of BNCT and discussion of the next-generation NCT[1]

A paradigm shift in neutron capture therapy

A critical review on the current limitations of BNCT and discussion of the next-generation NCT

Astrid L. Garretsen, MSc. LL.M [1,2,3], Diederik Feilzer [1], Else A Aalbersberg, MSc[2], Zoltán Perkó, PhD[1], Irene Bodeldijk, PhD[4], Klaas Bakker, PhD[4], Sander de Groot, MSc [4], Danny Lathouwers, PhD[1], Dennis R. Schaart, MSc. PhD [1], Antonia G. Denkova, MSc. PhD[1], Wouter V. Vogel, MD, PhD [2,3]

1. Radiation Science & Technology, Technical University Delft, Delft, NL
2. Nuclear Medicine, The Netherlands Cancer Institute, Amsterdam, NL
3. Radiation Oncology, The Netherlands Cancer Institute, Amsterdam, NL
4. Irradiation solutions, NRG, Petten, NL

Corresponding author:

Wouter V. Vogel, MD, PhD. Departments of Nuclear Medicine and Radiation Oncology, The Netherlands Cancer Institute. Plesmanlaan 121, 1066 CX Amsterdam, the Netherlands. Tel: +31 20 512 2285. Fax: +31 20 512 2290. E-mail: w.vogel@nki.nl

[1] As this critical review is intended for publication, it is provided here as a paper, with a reference list of its own.

2.1 Abstract

Neutron capture therapy (NCT) is a binary form of radiotherapy that utilizes the high cross section for thermal neutron capture of some nonradioactive isotopes, typically boron-10, to deliver ionizing radiation selectively to tissues with specific characteristics. The energetic charged particles (electrons and alpha particles) released in the capture reaction cause a high, localized dose deposition at the location of accumulated Boron tracer molecules, thus sparing surrounding normal tissue. For almost a century, NCT has been regarded as the holy grail of targeted radiotherapy, but its superiority over other available treatments has not been demonstrated so far. Limitations included amongst others a poor and non-selective biodistribution of Boron carrier molecules, a limited availability of suitable neutron sources, a lack of tools for patient selection and individualized dosimetry, and challenges related to treating patients in poor condition in an out-of-hospital reactor environment. However, several technical developments now indicate interesting new options for NCT.

Recent developments in molecular imaging have resulted in a plethora of new tracers for cancer-specific targets, which can be labelled with a range of useful elements. This could potentially enable the distribution of typical NCT-isotopes with unprecedented tumour-to-background ratios, and consequently to more selective dose delivery to tumour cells. At the subcellular level, many ligands exhibit preferential accumulation in structures with radiobiological relevance like the cell membrane, mitochondria, lysosomes or DNA. When applied with gadolinium-157, which has a much higher cross-section than boron-10 and induces Auger electrons with ultrashort path lengths, NCT dose can potentially be delivered selectively to such subcellular targets. The development of chemically parallel tracers for PET and MRI allows a theranostic approach with optimal patient selection and individualized dosing. Advances in the neutron energy transport modelling offers perspectives for modern treatment planning based on anatomy and tracer biodistribution. And lastly, (epi)thermal neutrons are becoming available from in-hospital accelerators, which reduces the dependency on reactor-based neutron beams.

These advances may allow a paradigm shift in NCT, from a forgotten niche to a modern, targeted and personalized treatment modality for a broad selection of tumours with actionable molecular targets. This justifies a new exploration of NCT, based on modern techniques. This paper provides a critical review of current literature, and discusses the potential of next-generation NCT.

2.2 Introduction

2.2.1 Classical BNCT

Neutron capture therapy (NCT) is a treatment modality that aims to selectively irradiate tumours using inter- and/or intracellular induction of ionizing particles [(Moss 2014, Nedunchezhian 2016)]. Classical NCT applies the stable isotope boron-10 as a target for the capturing of thermal neutrons, generally referred to as BNCT. Boron is distributed using a tracer molecule that accumulates preferentially in tumour, typically the amino-acid Boron-phenylalanine (BPA) [(e.g. Moss 2014, Nedunchezhian 2016)]. After loading with boron, the tumour area is irradiated with (epi)thermal neutrons. Neutron capture by boron-10 induces emission of alpha particles (helium-4) and recoiling nuclei (lithium-7), both high-LET particles (alpha particle approximately 150 keVμm^{-1}, and Li-7 nucleus approximately 175 keVμm^{-1}) with short path lengths of 4.5-10 μm [(e.g. Sauerwein 2012)]. These emissions induce concentrated ionizations around the location of boron-10, in a range comparable to the diameter of a single human cell. Surrounding normal tissue cells will receive a limited dose, for example from neutron capture events in normal tissue components or physiological tracer distribution [(Hawthorne 1993)], or from gamma contamination of the neutron beam. Depending on the specificity of the tracer and the quality of the neutron beam, the net result is highly selective damage to tumour cells that accumulated the tracer with relative sparing of normal tissues.

BNCT provides several theoretical advantages over other treatment options like external beam radiotherapy, brachytherapy, and systemic radionuclide therapy. Biological tumour targeting followed by wide regional neutron irradiation ensures complete tumour coverage, and reduces reliance on observer-dependent manual target delineation. Undetected locoregional microscopic tumour spread is automatically included in the beam penumbra. This characteristic also reduces the effect of small setup errors and tissue motion or deformation. The highly selective dose to malignant cells allows delivery in one fraction, and it permits re-irradiation in areas where the maximum tolerance for normal tissues has already been reached.

Despite these strong technical and radiobiological characteristics, the superiority of NCT relative to current standard treatment options could never be demonstrated to date. The reasons for this disappointing situation will be discussed in this critical review. First, a description of developments in time will be given, followed by an overview of current challenges. Afterwards, we will discuss some recent developments, which we believe justify a new exploration of the possibilities for NCT.

2.3 Challenges to be solved

2.3.1 History of development

Only 4 years after the discovery of the neutron by Chadwick in 1932 [(Chadwick 1932)], Locher had proposed the principle of selective accumulation of boron-10 in tumour followed by exposure to thermal neutrons to provide a high radiation dose relative to adjacent normal tissues [(Locher 1936)]. It took 15 years until BNCT was first attempted in clinical applications. From February 1951 to January 1953, the first ten patients suffering from malignant glioma received BNCT at the Brookhaven Graphite Research Reactor [(Farr 1954, Sauerwein, 2012)]. Although the clinical situation of nine out of ten patients was improved for a short time, all patients died of their progressive disease [(Sauerwein 2012)]. Yet the BNCT concept was

considered sufficiently promising to initiate two subsequent trials with 40 [Archambeau 1970] and 18 patients [Sweet 1963].

These first attempts used simple boron carriers with rather non-specific biodistributions, like boron-10-enriched borax, sodium pentaborate, boronic acid and disodium decahydrodecarborate ($Na_2B_{10}H_{10}$) [Nedunchezhian 2016, Sauerwein 2012]. The presence of tracer in normal tissues surrounding the irradiated tumour led to significant dose deposition and toxicity, with reports of radiodermatosis and deep skin ulcerations [Archambeau 1970], cerebral oedema and shock [Slatkin 1991], and brain necrosis [Asbury 1972]. Eventually it was concluded that the toxicity of BNCT was comparable with standard radiotherapy [Slatkin 1991], and in 1961, BNCT was ceased in the USA for three decades. In addition to the non-selective boron carriers, Sauerwein et al provide several explanations for the disappointing BNCT results in the USA: a poor depth-dose distribution of the thermal neutrons, causing a low dose to the tumour and a high dose to the skin [Gabel 1994, Sauerwein 2012], the underestimation of the dose from incident fast neutrons and photons as well as from the protons and gamma rays produced by the nuclear reactions in the patient [Coderre 1989, Goodman 1990, Farr 1991], and the fact that corticosteroids to avoid brain oedema after high-dose irradiation were not available yet [Sauerwein 2012].

In 1968, new clinical efforts were performed in Japan, based on the carrier sodium borocaptate, $Na_2B_{12}H_{11}SH$ (BSH) [Hatanaka 1990], which provided a better tumour-to-background uptake ratio of about 3-4 [Doi 2008]. At the same time, the low depth penetration and high superficial skin dose from low energy thermal neutrons were circumvented by surgical removal of the skull and direct exposure of the brain to the neutron beam [Hatanaka 1990]. This rather invasive approach allowed relevant clinical results, with a 5-year overall survival of 58% for recurrent brain tumours, which was unprecedented at that time [Hatanaka 1990]. Even though these results were not obtained in accordance with the strict rules of controlled prospective clinical trials, the promising data led to a reconsideration of clinical applications of BNCT among the globe [Moss 2014].

Around the same time, in 1987 in Japan, alternative carrier molecules were developed like Boron-phenylalanine (BPA) [Ichihashi 1982, Coderre 1990] and BPA-fructose [Coderre 1994], and used by Mishima to treat superficial malignant melanoma [Mishima 1989], which was an important step in the application of BNCT to tumours outside the central nervous system [Sauerwein 2012]. In addition, infusion techniques were improved, and this allowed gradual improvements of tracer biodistribution with better tumour-to-background ratios [Gabel 1994]. Another improvement was the shift to higher energy (epithermal) neutrons, which have a greater depth penetration and provide a more convenient thermal neutron flux at deeper-seated tumour locations with a skin-sparing effect that obviated the need for craniotomy [Gabel 1994, Sauerwein 2012].

These facilities created the conditions for the re-emergence of BNCT, and the possibility to start controlled trials. The first of these trials took place in Brookhaven [Chanana 1999] and Cambridge (MA) [Busse 2003], followed by BNCT trials in Europe at Petten [Sauerwein and Zurlo 2002], then in Finland [Joensuu 2003], Sweden [Capala 2003], and the Czech Republic [Dbaly 2002]. Also in Japan [Nakagawa 2003, Ono 1997], and later in Argentina [Gonzalez 2004] and in Taiwan [Liu 2004] patients were treated using BNCT. In these trials, BNCT was applied to different tumour types and target areas, including recurrent head-neck tumours [Kato 2004, Aihara 2006, Kankaanranta 2007], meningioma [Tamura 2006], pleural mesothelioma [Suzuki 2008], and hepatocellular carcinoma [Suzuki 2007]. Recently, in Japan clinical investigations also took place on patients with locally recurrent lung tumours [Suzuki 2012], and patients with extra-mammary Paget's disease [Sasaoka 2012].

2.3.2 Current status

Despite the 60 years of research and clinical work and the recent investigations applying BNCT to multiple tumour types, BNCT currently still has to be considered as an experimental modality. The trials performed thus far have mostly been phase I, I/II and II clinical trials, as well as, especially in Japan, clinical investigations performed outside clinical trial protocols (Moss 2014). Before BNCT can be considered a proper clinically available therapy, typically phase III trials have to be carried out. A phase III trial would typically investigate the therapeutic effect of BNCT in comparison with the effect of the current "gold standard" treatment. In order to determine the therapeutic effect, typically large patient groups are required, which often implies the involvement of multiple centres. Due to the relatively small number of centres capable of providing BNCT, in order to successfully perform such trials one would first, because of the differences that exist between the radiation beams of the different centres, need to resolve questions concerning an international standard for describing the boron-10 concentration and distribution, as well as the prescribing and reporting of the irradiation dose (Moss 2014). Consequently, due to the patient numbers, long duration, and difficulties regarding the treatment facilities both with respect to the availability and the unease of patients to be irradiated at out-of-hospital nuclear research reactors, phase III trials for BNCT would be extremely expensive and time-consuming, if possible at all (Moss 2014).

This situation is further complicated by the fact that most of the nuclear reactors used for clinical trials during the 1990s are no longer operational for BNCT anymore. As Sauerwein et al state, these closures were due to political and economic reasons rather than due to disappointing clinical results of BNCT (Sauerwein 2012), but the fact remains that the availability of suitable nuclear reactors is even smaller than two decades ago. Currently, BNCT treatments would only be possible in Japan, Taiwan, Finland, and Argentina (Sauerwein 2012, Moss 2014).[2]

Another complicating factor to performing (phase III) clinical trials with BNCT is the fact that the boron carriers that have been used so far during trials are still the same two compounds as used almost 60 years ago (Moss 2014). These compounds, BSH and BPA, are known to have low tumour-to-background ratios (Luderer2015), which obviously corrupts the efficacy of BNCT.

Finally, as in the meantime other treatment options like surgery, chemotherapy and conformal radiotherapy continued to improve, demonstrating the superiority of BNCT over other available treatments has become a more and more difficult task. The current reality is that progress has to be made regarding several aspects for BNCT to be resuscitated.

2.4 New developments

Fortunately, the technical and radiobiological superiority of the NCT approach is still recognised, and further improvements are still being pursued (Moss 2014, Nedunchezhian 2016). Some recent developments provide hope for a new exploration of the possibilities of NCT. However, there are many issues that require a solution before a broad interest in NCT can be revived. We will discuss recent developments pertinent to several of these issues in the remainder of this review.

[2] This statement concerns 'mainstream BNCT'. Outside of 'mainstream BNCT' several initiatives are investigated, such as extracorporeal BNCT in Pavia (Italy), and neutron capture-enhanced fast neutron therapy in Essen and Munich (Germany) (Sauerwein 2012).

2.4.1 Target isotopes

As previously described, boron-10 has been the isotope typically applied in NCT. Most other isotopes have no suitable characteristics for neutron capture, are not stable, or do not have characteristics to allow a favourable and safe biodistribution. However, gadolinium (Gd) is another promising candidate as a target element for NCT, with which some (preclinical) investigations have already been made (Akine 1990, Matsumoto 1992, De Stasio 2001, De Stasio 2005, Enger 2006a,b, Tokumitsu 1999, Gierga 2000, Goorley 2002, Goorley and Nikjoo 2002, Hosmane 2011, Jono 1999, Martin 1988, Martin 1989, Masiakowski 1992, Salt 2004, Brugger and Shih 1989, Shih and Brugger 1992a,b, Stepanek 2003, Takagaki and Hosmane 2007, Tokuuye 2000, Cerullo 2009). The differences between boron and gadolinium illustrate the potential for new applications.

2.4.1.1 Boron

Boron is a metalloid element with atomic number 5. The stable isotope boron-10 makes up 20% of natural boron and has a high cross-section for capture of thermal neutrons (0.025 eV) of 3,835 barn (Sauerwein 2012), as compared to 0.01-1 barn for standard elements in surrounding normal tissues (e.g. Panza and Prosperi 2012, De Stasio 2005). Neutron capture by boron-10 follows the reaction B-10 + n → B-11* → α + Li-7 + 2.79 MeV. The alpha particle (Helium core) and recoiling Lithium core both have an estimated path length of 4.5-10 um (e.g. Sauerwein 2012), which is in the order of the diameter of a typical cell (e.g. Zhao 2008). This distribution of high-LET particles is very convenient for selective dose deposition in tumour cells, while sparing surrounding normal tissues.

However, the use of boron also has disadvantages. The particle path length of one cell diameter prevents significant[3] cross-fire to adjacent tumour cells, and therefore boron depends on 100% tumour cell coverage by the carrier molecule which may not always be achievable. At the same time, this path length will generate a dose deposition spread over the entire tumour cell. It is not possible to deliver dose more selectively to relevant cell structures like DNA, which may allow improvement of the radiobiological effectiveness (RBE) of the treatment (Bos 2007). In addition, it is not always easy to label small tracer molecules with boron without affecting their biodistribution or binding affinity. This usually involves a covalent binding, like for BSH and BPA, which limits efforts to produce chemically parallel tracers with different labels for imaging and dosimetry purposes (Panza and Prosperi 2012).

2.4.1.2 Gadolinium

Gadolinium is a rare earth element with atomic number 64. Natural Gd contains a mixture of isotopes with different characteristics for neutron capture (see Table 1), and has an average cross-section for thermal neutrons of 49,700 barn (Munter 1992), which is about one order of magnitude larger than boron-10 (3,835 barn). Yet, Gd isotopes can be enriched selectively to achieve an even higher cross section. For example, Gd-155 has a higher cross-section for thermal neutrons of 61,100 barn, and Gd-157 has the highest cross-section of all known stable elements with 259,000 barn (Munter 1992). This unique

[3] There might be some background dose due to low linear energy transfer gamma rays (resulting from neutron capture by hydrogen atoms in tissue) and high linear energy transfer protons (resulting from either the scattering of fast neutrons or from neutron capture by nitrogen atoms (Barth 2005).

characteristic allows Gd-157 to reach a total cross-section for NCT in tissue similar to boron-10, but with about 66x lower concentration.

Table 1: Isotopes of natural gadolinium with their natural abundance (%) and cross section (barn) [(Munter 1992)].

Isotope	Natural abundance (%)	Cross section thermal neutrons (barn)
Gd (natural)	--	49,700
^{152}Gd	0.2	735
^{154}Gd	2.1	85
^{155}Gd	14.8	61,100
^{156}Gd	20.6	1.5
^{157}Gd	15.7	259,000
^{158}Gd	24.8	2.2
^{160}Gd	21.8	0.77

Neutron capture by Gd-157 follows the reaction Gd-157 + n → Gd-158 + γ + 7.94 MeV. The reaction product remains the same element, which is favourable to retain tracer stability and avoid degradation to potentially toxic fragments. The reaction generates low-LET prompt gamma radiation with energies up to 7.8 MeV [(De Stasio 2001, Enger 2013)], and long path lengths of about 10 cm, which induces a diffuse background dose, thus limiting the selectivity [(De Statio 2001, Cerullo 2009)]. However, depending on local anatomy most of these photons can leave the body without further interaction with tissues. In addition, the neutron capture reaction induces internal conversion (IC) electrons ranging in energy from 79 keV to 6.9 MeV [(Stepanek, 2003)]. IC electrons leave orbital electron vacancies that de-excite by emitting X-rays or high LET Auger electrons [(Enger 2013)]. Simulations of the Gd-157 neutron capture reaction indicated a yield of 0.69 internal conversion electrons, 4.93 Auger electrons, and about 0.8 X-rays [(Goorley and Nikjoo 2000, De Statio 2005, Enger 2013)]. Among these, the most biologically relevant are the Auger electrons and the internal conversion electrons [(De Stasio 2005)]. The IC electrons provide a convenient range of about 3-4 tumour cell diameters that allow cross-fire to adjacent tumour cells that have not accumulated sufficient tracer, while still sparing surrounding tissues [(Enger 2013)]. The Auger electrons have energies up to 50 keV with an average of 4.2 keV, and an average LET of 0.3 MeV/µm [(De Stasio, 2005)]. In comparison, the average LET in BNCT is 0.2 MeV/µm, for both alpha and Li-7 particles [(De Stasio 2005)]. However, the range of Auger electrons is limited to 0-150 nm, with an average path length of 12.5 nm for the average energy of 4.2 keV [(Goorley and Nikjoo 2000, Powell 2000)]. Consequently, the Auger electrons provide an extremely concentrated dose deposition at the location of the tracer, which improves the selectivity of the treatment. It should, however, be stressed that the distribution of the Auger electrons requires Gd to accumulate exactly at the location of the radiobiological target, for example within nanometres from tumour DNA. Gd-157 NCT using a tracer that distributes randomly within tumour cells largely loses the benefit of Auger electron emission, and may not demonstrate the expected benefits. This might be one of the reasons why thus far no real benefit has been shown in preclinical investigations

with Gd-157 NCT [Sauerwein 2012]. Therefore, the use of Gd imposes new requirements on the biodistribution of applied tracer molecules.

An additional advantage of gadolinium as a target isotope is the high flexibility and acceptance for clinical applications. Gd isotopes can be labelled conveniently to small molecules using a chelator, which also allows the development of chemically parallel tracers with other isotopes. Natural gadolinium is already used as a contrast enhancer in more than 30% of all clinical magnetic resonance imaging (MRI) investigations because of its paramagnetic characteristics, usually intravenously injected in chelated formulations [Enger 2013].

2.4.2 Improved delivery of target isotopes

Rather than the target isotope, is the biodistribution of the isotope carrier molecule the biological Achilles' heel of NCT. In the case of boron carrier molecules, several ideal properties have been formulated in the literature, which involve the ability to reach tumour concentrations of 20-50 µg boron-10 per gram tumour [Barth 1992], a preferred intracellular localization inside or near the nucleus, high tumour-to-background concentrations with rapid clearance from blood and normal tissues, persistence in tumour during treatment, and low systemic toxicity [Barth 1992, Nakamura and Kirihata 2012, Moss 2014, Nedunchezhian 2016]. The traditional boron delivery agents, like BPA and BSH, can provide the desired boron concentration in tumour, but with rather poor ratios with normal tissues and blood [Luderer 2015]. In the last decade, several developments have taken place, both regarding techniques to improve BPA and BSH uptake in tumour, and regarding new delivery agents.

2.4.2.1 Techniques to improve uptake of traditional boron carriers in tumour cells

Several methods have been proposed that could increase the uptake of boron in tumour cells. First, it is suggested to vary the infusion procedure (intravenously, intra-arterially, or internal carotid artery) and the infusion rate of the administered agent [Sköld 2010]. Another common strategy is the pretreatment of cells with amino acid analogs that are structurally similar to BPA, and may enter the cell through the same amino acid transport system [Capuani 2009]. It is presumed and validated that this transport system utilizes a substrate coupled antiport (exchange) mechanism, due to which pretreatment with a specific amino acid can improve the subsequent accumulation of BPA via this antiport mechanism [Luderer 2015]. Another technique used to increase the uptake of boron in tumours is the disruption of the blood-brain barrier (BBB) by a hyperosmotic agent, such as mannitol [Barth 2000]. However, disruption of the BBB by mannitol has nonspecific effects, due to which the boron uptake in healthy tissue might also be increased [Tani 2014]. This limits the applicability of hyperosmotic agents [Luderer 2015].

2.4.2.2 Recent efforts with nonspecific small molecules

In addition to techniques to increase the uptake of traditional boron carriers, new delivery agents have been developed. One group of new agents comprises small boron molecules. A small boron molecule includes a boron-10 moiety and a tumour-affinity function (although it is usually not tumour-specific) [Nakamura and Kirihata 2012]. As boron-10 moieties in the molecules boronic acid, carboranes and various boron

clusters are generally used [Adams 2002, El-Zaria 2002]. Small boron molecules can be divided in several classes: nucleoside and carbohydrate analogs, unnatural amino acids and porphyrins and related derivatives [Nakamura and Kirihata 2012, Luderer 2015].

Nucleoside and carbohydrate analogs use the higher metabolic activity of tumour cells to selectively increase the uptake of boron [Snajdr 2014]. Linked to a DNA binding unit, these molecules have the potential advantage of intra-nuclear accumulation (DNA incorporation), which might lower dosing requirements for effective BNCT [Luderer 2015]. One potential disadvantage however is that their intracellular trapping is likely cell-cycle dependent, due to which the treatment response might be cell-cycle dependent as well [Barth 2005, Khalil 2013].

Unnatural amino acids have been observed to preferentially accumulate in malignant melanoma cells compared to BPA [Kabalka 2009]. Although the overall mechanism for their tumour selectivity is still largely unknown, the advantage of unnatural amino acids is that their ability to penetrate the nucleus might provide high tumour-to-background ratios and lower dosing requirements for effective BNCT [Luderer 2015]. Unnatural amino acids however have the disadvantage that they deliver only a single boron atom per molecule [Luderer 2015].

Porphyrins and related derivatives are known to accumulate in a wide variety of solid tumours [Nakamura and Kirihata 2012]. In addition to their application in photodynamic therapy as a photosensitizer, porphyrins have been conjugated to boron-rich moieties to be applied for BNCT [Maderna 2002]. Porphyrins offer several advantages for application in BNCT, such as high water solubility, minimal cytotoxicity, a high percent boron composition, and the possibility to determine their concentration levels in tissue by relatively simple spectrophotofluorimetric analysis [Jori 2009]. A disadvantage of porphyrins however is that if they are administered intravenously, intracellular boron levels above 20 ppm required for effective BNCT might not be achieved [Luderer 2015].

2.4.2.3 Boron-conjugated biological complexes

As discussed, the effect of BNCT depends on the selective uptake of large amounts of boron-10 in tumour cells, while sparing adjacent normal tissue. Due to the limited tumour selectivity of small boron molecules, another group of boron delivery agents have been developed, which are boron-conjugated biological complexes. Several classes of biological complexes have been investigated, such as boron-containing polymers, boron peptides and antibodies, boron-encapsulated liposomes, and nanoparticles [Nakamura and Kirihata 2012, Luderer 2015]. Most of these complexes have in common that they include targeting moieties, which target receptors overexpressed on the surface of many tumour cells [Nakamura and Kirihata 2012]. Consequently, high tumour-to-background ratios might be achieved. Several (preclinical) investigations have been performed on different tumour types, such as gliomas [Yang 2008,2009; Michiue 2014], but also rat colon carcinoma [Azab 2005], and rat osteosarcoma [Achilli 2014], mouse melanomas and mouse mammary adenocarcinoma [Luderer 2015], and hamster cheek pouches as model for oral cancer [Heber 2014], to test the cytotoxicity and the tumour-to-background ratios of the biological complexes. In general, tumour-to-background ratios were higher compared to BPA/BSH, while the cytotoxicity was similar [Luderer 2015], which indicates the suitability of the biological complexes for BNCT. On the other hand, most of these complexes also have in common that they are rather large in size, due to which they, in case

of treating gliomas, have difficulties to penetrate the BBB and, in general, may undesirably accumulate in filtrating organs [Luderer 2015].

2.4.2.4 New tracer molecules

The traditional tracers like BSH and BPA targeted molecular pathways that were not exclusively activated in tumour cells, and therefore exhibited a rather non-specific biodistribution with limited tumour-to-background ratios. Ongoing efforts in molecular imaging, predominantly aimed at development of small tracer molecules for positron emission tomography (PET) imaging, have resulted in many new ligands that bind selectively to cancer-specific targets. These tracer molecules are inherently designed to carry specific isotopes, and many accumulate in tumour with unprecedented tumour-to-background ratios. In addition, several of these tracers have an intracellular distribution that is favourable over classical BSH or BPA for the purpose of NCT. An example of a potential new tracer molecule for application in NCT is PSMA.

PSMA

The prostate-specific membrane antigen (PSMA), also known as Glutamate carboxypeptidase II (GCPII), is a cell membrane epitope with a presently uncertain function. Several cancer types abundantly (i.e. 100-1000 times more than normal cells [Silver 1997]) express PSMA on their surface, while most normal tissues do not. Typical cancer types with a high likelihood of being PSMA-positive include prostate cancer (>90% of tumours express PSMA [Lückerath 2018]), renal cell carcinoma and salivary gland tumours, but many more can express the epitope. For prostate cancer, up to ~$1.5*10^6$ receptors per cell have been described [Taylor 2012]. PSMA-ligands are small molecules that selectively bind to the PSMA epitope in vivo. After intravenous injection, their biodistribution reflects areas with PSMA expression. Several PSMA-ligands are available with a DOTA chelator group, which allows labelling with e.g. Gallium-68 for PET imaging or with Lutetium-177 for radionuclide treatment. Figure 1 demonstrates the highly selective and intense uptake in metastases from prostate cancer that can be seen with PSMA-ligand PET.

A tumour-to-background ratio of up to 100:1 as compared to directly surrounding normal tissues has been described at 1 hour post-injection, and this ratio is known to improve further over time in the hours and days after injection [Afshar-Oromieh 2014]. Most bound ligand-receptor complexes remain at the cell surface, but a significant fraction is internalized and seems to accumulate in the vicinity of the nucleus [Meneghetti 2012, Banerjee 2015]. This indicates a promising biodistribution for NCT, with a significant proportion of the administered isotopes close to tumour DNA.

Isotope binding

Tracer molecules like PSMA have been expanded with a DOTA chelator group, which is most often primarily intended for labelling with Gallium-68 for PET imaging [Lenzo 2018]. The presence of a DOTA group also allows convenient labelling with other metallic elements for diagnostic and therapeutic purposes, with large similarities in the required procedures and quality control [Viola-Villegas and Doyle 2009]. This universal approach allows fast exchange of knowledge, and allows substitution in available

molecules for different applications like imaging and therapy. Consequently, this also facilitates relatively easy development and implementation of new tracer molecules labelled with DOTA-Gadolinium for preclinical and clinical use.

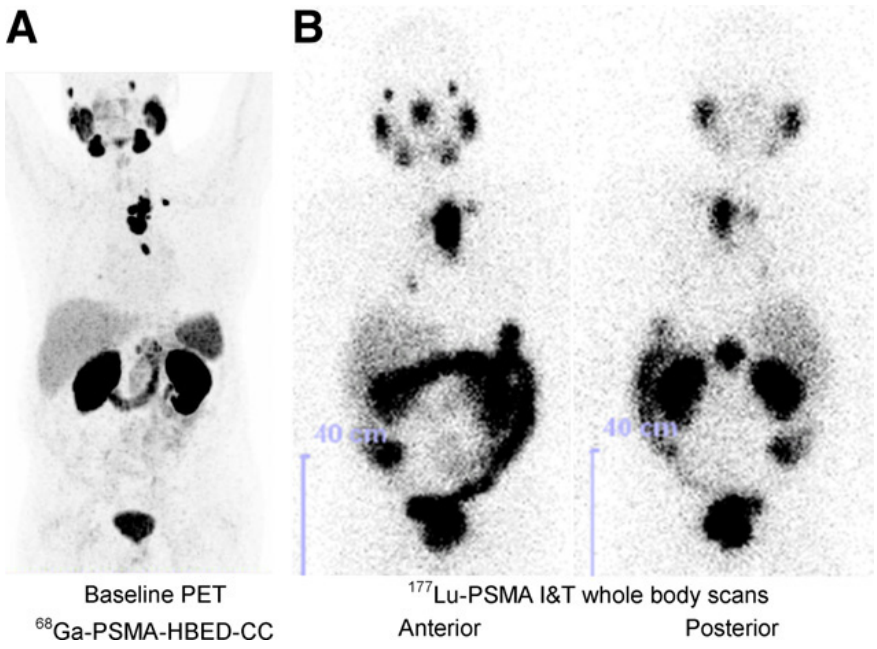

Figure 1: (A) 68Ga-PSMA PET/CT scan made 60 min after injection with corresponding (B) whole body scan of 177Lu-PSMA after 47h uptake. Intense tracer accumulation in metastates is shown [(Weineisen 2015)].

2.4.3 Imaging of tracer distribution

One of the theoretically strong aspects of NCT is the limited toxicity profile, which is mainly achieved by low induction of local and regional toxicity. This favourable treatment characteristic would be lessened when the administered tracer induces systemic toxicity. Early boron carriers like boronic acid suffered from such toxicity, but this has not been described for BSH or BPA in the doses that were typically applied for BNCT. Newly developed carrier molecules will have to adhere to current safety regulations, which include production according to good clinical practice (GMP) and appropriate toxicity evaluation in mice and man. The safety profile of a carrier molecule further improves when a very low (tracer) dose can be administered to achieve the desired concentrations in target tissues, which is facilitated by a biodistribution with very tumour-specific uptake. For these considerations, it is of great help when the pharmacological characteristics of a tracer molecule can be evaluated with non-invasive techniques in vitro, like imaging with PET, SPECT or MRI. In the case of boron-10, BPA could be labelled with F-18 which allows the evaluation of the tracer distribution using PET. In addition, the detection of boron compounds by MRI is available for clinical use [(Moss 2014)]. As natural gadolinium is regularly applied in the clinic for MRI, this also provides an opportunity to evaluate the distribution of gadolinium used for NCT.

2.4.4 Theranostic approach using parallel tracers

The use of DOTA chelators for PET-tracers allows the analogous development and direct comparison of the same molecules labelled with Gd-157 for NCT treatment and with Gallium-68 for imaging. This provides the opportunity to evaluate the distribution of the NCT agent using PET, which allows for a theranostic approach with proper patient selection and individualized dose optimization for treatment.

The term 'theranostics' epitomizes the inseparability of diagnosis and therapy, the two pillars of medicine. In the context of nuclear medicine, it refers to the use of molecular targeting agents labelled either with diagnostic radionuclides (e.g. positron or gamma emitters), or with therapeutic radionuclides for respectively diagnosis and therapy of a particular disease, targeted specifically by the agent at its molecular level. Therefore, molecular imaging and diagnosis of the disease can be effectively followed by personalized treatment utilizing the same molecular imaging agent (Baum and Kulkarni 2012).

The potential of a theranostic approach in the context of NCT is very promising, as merely those patients will be selected for trials which are expected to benefit from the treatment, and potential harm due to for example undesired accumulation of tracer in normal tissue, could be prevented as this will be known before the irradiation commences.

2.4.5 Improved treatment planning

Information obtained about the biodistribution of the PET tracer in individual patients may help to improve the treatment planning in NCT. Treatment planning involves the computation and analysis of the radiation dose distribution in an individual patient. This is done in order to determine the beam orientation and the radiation fluence, to enable delivery of an optimized dose distribution, which complies with the dose prescribed, while respecting dose limits for normal tissues and organs at risk as much as possible (Kiger III and Kumada 2012). As Kiger and Kumada contend, treatment planning for NCT differs significantly from treatment planning for photons or electrons in conventional radiotherapy, and is in some ways much more complex.

In conventional radiotherapy, the dose from primary photons or electrons is computed, which is ultimately delivered by low-LET electrons in both cases. In contrast, in the case of NCT the radiation field is a complex mixture of high- and low-LET dose components with varying biological effectiveness, which depends on both the tissue and the delivery agent (Kiger III and Kumada 2012). Consequently, in NCT treatment planning, several different dose components, arising from neutron and photon interactions in tissue, must be taken into account. To make things more complicated, each of these dose components has a different spatial distribution, which depends on the tissue composition as well as the neutron and photon fluence spectra (Kiger III and Kumada 2012).

Because of the complex, scatter-dominated nature of the radiation interactions involved, NCT treatment planning systems thus far exclusively rely on Monte Carlo simulation for the calculation of doses in the patient (Kiger III and Kumada 2012). Recently, several treatment planning systems have been developed, which could be used for NCT (Moss 2014). These systems include BNCT_Rtpe, NCTPlan, JCDS, SERA and THORPlan (Kiger III and Kumada 2012). Prior acquired PET/CT and/or PET/MRI data on anatomy and tracer biodistribution can be used as input for these treatment planning systems (Nichols 2002).

2.4.6 Neutron beams

The availability of proper neutron beams is another issue that needs to be resolved before a broad interest in NCT can be revived. For NCT, a proper neutron beam is a beam with a sufficiently high fluence rate, which delivers neutrons at the 'right' energy. The radiation beam directed towards the tumour area, should also have as little contaminants (e.g. gamma photons) as possible [Moss 2014, Nedunchezhian 2016]. Thus far, all reported NCT irradiations on patients have been performed at nuclear research reactors in a variety of countries [Moss 1997, Nigg 2006, Harling and Riley 2012]. As discussed before, many of these reactors are either no longer open, have ceased their NCT activities or are on the verge of closure [Moss 2014]. Yet for future development of NCT, suitable neutron beams are essential. There might however be hope because of the developments regarding Accelerator-Based Neutron Sources (ABNS), as discussed in the following.

2.4.6.1 In-hospital availability using accelerators

With regard to accelerator-based neutron sources, there are many different types that have and are being considered for NCT applications. ABNS range from low-energy electrostatic machines to higher energy cyclotrons, to still much higher-energy Linacs or synchrotrons [Moss 2014]. The generation of neutrons by accelerators is different from reactor sources: in general, a proton beam is produced by the accelerator and impinges on a target, releasing neutrons [Moss 2014]. The beam of neutrons produced accordingly, tends to have a low fluence rate compared to beams from nuclear reactors [Moss 2014]. Although an increase in beam intensity by more than an order of magnitude is necessary in many types of accelerators, the promise of ABNS with suitable fluence rates appears to be possible [Nigg 2006, Kreiner 2012]. At present, there are several initiatives to develop accelerator-based BNCT around different types of accelerators [Kreiner 2014]. There are projects going on in Japan [Tanaka 2011, Kumada 2011, Nakamura and Kirihata 2012], Russia [Aleynik 2011, Kononov 2004], UK [Ghani 2008], Argentina [Kreiner 2011,2013, Burlon 2011], Israel [Halfon 2011], and Italy [Ceballos 2011]. Some of these accelerators are already developed and ready to be used for clinical trials (Russia, UK, two out of three projects in Japan and Israel), and some are still under construction (Argentina, one out of three in Japan and Italy) [Kreiner 2014].

In addition to the reduction of the dependency on reactor-based neutron beams, accelerators have some other advantages over reactor-based sources. An important advantage of accelerators is that the neutron energy spectrum from certain nuclear reactions is much 'softer' (i.e. less energetic) than the one coming from fission, which, according to Kreiner, makes it easier to generate the 'ideal' epithermal neutron spectrum needed for treatment of deep-seated tumours, and consequently, the quality of the neutron field can be designed to significantly exceed the quality of the neutron field for reactor-based neutron beams [Kreiner 2012]. Another major advantage of ABNS is the potential for situating it within a hospital. The presence of accelerators in health-care institutions is expected to increase institutional commitment and to ease patient recruitment and the use of on-site resources, which is deemed necessary for a significant improvement in the data and experience gathered regarding NCT [Kreiner 2012]. Since (electron as well as ion) accelerators have been a prominent feature of radiotherapy departments in hospitals for years, and clinicians consequently have a long-standing experience with similar devices for patient irradiation, it is very likely that clinicians will prefer accelerators to reactor-based sources. Other advantages of accelerators include the fact that they can easily be turned off when the neutron field is no longer required, that the licencing, installation and maintenance of accelerators are simpler, and that the capital expense of accelerators is substantially lower [Kreiner 2012,

Moss 2014). As such, the availability of accelerators may be decisive for the future of NCT. It is therefore hoped that accelerators suitable for NCT will become broadly available in due time.

2.5 Conclusions

Due to the use of non-specific delivery agents with low tumour-to-background ratios, the limited availability of neutron sources, and a shortage of properly conducted clinical trials, BNCT thus far has never been shown to be better than state of the art treatments.

However, the recent developments described in this work, regarding new, highly targeted delivery agents, dose optimization using a theranostic approach, advanced treatment planning, and the availability of in-hospital accelerators for neutron production, together may allow for a paradigm shift in NCT, from an exotic niche to a mainstream and technically superior treatment modality for a broad selection of tumours. This justifies a renewed exploration of the potential of NCT, utilizing modern methodologies and techniques.

In particular with respect to the new tracer molecules, due to their highly specific uptake, we foresee broad new applications and potential for personalized treatment. Potential applications of next-generation NCT include regional ablation of macroscopic and microscopic tumour, potentially in a single session with limited toxicity, which can notably be effective and safe, even in the case of distorted anatomy or prior high-dose radiotherapy.

2.6 Bibliography

1. Moss RL. Critical review, with an optimistic outlook, on Boron Neutron Capture Therapy (BNCT). Appl Radiat Isot. 2014 Jun; 88:2-11.
2. Nedunchezhian K, Aswath N, Thiruppathy M, Thirugnanamurthy S. Boron Neutron Capture Therapy - A Literature Review. J Clin Diagn Res. 2016 Dec; 10(12): ZE01-ZE04.
3. Sauerwein WAG, Moss RL, Wittig, A, Nakagawa, Y (eds), Neutron Capture Therapy; Principles and applications. Springer-Verlag. 2012; Heidelberg.
4. Hawthorne MF. The Role of Chemistry in the Development of Boron Neutron Capture Therapy of Cancer. Angew. Chem. Int. Ed. Engl. 1993; 32: 950-984.
5. Chadwick J. The existence of a neutron. Proc R Soc Lond. 1932; A136:692–708.
6. Locher GL. Biological effects and therapeutic possibilities of neutrons. Am J Roentgenol Radium Ther. 1936; 36(1):1–13.
7. Farr LE, Sweet WH, Locksley HB, Robertson JS. Neutron capture therapy of gliomas using boron. Trans Am Neurol Assoc. 1954; 13(79th Meeting):110-3.
8. Archambeau JO. The effect of increasing exposures of the 10-B(n,alpha)7-Li reaction on the skin of man. Radiology. 1970 Jan; 94(1):179-87.
9. Sweet WH, Soloway AH, Brownell GL. Boron-slow neutron capture therapy of gliomas. Acta Radiol Stockholm. 1963; 1:114–21.
10. Slatkin DN. A history of boron neutron capture therapy of brain tumours. Brain. 1991 Aug; 114 (Pt 4):1609-29.
11. Asbury AK, Ojemann RG, Nielsen SL, Sweet WH. Neuropathologic study of fourteen cases of malignant brain tumour treated by boron-10 slow neutron capture radiation. J Neuropathol Exp Neurol. 1972 Apr; 31(2):278-303.
12. Gabel D. Present status and perspectives of boron neutron capture therapy. Radiotherapy and Oncology. 1994; 30: 199-205.
13. Coderre JA, Glass JD, Micca P, Fairchild RG. Neutron capture therapy for melanoma. Basic Life Sciences. 1989; 50(219):219–232.
14. Goodman JH, Fairchild RG. Boron neutron capture therapy for cerebral neoplasia. Perspect Neuroogical Surgery 1990; 1(1):93–110.
15. Farr LE. Neutron capture therapy: years of experimentation – years of reflection. Report BNL-47087. 1991; Brookhaven National Laboratory, New York.
16. Hatanaka H. Clinical results of boron neutron capture therapy. Basic Life Sci. 1990; 54(15):15–21.
17. Doi A, Kawabata S, Iida K, Yokoyama K, Kajimoto Y, Kuroiwa T, Shirakawa T, Kirihata M, Kasaoka S, Maruyama K, Kumada H, Sakurai Y, Masunaga S, Ono K, Miyatake S. Tumour-specific targeting of sodium borocaptate (BSH) to malignant glioma by transferrin-PEG liposomes: a modality for boron neutron capture therapy. J Neurooncol. 2008 May; 87(3):287-94. doi: 10.1007/s11060-008-9522-8. Epub 2008 Jan 25. PubMed PMID: 18219552.
18. Ichihashi M, Nakanishi T, Mishima Y. Specific killing effect of 10B1-para-boronophenylalanine in thermal neutron capture therapy of malignant melanoma: in vitro radiobiological evaluation. J Invest Dermatol. 1982 Mar; 78(3):215-8. PubMed PMID: 7057053.
19. Coderre JA, Glass JD, Fairchild RG, Micca PL, Fand I, Joel DD. Selective delivery of boron by the melanin precursor analogue p-boronophenylalanine to tumours other than melanoma. Cancer Res. 1990 Jan 1; 50(1):138-41. PubMed PMID: 2293547.
20. Coderre JA, Button TM, Micca PL, Fisher CD, Nawrocky MM, Liu HB. Neutron capture therapy of the 9L rat gliosarcoma using the p-boronophenylalanine-fructose complex. Int J Radiat Oncol Biol Phys. 1994 Oct 15; 30(3):643-52. PubMed PMID: 7928496.
21. Mishima Y, Ichihashi M, Hatta S, Honda C, Yamamura K, Nakagawa T, et al. First human clinical trial of melanoma neutron capture. Diagnosis and therapy. Strahlenther Onkol. 1989; 165(2–3):251–54.

22. Chanana AD, Capala J, Chadha M, Coderre JA, Diaz AZ, Elowitz EH, Iwai J, Joel DD, Liu HB, Ma R, Pendzick N, Peress NS, Shady MS, Slatkin DN, Tyson GW, Wielopolski L. Boron neutron capture therapy for glioblastoma multiforme: interim results from the phase I/ II dose-escalation studies. Neurosurgery. 1999; 44(6):1182–1193.
23. Busse PM, Harling OK, Palmer MR, Kiger WS 3rd, Kaplan J, Kaplan I, Chuang CF, Goorley JT, Riley KJ, Newton TH, Santa Cruz GA, Lu XQ, Zamenhof RG. A critical examination of the results from the Harvard-MIT NCT program phase I clinical trial of neutron capture therapy for intracranial disease. J Neurooncol. 2003; 62(1–2):111–121.
24. Sauerwein W, Zurlo A. The EORTC boron neutron capture therapy (BNCT) group: achievements and future projects. Eur J Cancer. 2002; 38(Suppl 4):S31–S34.
25. Joensuu H, Kankaanranta L, Seppala T, Auterinen I, Kallio M, Kulvik M, Laakso J, Vahatalo J, Kortesniemi M, Kotiluoto P, Seren T, Karila J, Brander A, Jarviluoma E, Ryynanen P, Paetau A, Ruokonen I, Minn H, Tenhunen M, Jaaskelainen J, Farkkila M, Savolainen S. Boron neutron capture therapy of brain tumours: clinical trials at the Finnish facility using boronophenylalanine. J Neurooncol. 2003; 62(1–2):123–134.
26. Capala J, Stenstam BH, Skold K, Rosenschold PM, Giusti V, Persson C, Wallin E, Brun A, Franzen L, Carlsson J, Salford L, Ceberg C, Persson B, Pellettieri L, Henriksson R. Boron neutron capture therapy for glioblastoma multiforme: clinical studies in Sweden. J Neurooncol. 2003; 62(1–2):135–144.
27. Dbaly V, Tovarys F, Honova H, Petruzelka L, Prokes K, Burian J, Marek M, Honzatko J, Tomandl I, Kriz O, Janku I, Mares V. Contemporary state of neutron capture therapy in Czech Republic (part 2). Ces a slov Neurol Neurochir. 2002; 66/99(1):60–63.
28. Nakagawa Y, Pooh K, Kobayashi T, Kageji T, Uyama S, Matsumura A, Kumada H. Clinical review of the Japanese experience with boron neutron capture therapy and a proposed strategy using epithermal neutron beams. J Neurooncol. 2003; 62(1–2):87–99.
29. Ono K, Ueda S, Oda Y, Nakagawa Y, Miyatake S, Osawa M, Kobayashi T. Boron neutron capture therapy for malignant glioma at Kyoto University reactor. In: Larsson B, Crawford J, Weinreich R (eds) Advances in neutron capture therapy. 1997; vol I. Elsevier Science, Amsterdam, pp 39–45.
30. Gonzalez SJ, Bonomi MR, Santa Cruz GA, Blaumann HR, Calzetta Larrieu OA, Menendez P, Jimenez Rebagliati R, Longhino J, Feld DB, Dagrosa MA, Argerich C, Castiglia SG, Batistoni DA, Liberman SJ, Roth BM. First BNCT treatment of a skin melanoma in Argentina: dosimetric analysis and clinical outcome. Appl Radiat Isot. 2004; 61(5):1101–1105.
31. Liu YW, Huang TT, Jiang SH, Liu HM (2004) Renovation of epithermal neutron beam for BNCT at THOR. Appl Radiat Isot 61(5):1039–1043.
32. Kato I, Ono K, Sakurai Y, Ohmae M, Maruhashi A, Imahori Y, Kirihata M, Nakazawa M, Yura Y. Effectiveness of BNCT for recurrent head and neck malignancies. Appl Radiat Isot. 2004; 61(5):1069–1073.
33. Aihara T, Hiratsuka J, Morita N, Uno M, Sakurai Y, Maruhashi A, Ono K, Harada T. First clinical case of boron neutron capture therapy for head and neck malignancies using 18 F-BPA PET. Head Neck. 2006; 28(9):850–855.
34. Kankaanranta L, Seppala T, Koivunoro H, Saarilahti K, Atula T, Collan J, Salli E, Kortesniemi M, Uusi-Simola J, Makitie A, Seppanen M, Minn H, Kotiluoto P, Auterinen I, Savolainen S, Kouri M, Joensuu H. Boron neutron capture therapy in the treatment of locally recurred head and neck cancer. Int J Radiat Oncol Biol Phys. 2007; 69(2):475–482.
35. Tamura Y, Miyatake S, Nonoguchi N, Miyata S, Yokoyama K, Doi A, Kuroiwa T, Asada M, Tanabe H, Ono K. Boron neutron capture therapy for recurrent malignant meningioma. Case report. J Neurosurg. 2006; 105(6):898–903.
36. Suzuki M, Endo K, Satoh H, Sakurai Y, Kumada H, Kimura H, Masunaga S, Kinashi Y, Nagata K, Maruhashi A, Ono K. A novel concept of treatment of diffuse or multiple pleural tumours by boron neutron capture therapy (BNCT). Radiother Oncol. 2008; 88(2):192–195.

37. Suzuki M, Sakurai Y, Hagiwara S, Masunaga S, Kinashi Y, Nagata K, Maruhashi A, Kudo M, Ono K. First attempt of boron neutron capture therapy (BNCT) for hepatocellular carcinoma. Jpn J Clin Oncol. 2007; 37(5):376–381.
38. Suzuki M et al. Reirradiation for locally recurrent lung cancer in the chest wall with boron neutron capture therapy (BNCT): A case report. In: Presented at the 15th international congress on neutron capture therapy. Tsukuba, Japan, 2012. September 10–14.
39. Sasaoka S. The first clinical trial of boron neutron captures therapy using 10B-para-boronophenylalanine for treating extra-mammary Paget's disease. In: Presented at the 15th International Congress on Neutron Capture Therapy, Tsukuba, Japan, 2012. September 10-14.
40. Akine Y, Tokita N, Matsumoto T, Oyama H, Egawa S, Aizawa O. Radiation effect of gadolinium-neutron capture reactions on the survival of Chinese hamster cells. Strahlenther Onkol. 1990; 166(12):831–833
41. Matsumoto T. Transport calculations of depth-dose distributions for gadolinium neutron capture therapy. Phys Med Biol. 1992; 37(1):155–162.
42. De Stasio, G., Casalbore, P., Pallini, R., Gilbert, B., Sanita, F., Ciotti, M.T., Rosi, G., Festinesi, A., Larocca, L.M., Rinelli, A., Perret, D., Mogk, D.W., Perfetti, P., Mehta, M.P., Mercanti, D. Gadolinium in human glioblastoma cells for gadolinium neutron capture therapy. Cancer Res. 2001; 61, 4272e4277.
43. De Stasio G, Rajesh D, Casalbore P, Daniels MJ, Erhardt RJ, Frazer BH, Wiese LM, Richter KL, Sonderegger BR, Gilbert B, Schaub S, Cannara RJ, Crawford JF, Gilles MK, Tyliszczak T, Fowler JF, Larocca LM, Howard SP, Mercanti D, Mehta MP, Pallini R. Are gadolinium contrast agents suitable for gadolinium neutron capture therapy? Neurological Research. 2005 June; 27:387-398.
44. Enger, S.A., Rezaei, A., Munck af Rosenschöld, P., Lundqvist H. Gadolinium neutron capture brachytherapy (GdNCB), a new treatment method for intravascular brachytherapy. Med. Phys. 2006a; 33, 46e51.
45. Enger, S.A., Munck af Rosenschöld, P., Rezaei, A., Lundqvist, H. Monte Carlo calculations of thermal neutron capture in gadolinium: a comparison of GEANT4 and MCNP with measurements. Med. Phys. 2006b; 33, 337e341.
46. Tokumitsu, H., Ichikawa, H., Fukumori, Y., Block, L.H. Preparation of gadopentetic acid-loaded chitosan microparticles for gadolinium neutron-capture therapy of cancer by a novel Emulsion-Droplet coalescence technique. Chem. Pharm. Bull. 1999; 47, 838e842.
47. Gierga, D.P., Yanch, J.C., Shefer, R.E. An investigation of the feasibility for neutron capture synovectomy. Med. Phys. 2000; 27, 1685e1692.
48. Goorley, T., Kiger, W.S., Zamenhof, R.G. Reference dosimetry calculations for neutron capture therapy with comparison of analytical and voxel models. Med. Phys. 2002; 29, 145e156.
49. Goorley, T., Nikjoo, H. A comparison of three gadolinium based Approaches to cancer therapy. Radiat. Res. 2002; 154, 556e563.
50. Hosmane, N.S. Boron Science: New Technologies and Applications. Taylor & Francis Books/CRC Press, 2011; Boca Raton, FL, USA.
51. Jono, K., Ichikawa, H., Fujioka, K., Fukumori, Y., Akine, Y., Tokuuye, K. Preparation of lecithin microcapsules by a dilution method using the Wurster process for intra-arterial administration in gadolinium neutron capture therapy. Chem. Pharm. Bull. 1999; 47, 54e63.
52. Martin, R.F., D'Cunha, G., Pardee, M., Allen, B.J. Induction of double strand breaks following neutron capture by DNA bound 157Gd. Int. J. Radiat. Biol. 1988; 54, 205e208.
53. Martin RF, D'Cunha G, Pardee M, Allen BJ. Induction of DNA double-strand breaks by 157-Gd neutron capture. Pigment Cell Res. 1989; 2(4):330–332
54. Masiakowski, J.T., Horton, J.L., Peters, L.J. Gadolinium neutron capture therapy for brain tumours: a computer study. Med. Phys. 1992; 19, 1277e1284.
55. Salt, C., Lennox, A.J., Takagaki, M., Maguire, J.A., Hosmane, N.S. Boron and gadolinium neutron capture therapy. Russ. Chem. Bul. 2004; 53, 1871e1888.

56. Brugger RM, Shih JA. Evaluation of gadolinium-157 as a neutron capture therapy agent. Strahlenther Onkol. 1989; 165(2–3):153–156
57. Shih, J.A., Brugger, R.M. Gadolinium as a neutron capture therapy agent. Med. Phys. 1992a; 19, 733e744.
58. Shih, J.A., Brugger, R.M. Neutron induced brachytherapy: neutron capture therapy and Brachytherapy. Med. Phys. 1992b; 19, 369e375.
59. Stepanek, J. Emission spectra of gadolinium-158. Med. Phys. 2003; 30: 41-43.
60. Takagaki, M., Hosmane, N.S. Gadolinium neutron capture. Aino J. 2007; 6, 39e44.
61. Tokuuye, K., Tokita, N., Akine, Y., Nakayama, H., Sakurai, Y., Kobayashi, T., Kanda, K., Comparison of radiation effects of gadolinium and boron neutron capture reactions. Strahlenther Onkol. 2000; 176, 81e83.
62. Cerullo N, Bufalino D et al. Progress in the use of gadolinium for NCT. Appl Radiat Isot. 2009; 67(7–8 Suppl): S157–S160.
63. Panza L and Prosperi D. Boron chemistry. In Sauerwein, WAG, Moss, RL, Wittig, A, Nakagawa, Y (eds), Neutron Capture Therapy; Principles and applications. Springer-Verlag. 2012; Heidelberg.
64. Zhao L, Kroenke CD, Song J, Piwnica-Worms D, Ackerman JJ, Neil JJ. Intracellular water-specific MR of microbead-adherent cells: the HeLa cell intracellular water exchange lifetime. NMR Biomed. 2008 Feb; 21(2):159-64
65. Bos AJJ, Draaisma FS, Okx WJC. Inleiding tot de stralingshygiëne. Sdu Uitgevers bv. 2007; Den Haag.
66. Munter A. Special Feature section of neutron scattering lengths and cross sections of the elements and their isotopes. Neutron News. 1992; 3(3):29-37.
67. Enger SA, Giusti V, Fortin M-A, Lundqvist H, Munck af Rosenschöld P. Dosimetry for gadolinium neutron capture therapy (GdNCT). Radiation Measurements. 2013; 59: 233-240.
68. Goorley T, Nikjoo H. Electron and photon spectra for three gadolinium-based cancer therapy approaches. Radiat Res 2000; 154: 556–563
69. Powell CJ, Jablonski A. NIST Electron Inelastic-Mean-Free-Path Database – Version 1.1, 2000; National Institute of Standards and Technology, Gaithersburg, MD.
70. Barth RF, Soloway AH, Fairchild RG, Brugger RM. Boron neutron capture therapy for cancer. Realities and prospects. Cancer. 1992 Dec 15; 70(12): 2995-3007.
71. Nakamura H and Kirihata M. Boron Compounds: New Candidates for Boron Carriers in BNCT. In Sauerwein, WAG, Moss, RL, Wittig, A, Nakagawa, Y (eds), Neutron Capture Therapy; Principles and applications. Springer-Verlag, Heidelberg, 2012.
72. Luderer M J, Puente P de la, Azab AK. Advancements in Tumour Targeting Strategies for Boron Neutron Capture Therapy. Pharm Res. 2015; 32: 2824-2836.
73. Sköld, K., Stenstam,B.H., Diaz,A.Z., Giusti,V., Pellettieri,L., Hopewell,J.W. Boron Neutron Capture Therapy for glioblastoma multiforme:advantage of prolonged infusion of BPA-f. Acta Neurol. Scand. 2010; (122), 58–62.
74. Capuani S, Gili T, Bozzali M, Russo S, Porcari P, Cametti C, et al. Boronophenylalanine uptake in C6 glioma model is dramatically increased by l-DOPA preloading. Appl Radiat Isot. 2009; 67(7–8): S34–S6.
75. Barth, R.F., Yang,W., Rotaru,J.H., Moeschberger,M.L., Boesel,C.P., Soloway,A.H., Joel, D.D., Nawrocky,M.M., Ono,K., Goodman,J.H., Boron Neutron Capture Therapy of brain tumours: enhanced survival and cure following blood–brain barrier disruption and intracarotid injection of sodium borocaptate and boronophenylalanine. Int. J. Radiat. Oncol. Biol. Phys. 2000; 47,209–218.
76. Tani H, Kurihara H, Hiroi K, Honda N, Yoshimoto M, Kono Y, et al. Correlation of (18)F-BPA and (18)F-FDG uptake in head and neck cancers. Radiother Oncol. 2014; 113(2):193–7.
77. Adams L, Hosmane SN, Eklund JE et al. A new synthetic route to boron-10 enriched pentaborane (9) from boric acid and its conversion to anti- 10 B 18 H 22. J Am Chem Soc. 2002; 124:7292–7293.
78. El-Zaria ME, Dor fl er U, Gabel D. Synthesis of (aminoalkylamine)-N-aminoalkyl) azanonaborane(11) derivatives for boron neutron capture therapy. J Med Chem. 2002; 45:5817–5819.

79. Snajdr I, Janousek Z, Takagaki M, Cisarova I, Hosmane NS, Kotora M. Alpha (alpha-) and beta (beta-carboranyl-Cdeoxyribosides: syntheses, structures and biological evaluation. Eur J Med Chem. 2014; 83:389–97.
80. Barth RF, Coderre JA, Vicente MGH, Blue TE. Boron neutron capture therapy of cancer: current status and future prospects. Clin. Cancer Res. 2005; 11(11):3987–4002.
81. Khalil A, Ishita K, Ali T, Tjarks W. N3-substituted thymidine bioconjugates for cancer therapy and imaging. Future Med Chem. 2013; 5(6):677–92.
82. Kabalka GW, Yao ML, Marepally SR, Chandra S. Biological evaluation of boronated unnatural amino acids as new boron carriers. Appl Radiat Isot. 2009; 67(7–8):S374–S9.
83. Maderna A, Huertas R, Hawthorne MF, Luguya R, Vicente MGH. Synthesis of a porphyrin-labelled carboranyl phosphate diester: a potential new drug for boron neutron capture therapy of cancer. Chem Commun. 2002; 16:1784–5.
84. Jori G, Soncin M, Friso E, Vicente MG, Hao E, Miotto G, et al. A novel boronated-porphyrin as a radio-sensitizing agent for boron neutron capture therapy of tumours: in vitro and in vivo studies. Appl Radiation Isot: Incl Data, Instrum Methods Agric, Ind Med. 2009; 67(7–8 Suppl):S321–4.
85. Yang W, Wu G, Barth RF, Swindall MR, Bandyopadhyaya AK, Tjarks W, et al. Molecular targeting and treatment of composite EGFR and EGFRvIII-positive gliomas using boronated monoclonal antibodies. Clin Cancer Res: Off J Am Assoc Cancer Res. 2008; 14(3):883–91.
86. Yang W, Barth RF, Wu G, Tjarks W, Binns P, Riley K. Boron neutron capture therapy of EGFR or EGFRvIII positive gliomas using either boronated monoclonal antibodies or epidermal culture factor as molecular targeting agents. Appl Radiation Isot: InclData, Instrum Methods Agric, Ind Med. 2009;67(7–8 Suppl):S328–31.
87. Michiue H, Sakurai Y, Kondo N, Kitamatsu M, Bin F, Nakajima K, et al. The acceleration of boron neutron capture therapy using multi-linked mercaptoundecahydrododecaborate (BSH) fused cell penetrating peptide. Biomaterials. 2014. Epub 2014/01/24.
88. Azab AK, Srebnik M, Doviner V, Rubinstein A. Targeting normal and neoplastic tissues in the rat jejunum and colon with boronated, cationic acrylamide copolymers. J Controlled Release: Off J Controlled Release Soc. 2005; 106(1–2):14–25.
89. Achilli C, Grandi S, Ciana A, Guidetti GF, Malara A, Abbonante V, et al. Biocompatibility of functionalized boron phosphate (BPO4) nanoparticles for boron neutron capture therapy (BNCT) application. Nanomed: Nanotechnol, Biol Med. 2014; 10(3):589–97.
90. Heber EM, Hawthorne MF, Kueffer PJ, Garabalino MA, Thorp SI, Pozzi EC, et al. Therapeutic efficacy of boron neutron capture therapy mediated by boron-rich liposomes for oral cancer in the hamster cheek pouch model. Proc Natl Acad Sci U S A. 2014; 111(45):16077–81.
91. Silver DA, Pellicer I, Fair WR, Heston WD, Cordon-Cardo C. Prostate-specific membrane antigen expression in normal and malignant human tissues. Clin Cancer Res. 1997 Jan; 3 (1): 81-85.
92. Lückerath K, Stuparu AD, Wei L, Kim W, Radu CG, Mona CE, Calais J, Rettig M, Reiter RE, Czernin J, Slavik, R, Herrmann K, Eiber M, Fendler WP. Detection threshold and reproducibility of ^{68}Ga-PSMA-11 PET/CT in a mouse model of prostate cancer. J Nucl Med. 2018 March 30 (Epub ahead of print): 1-29.
93. Taylor RM, Severns V, Brown DC, Bisoffi M, Sillerud LO. Prostate Cancer Targeting Motifs: Expression of αvβ3, Neurotensin Receptor 1, Prostate Specific Membrane Antigen, and Prostate Stem Cell Antigen in Human Prostate Cancer Cell Lines and Xenografts. The Prostate. 2012; 72(5):523-532. doi:10.1002/pros.21454.
94. Weineisen M, Schottelius M, Simecek J, Baum RP, Yildiz A, Beykan S, Kulkarni HR, Lassmann M, Klette I, Eiber M, Schwaiger M, Wester HJ. 68Ga- and 177Lu-Labeled PSMA I&T: Optimization of a PSMA-Targeted Theranostic Concept and First Proof-of-Concept Human Studies. J Nucl Med. 2015 Aug 1; 56 (8):1169-1176.
95. Afshar-Oromieh, A., Malcher, A., Eder, M. et al. PET imaging with a [68Ga]-labelled PSMA ligand for the diagnosis of prostate cancer: biodistribution in humans and first evaluation of tumour lesions. Eur J Nucl Med Mol Imaging. 2013; 40: 486.

96. Meneghetti M, Scarsi A, Litti L, Colombatti M. Serrs: Plasmonic Nanostructures for SERRS Multiplexed Identification of Tumour-Associated Antigens. Small. 2012 December; 8 (24).
97. Banerjee SR, Ngen EJ, Rotz MW, Kakkad S, Lisok A, Pracitto R, Pullambhatla M, Chen Z, Shan T, Artemov D, Meade TJ, Bhujwalla ZM, Pomper MG. Synthesis and Evaluation of GdIII-Based Magnetic Resonance Contrast Agents for Molecular Imaging of Prostate-Specific Membrane Antigen; Supporting Information. Angew. Chem. Int. Ed. 2015; 54: 10778-10782.
98. Lenzo NP, Meyrick D, Turner JH. Review of Gallium-68 PSMA PET/CT Imaging in the Management of Prostate Cancer. Diagnostics. 2018; 8 (16): 1-17.
99. Viola-Villegas N, Doyle RP. The coordination chemistry of 1,4,7,10-tetraazacyclododecane-N,N',N'',N'''-tetraacetic acid (H4DOTA): Structural overview and analyses on structure–stability relationships. Coordination Chemistry Reviews. 2009 July; 253(13-14): 1906-1925.
100. Baum RP, Kulkarni HR. THERANOSTICS: From Molecular Imaging Using Ga-68 Labeled Tracers and PET/CT to Personalized Radionuclide Therapy - The Bad Berka Experience. Theranostics. 2012; 2(5):437-447. doi:10.7150/thno.3645.
101. Kiger III WS, Kumada H. Treatment Planning. In Sauerwein, WAG, Moss, RL, Wittig, A, Nakagawa, Y (eds), Neutron Capture Therapy; Principles and applications. Springer-Verlag. 2012; Heidelberg.
102. Nichols, T.L.,Kabalka,G.W., Miller, L.F.,Khan,M.K., Smith,G.T. Improved treatment planning for Boron Neutron Capture Therapy for glioblastoma multiforme using fluorine-18 labeled boronophenylalanine and positron emission tomography. Med.Phys. 2002; 29, 2351–2358.
103. Moss, R.L., Aizawa,O., Beynon,D., Brugger,R., Constantine,G., Harling,O., Liu,H.B., Watkins,P. The requirements and development of neutron beams for neutron capture therapy of brain cancer. J.Neurooncol. 1997; 33, 27–40.
104. Nigg,D.W. Neutron sources and applications in radiotherapy – a brief history and current trends. In:Nakagawa,Y., Kobayashi,T., Takamatsu, Fukuda H. (Eds.), Advances in Neutron Capture Therapy 2006 – Proceedings of the 12th International Congress on Neutron Capture Therapy, October9–13 Japan.
105. Harling, O.K., Riley,K.J. Fission reactor-based irradiation facilities for neutron capture therapy. In Sauerwein, WAG, Moss, RL, Wittig, A, Nakagawa, Y (eds), Neutron Capture Therapy; Principles and applications. Springer-Verlag. 2012; Heidelberg.
106. Kreiner AJ. Accelerator-Based BNCT. In Sauerwein, WAG, Moss, RL, Wittig, A, Nakagawa, Y (eds), Neutron Capture Therapy; Principles and applications. Springer-Verlag. 2012; Heidelberg.
107. Kreiner AJ, Bergueiro J, Cartelli D, et al. Present status of Accelerator-Based BNCT. Reports of Practical Oncology and Radiotherapy. 2016; 21(2):95-101. doi:10.1016/j.rpor.2014.11.004.
108. Tanaka H, Sakurai Y, Suzuki M. Experimental verification of beam characteristics for cyclotron-based epithermal neutron source (C-BENS) Appl Radiat Isot. 2011; 69:1642–1645.
109. Kumada H, Matsumura A, Sakurai H. New challenge for advanced BNCT in University of Tsukuba. In the front edge of BNCT development. Proceedings of Sixth Young Researchers BNCT Meeting; National Tsing Hua University; 2011. pp. 132–136.
110. Aleynik V, Bayanov B, Burdakov A. BINP accelerator based epithermal neutron source. Appl Radiat Isot. 2011; 69:1639–1641.
111. Aleynik V, Bayanov B, Burdakov A. BINP accelerator based epithermal neutron source. Appl Radiat Isot. 2011; 69:1639–1641.
112. Ghani Z, Green S, Wojnecki C. Proceedings of the 13th international congress on neutron capture therapy. ENEA. BNCT beam monitoring, characterization and dosimetry; 2008; 647–649.
113. Kreiner AJ, Castell W, Baldo M. Development of a tandem-electrostatic-quadrupole facility for accelerator-based boron neutron capture therapy. ARI. 2011; 69:1672–1675.
114. Kreiner AJ, Baldo M, Bergueiro RJ. Accelerator-based BNCT. Appl Radiat Isot. 2014; 88:185–189.
115. Burlon AA, Girola S, Valda AA, Minsky DM, Kreiner AJ, SanchezG. Design of a beam shaping assembly and preliminary modelling of a treatment room for accelerator-based BNCT. Appl. Radiat. Isot. 2011; (69): 1688–1691.

116. Halfon S, Paul M, Arenshtam A. High power liquid-lithium target prototype for accelerator-based boron neutron capture therapy. ARI. 2011; 69:1654–1656.
117. Ceballos C., Esposito J, Agosteo S. Towards the final BSA modeling for the accelerator-driven BNCT facility at INFN LNL. ARI. 2011; 69:1660–1663.

3 Synthesis of Gd-PSMA and *in vitro* evaluation

Although the concept of Gd-PSMA seems promising, no proof-of-concept has been established yet. In this research project, we will investigate the feasibility of applying Gd-PSMA for NCT. Several experimental steps have to be taken, before an in vitro proof-of-concept can be investigated. In this chapter, these experiments will be discussed. As some of these experiments build upon the results of previous experiments, experiments will be discussed subsequently. This chapter thus deviates from the classical lay-out of describing all materials and methods at once, followed by an overview of all results. Rather, first the labelling of Gd-PSMA will be discussed (paragraph 3.1). Secondly, the validation of the cell lines used in the remainder of our research will be described (paragraph 3.2), followed by an overview of several experiments regarding the uptake of PSMA (paragraph 3.3). Finally, the first neutron irradiations are discussed (paragraph 3.4).

3.1 Labelling of PSMA with Gd

In order to demonstrate the proof-of-concept of applying Gd-PSMA for NCT, first the possibility of labelling gadolinium with a PSMA tracer should be shown, and optimized if possible. Optimization is needed to avoid unneeded toxicity by unlabelled ligand or free Gd, and to ensure a workable procedure, that could eventually be applied in the clinic. Finally, it should be confirmed that the product synthesized by labelling PSMA with Gd, is Gd-PSMA. These aspects will be discussed in this paragraph.

Gadolinium molecule

For the labelling of (natural) gadolinium with PSMA, gadolinium(III) chloride hexahydrate is used. The structural formula of the molecule is shown in Figure 2. This molecule has a molar weight of 371.7 g/mol. When added to water, the molecule falls apart in gadolinium ions, chloride ions, and water. The gadolinium ions can consequently bind to another molecule.

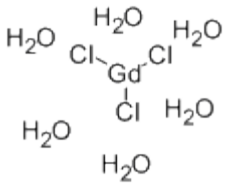

Figure 2: Structural formula of Gadolinium(III) Chloride Hexahydrate

PSMA molecule

The PSMA molecule used for the labelling is PSMA-617. PSMA-617 is a molecule which consists of three main components, i.e. a ligand part binding to the PSMA receptor on cells, a linker part to improve pharmacokinetics, and a chelator part, as shown in Figure 3. The chelator part is the part which enables the coupling of (metal) ions to the molecule, such as gadolinium ions. Theoretically, 1 gadolinium ion can bind to 1 PSMA-617 molecule. Unlabelled PSMA-617 molecules have a molar mass of 1042.1 g/mole [(ABX 2017)]. As natural gadolinium ions have a molar mass of 157.25 g/mole, a labelled Gd-PSMA-617 molecule is expected to have a molar mass of 1199.35 g/mole.

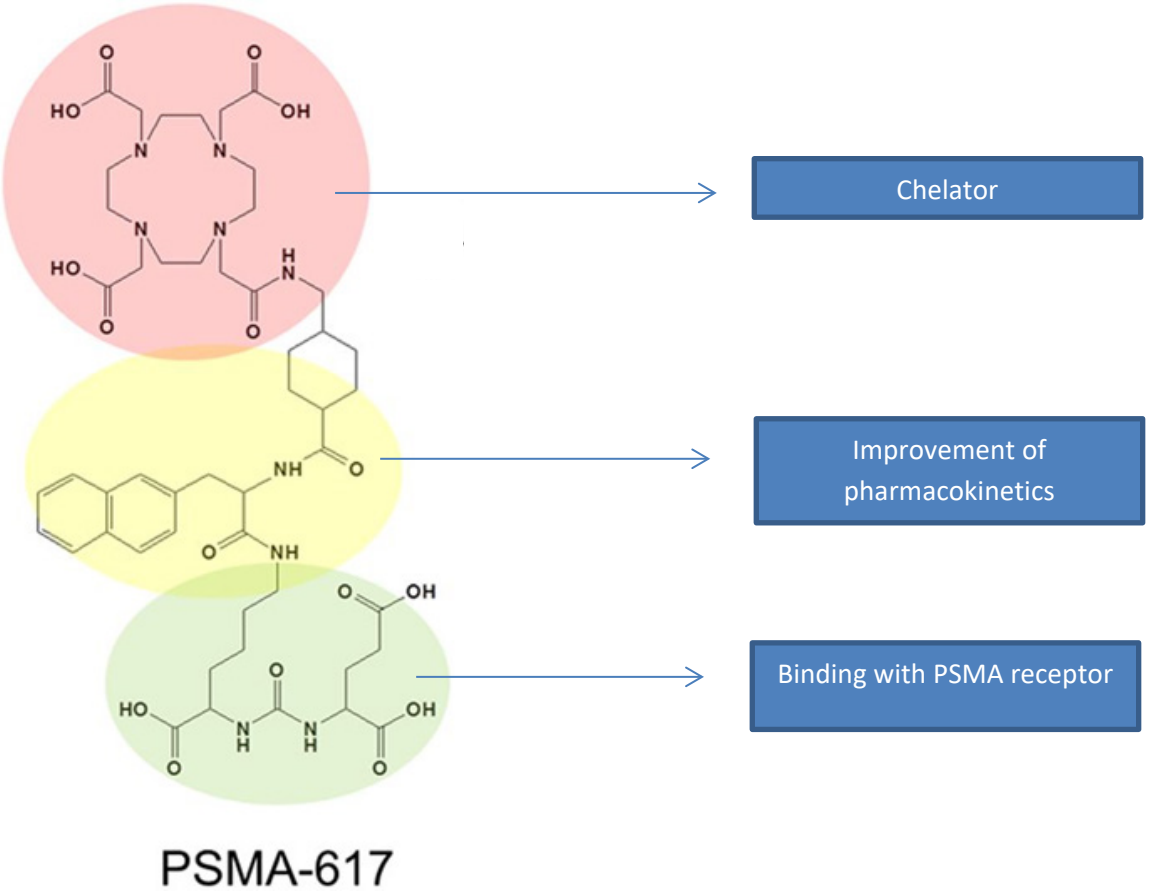

Figure 3: Structural formula of the PSMA-617 molecule, consisting of a ligand part binding to the PSMA receptor (green), a linker part to improve pharmacokinetics (yellow), and a chelator part (red), which can bind (metal) ions.

For the analysis and optimization of the labelling of Gd to PSMA, high-performance liquid chromatography with ultraviolet detection (HPLC-UV) was used. HPLC is a technique that can be used to separate, identify and quantify components in a mixture. It relies on pumps to pass a pressurized liquid solvent containing the sample mixture (i.e. the mobile phase) through a column filled with a solid adsorbent material (i.e. the stationary phase) [f.e Ahuja and Dong 2005, Snyder 2009]. Each component in the sample interacts slightly differently with the adsorbent material, causing different flow rates for the different components and leading to the separation of the components as they flow out the column. The components flowing out of the column are subsequently detected by a UV-VIS detector, as depicted in Figure 4. An UV-VIS detector uses light in the UV or visible wavelength range to analyse samples. It measures the absorbance of light (in mAU) and relates the magnitude of the absorbance to the concentration of analyte in the eluent passing through a flow cell contained within the detector. The corresponding chromatogram of the HPLC demonstrates the absorbance of the analyte as a function of the time needed for the analyte to flow through the column (i.e. the retention time).

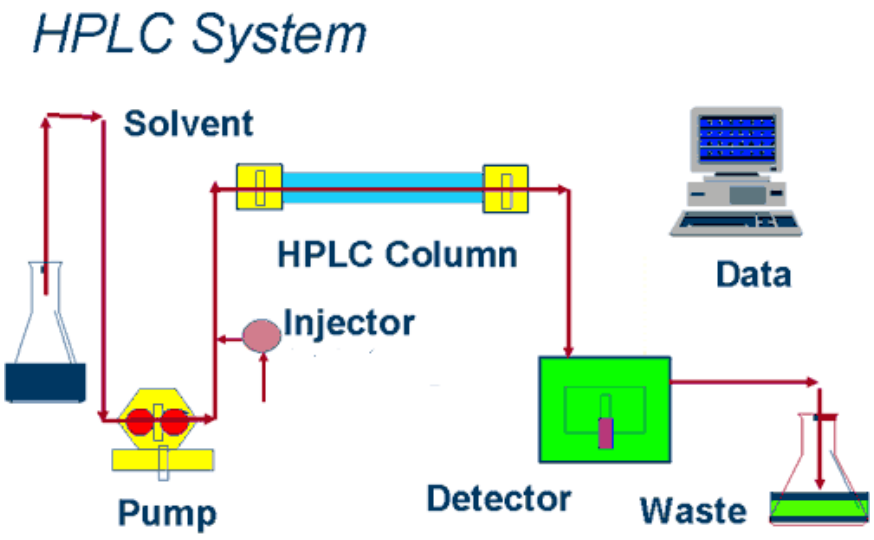

Figure 4: Schematic overview of the main parts of a HPLC system.

A shift in retention time may consequently indicate that a new component has been formed. However, such a shift does not confirm that the new component is the labelling product expected to be synthesized. For example during our experiments, it is not confirmed by the HPLC measurements that by adding gadolinium to PSMA, the new component formed is Gd-PSMA. Such a confirmation is not possible with HPLC measurements. Another technique is required to provide such a confirmation. For this purpose, high performance liquid chromatography-mass spectrometry (HPLC-MS) was selected. HPLC-MS is an analytical chemistry technique that combines the physical separation capabilities of HPLC with the mass analysis capabilities of mass spectrometry (MS). MS is a technique that converts samples into gaseous ions, with or without fragmentation, which are subsequently characterized by their mass to charge ratios (m/z) and their relative abundances (f.e. Mellon 2003). One of the advantages of combining HPLC with MS is that mass spectrometry analysis can be applied to fractions of a sample, separated over time, rather than measuring a sample at once. Consequently, it may be easier to identify the component desired in the samples analysed.

3.1.1 Materials and methods

For the experiments to label Gd to PSMA, the following materials and methods were used:

Gadolinium molecule

Gadolinium(III) chloride hexahydrate (99% titration, Sigma-Aldrich) is provided to us as a powder, the mass of which can be determined using an analytical balance. In order to make a stock solution, a certain amount of Gadolinium(III) chloride hexahydrate was weighed with an analytical balance (MC1 Analytic AC 210 s, Sartorius) with 0.1 mg readability, and added to a specified volume of water.

PSMA molecule

PSMA-617 (ABX GmbH) is provided to us as a powder. For the optimization of the labelling, PSMA-671 of GMP quality was used. Samples were filled with a minimum amount of net peptide of 100 µg and a maximum amount of 104 µg.

Analysis of labelling

The HPLC detector used for our experiments was an Ultimate 3000 (Dionex, Thermo Fisher) HPLC at a temperature of 20˚C. Samples of 15 µL were injected. As a stationary phase, a reversed phase Symmetry 300™ C18 column, 5 µm spherical silica, 4.6 mm * 250 mm was used. For the mobile phase, a mixture of two liquids was used, A) 0.1% of Trifluoroacetic acid (TFA) in MilliQ water, and B) 0.1% of Trifluoroacetic acid in acetonitrile. The flow of the mobile phase was 1.5 mL/min. A Dionex (Thermo Fisher) UV-VIS detector was used for detection. Absorbance was measured at a wavelength of 220 nm. Chromeleon™ software version 6.80 of Dionex Corporation was used to manage the data.

Optimal HPLC settings

First, it was determined experimentally what mobile phase conditions (with respect to gradient and time) provided chromatograms in which relevant peaks would be separated.

Optimization of labelling

Afterwards, the labelling of Gd-PSMA was optimized in terms of the amount of gadolinium required, the temperature of the labelling and the time needed. In terms of the amount of gadolinium, samples with a theoretical 1:1 ratio of gadolinium and PSMA-617 were investigated, as well as samples with a slight excess of PSMA-617. With respect to the temperature required, several extremities (i.e. room temperature and 60˚C) were tested and the labelling time and by-products were monitored. Samples were heated in an Eppendorf Thermomixer comfort set at 60˚C and at 700 rpm, to ensure proper mixing of the samples. When amount and temperature were optimized, the labelling time was investigated more systematically, by measuring a range of different time points.

Confirmation of Gd-PSMA

The optimized labelling method was used to prepare the samples that were to be measured with the HPLC-MS. Afterwards, quality control of the preparation was performed with the HPLC-UV. Samples of 15 µL were injected. As a stationary phase, a Symmetry 300™ C18 column, 5 µm spherical silica, 4.6 mm * 250 mm was used. For the mobile phase, the conditions were used that were experimentally determined to provide chromatograms in which relevant peaks would be separated.

After the quality control, the samples, columns and solvents were brought to the pharmacological laboratory of the NKI-AvL, where the HPLC-MS measurements were performed. For the HPLC-MS measurements, a HPLC-UV detector in parallel with a LTQ Orbitrap MS was used. This HPLC system had a LC-20AD (Shimadzu) pump and a SIL-HTc (Shimadzu) autosampler. The materials and methods used for the HPLV-UV part of this system were equal to the materials and methods used to validate the preparation of the Gd-PSMA samples. The MS system consists of a LTQ Orbitrap Discovery (Thermo Scientific) and is integrated with the HPLC system via electrospray ionization (ESI).

3.1.2 Results and Discussion

The HPLC experiments showed peaks at different retention times for samples with merely PSMA and samples that were presumed to have labelled products. Consequently, it was assumed to be possible to label Gd with PSMA-617.

Optimal HPLC settings

The following gradient scheme of the mobile phase turned out to be suitable for separation of the different components in the sample: 85% A to 80% A and 15% B to 20% B over 0-5 min, 20% B to 25% B over 5-12.5 min, 25% B to 30% B over 12.5-18 min, and finally 15% B over 18-25 min.

With this gradient scheme, the peak assumed to correspond with PSMA had a retention time of 12.5 ± 0.24 (2σ) min, and the peak assumed to correspond with Gd-PSMA had a retention time of 13.2 ± 0.09 (2σ) min.

Optimization of labelling

The labelling of Gd-PSMA was first optimized in terms of temperature. Figure 5 and Figure 6 show respectively the labelling of Gd to PSMA at room temperature and at 60 degrees Celsius over time. These results indicate that the reaction rate at room temperature was much slower and resulting in much less labelled product within an acceptable duration of incubation than the reaction rate at 60˚C.

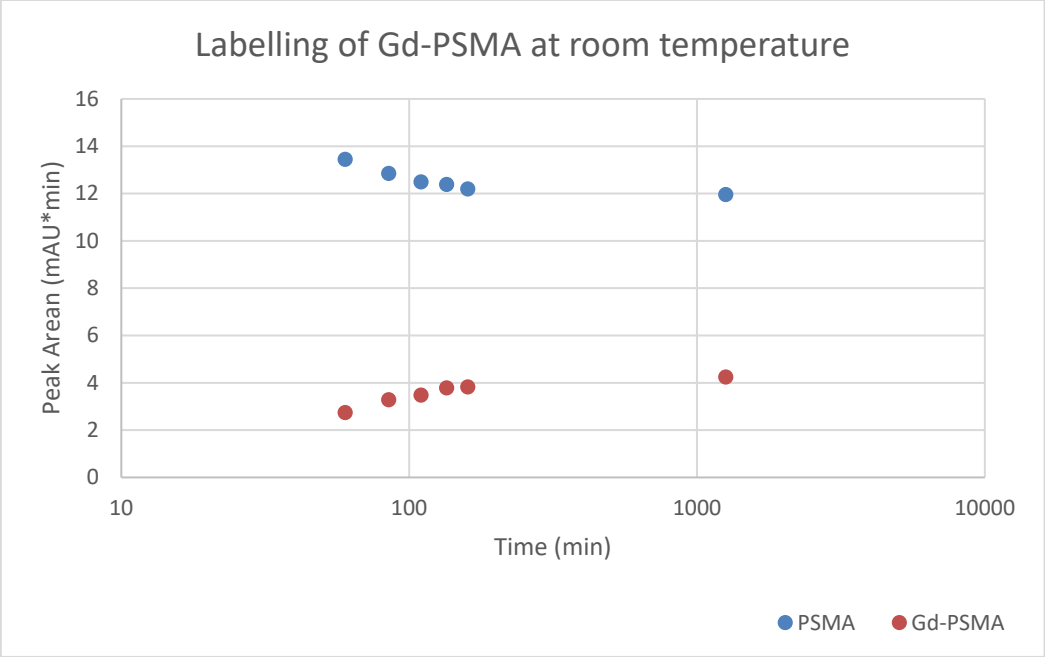

*Figure 5: Labelling of Gd-PSMA at room temperature. On the X-axis time (min) is shown, on the Y-axis the area of the peak (mAU*min) is shown. The plot shows a gradual increase over time in amount of Gd-PSMA labelled.*

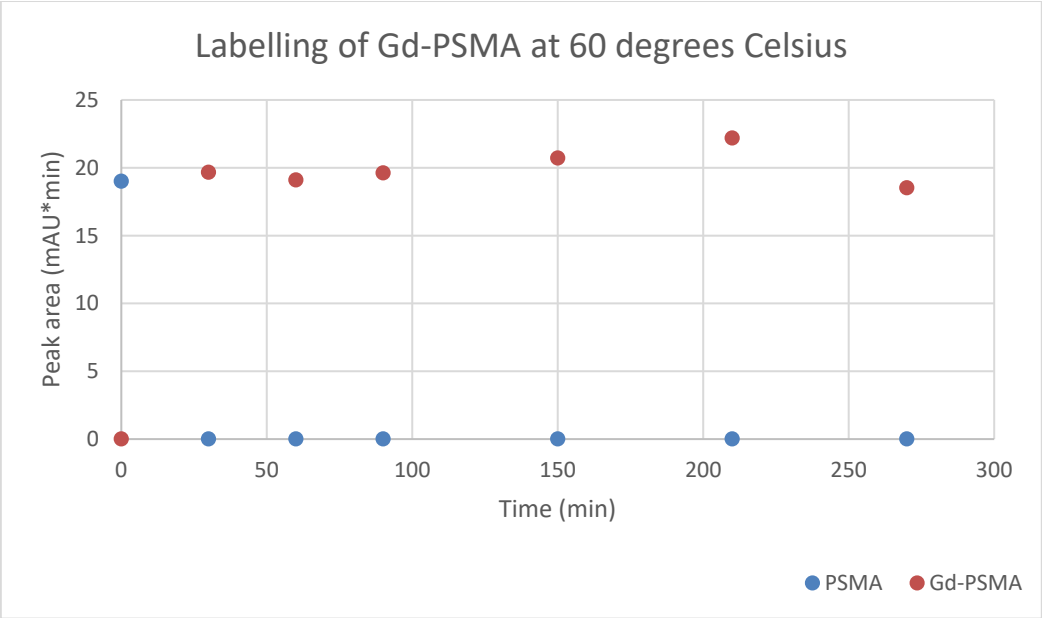

*Figure 6: Labelling of Gd-PSMA at 60˚C. On the X-axis time (min) is shown, on the Y-axis the area of the peak (mAU*min) is shown. The plot shows full labelling of Gd-PSMA from the first point of measurement onwards.*

Since the chromatogram of the labelling at 60˚C did not show significant debris (i.e. extra peaks in addition to the main peak) due to the heating of the sample (see Figure 7), it was decided that 60˚C was a suitable temperature for the labelling of Gd-PSMA.

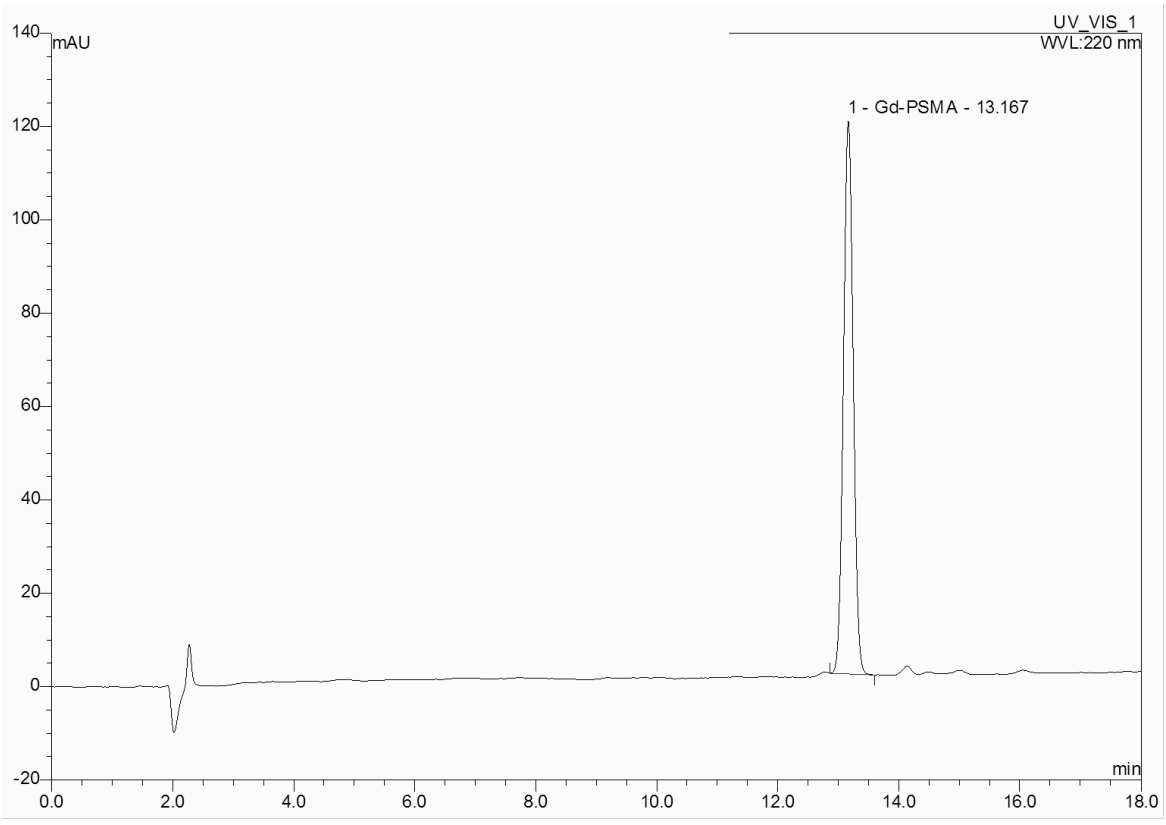

Figure 7: Chromatogram of HPLC-UV measurement of the preparation of Gd-PSMA in a 1:1 ratio at 60˚C. X-axis shows time in min, Y-axis shows absorbance in mAU. No significant extra peaks due to the heating of the sample are shown.

In terms of the amount of PSMA and gadolinium required, Figure 7 shows that with a 1:1 ratio of Gd:PSMA, which corresponds with the theoretical reaction ratio, no peak of PSMA is left. As a slight remainder of PSMA is preferred due to Gd-ions toxicity, a slight excess of PSMA was investigated as well. As Figure 8 shows, a ratio of 1:1.1 of Gd:PSMA did not demonstrate any remainder of PSMA either. A ratio of 1:1.25 of Gd:PSMA however, exhibited a PSMA peak with an area about 10% of the Gd-PSMA peak (3.4 mAU*min versus 33 mAU*min), as shown in Figure 9.

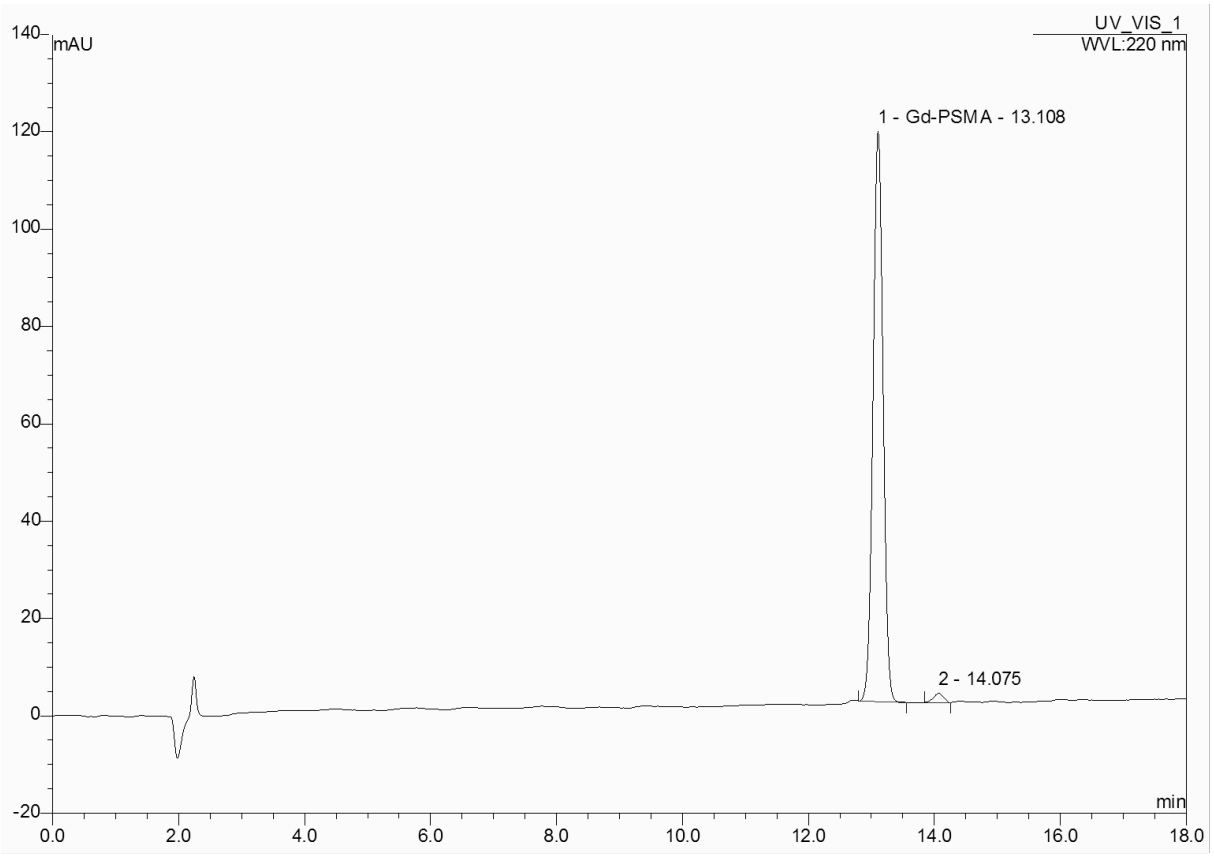

Figure 8: Chromatogram of HPLC-UV measurement of the preparation of Gd-PSMA in a 1:1.1 ratio at 60˚C. X-axis shows time in min, Y-axis shows absorbance in mAU. No remaining PSMA peak is visible. The peak assigned with number 2 is considered to be debris due to the heating of the sample.

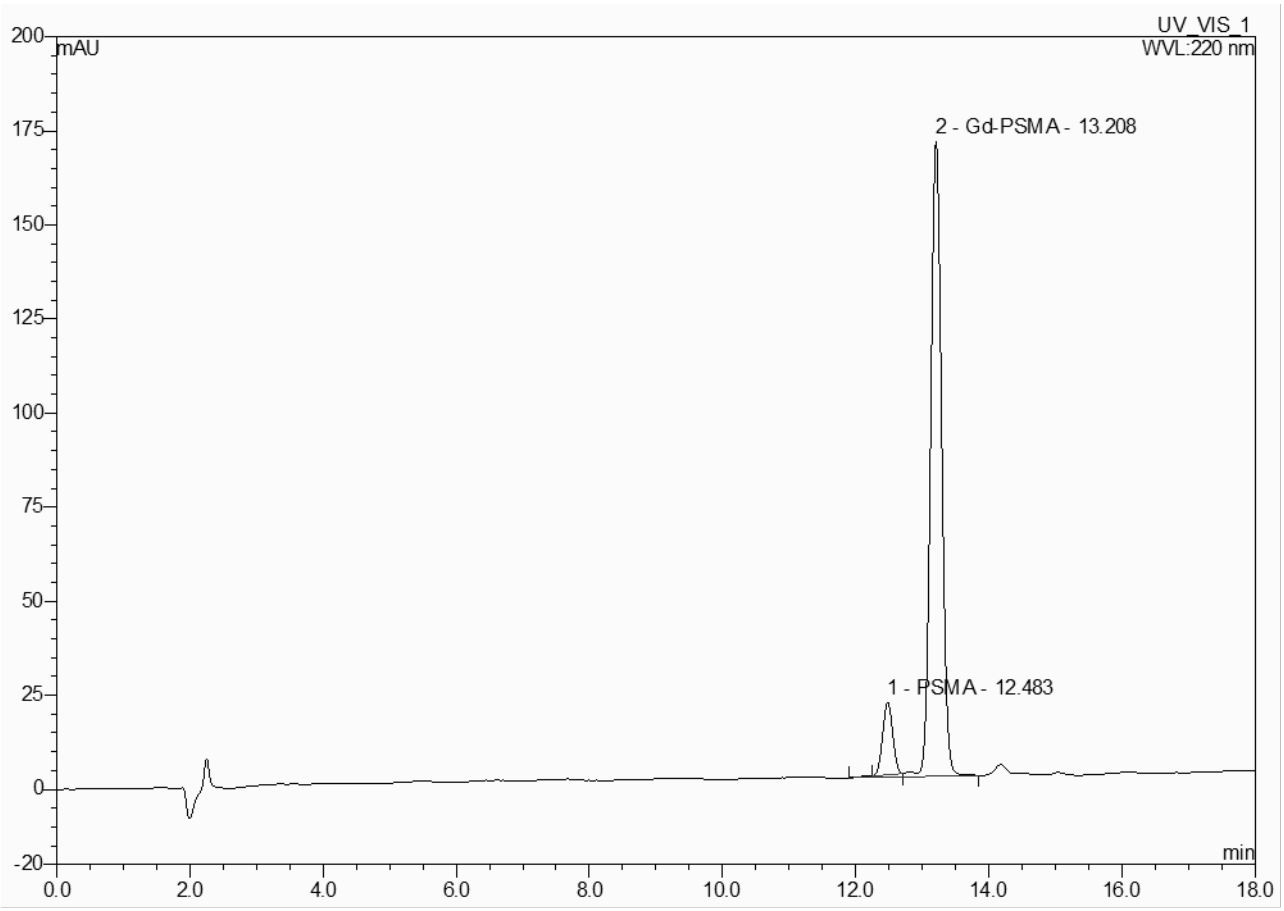

Figure 9: Chromatogram of HPLC-UV measurement of the preparation of Gd-PSMA in a 1:1.25 ratio at 60˚C. X-axis shows time in min, Y-axis shows absorbance in mAU. A remaining PSMA peak is visible, which has an area of about 10% of the Gd-PSMA peak.

As a 10% remainder of PSMA in the sample was deemed acceptable, a ratio of 1:1.25 of Gd:PSMA was considered a suitable ratio for the labelling of Gd-PSMA.

Finally, the optimal amount of time required for the labelling of Gd-PSMA was investigated. Several time points were measured in a range of 15 to 105 minutes. Measurements were performed in triplo (and the final time point due to time constraints in duplo). Figure 10 shows the results of the measurements over time of the labelling of Gd-PSMA at the previously determined conditions of 1:1.25 Gd:PSMA and 60˚C. Uncertainties were determined by taking the average and calculating the corresponding standard deviation from the results.

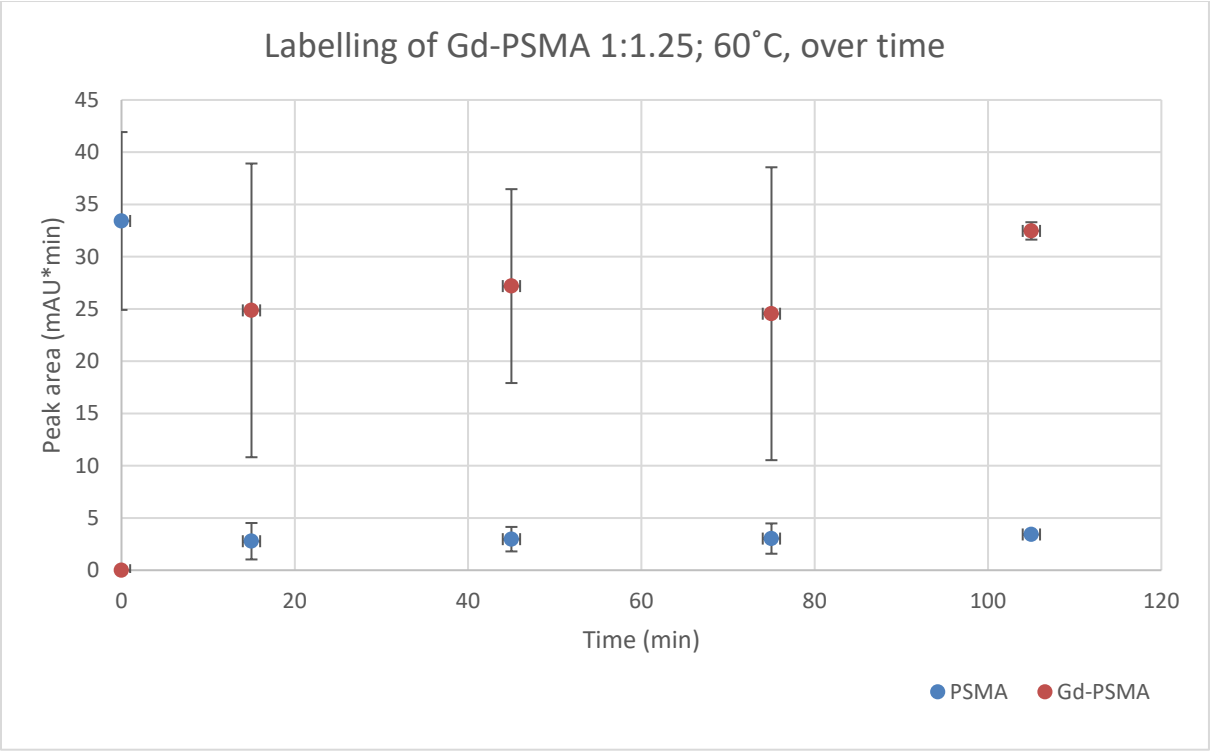

*Figure 10: Plot of the labelling of Gd-PSMA over time. On the X-axis time (min) is shown, on the Y-axis the area of the peak (mAU*min) is shown, with 2σ uncertainty bars. The labelling is performed at the previously optimized conditions of a Gd:PSMA ratio of 1:1.25 and at 60˚C. The plot shows no significant difference between the Gd-PSMA peak areas of different time points.*

The plot shows that within 2σ uncertainty margins, the peak areas of the Gd-PSMA peaks for different time points can be considered to be equal. Consequently, a labelling time of 15 minutes is considered to be optimal for the labelling of Gd-PSMA, as shorter labelling times are preferred in practice. In conclusion, the labelling of Gd-PSMA is optimal when performed with a Gd:PSMA ratio of 1:1.25, at a temperature of 60˚C, for 15 minutes of time.

This optimal labelling was temperature wise and amount wise in accordance with our expectations: for a similar kind of labelling of PSMA to Gd, a temperature of 60˚C was used as well [(Banerjee 2015)]. Also, a slight excess of PSMA was expected to be required in order to have a remainder of PSMA after the labelling. Timewise, it was not expected from the literature that the reaction rate was basically independent of time. Banerjee for example uses labelling times of several hours [(Banerjee 2015)], but does not provide any reasoning for these long labelling times. Presumably, he wants to be sure the product has been fully labelled. For clinical purposes, it is however very promising that the labelling times can be short: this enables labelling of the product on the day of clinical use.

Investigations on setup of clinical quality control procedure

In addition to an optimized labelling, one of the requirements for future clinical implementation of Gd-PSMA is the establishment of a clinical quality control procedure of the labelling. Such quality control could be performed with HPLC-UV. In order to set up a quality control procedure, a HPLC-UV validation protocol has to be carried out. It was investigated whether it was possible to set-up such a quality control procedure according to clinical standards. Due to small stock sizes of PSMA and small quantities

of samples used for HPLC-UV measurements in this study, it was concluded that setting up a quality control procedure was not conceivable yet.

Confirmation of Gd-PSMA

Figure 11 shows the chromatogram of the HPLC-UV quality control measurements with the Gd-PSMA samples prepared for analysis by HPLC-MS. The chromatogram indicates retention times of 11.5 min and 14.2 min for respectively the peak assumed to correspond with PSMA, and with Gd-PSMA .

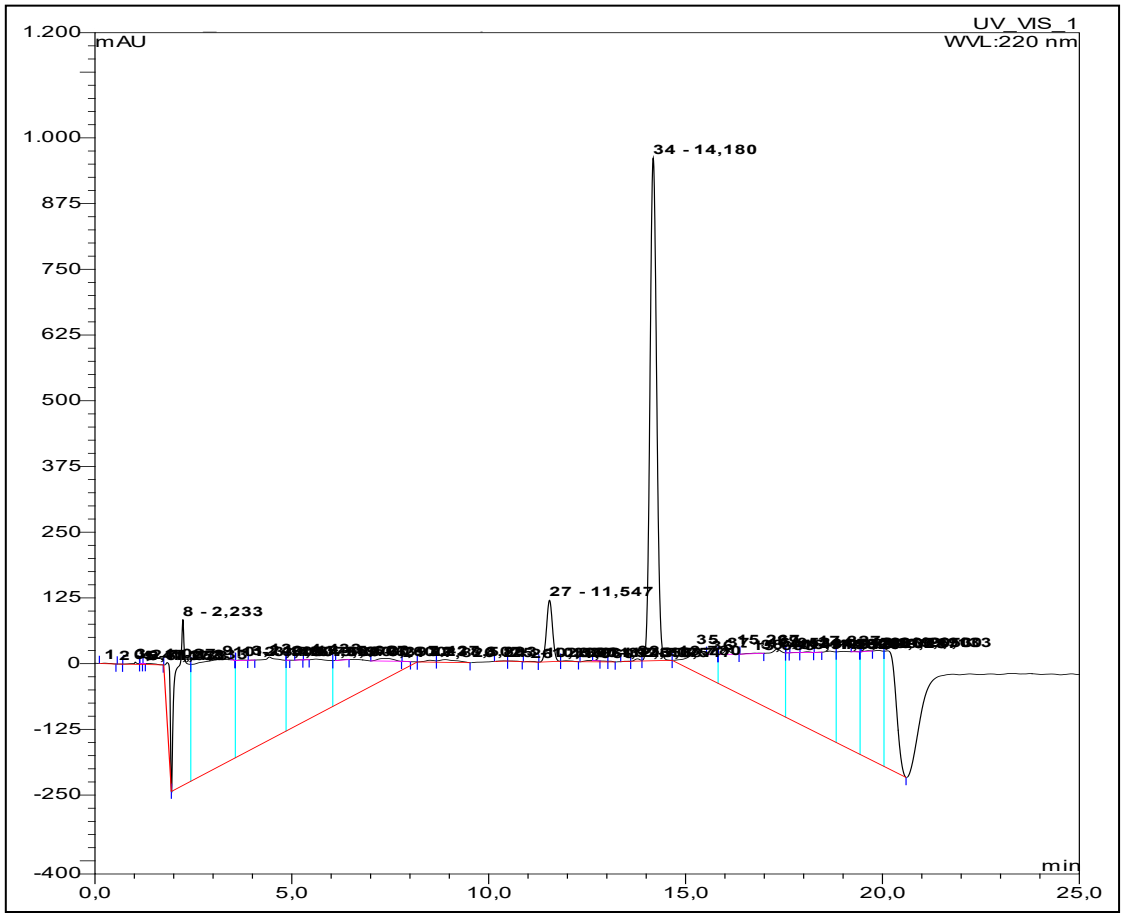

Figure 11: Chromatogram of HPLC-UV quality control measurement of preparation of Gd-PSMA. X-axis shows time in min, Y-axis shows absorbance in mAU. Peak 27 is assumed to correspond with PSMA, peak 34 is assumed to correspond with Gd-PSMA. Other peaks are considered to be dead time or background. The coloured lines indicate analysis of the peaks.

The fragments of both time points were analysed with MS.

In the first time frame, PSMA was expected to be found. The theoretical mean molar mass of PSMA-617 (with molecular formula $C_{49}H_{71}N_9O_{16}$) is 1042.13 gram/mole. The theoretical monoisotopic mass of PSMA-617 however, calculated with the mass of the most abundant isotope of each element in the molecule, is 1041.50188 gram/mole. Consequently, the theoretical monoisotopic $[M+H]^+$ mass would be 1042.50971 m/z. Figure 12 shows the mass spectrum of the first time frame. The peak with the highest abundance corresponds with an observed $[M+H]^+$ mass of 1042.51135 m/z. So, the values are very similar, with a mass error of 1.58 ppm.

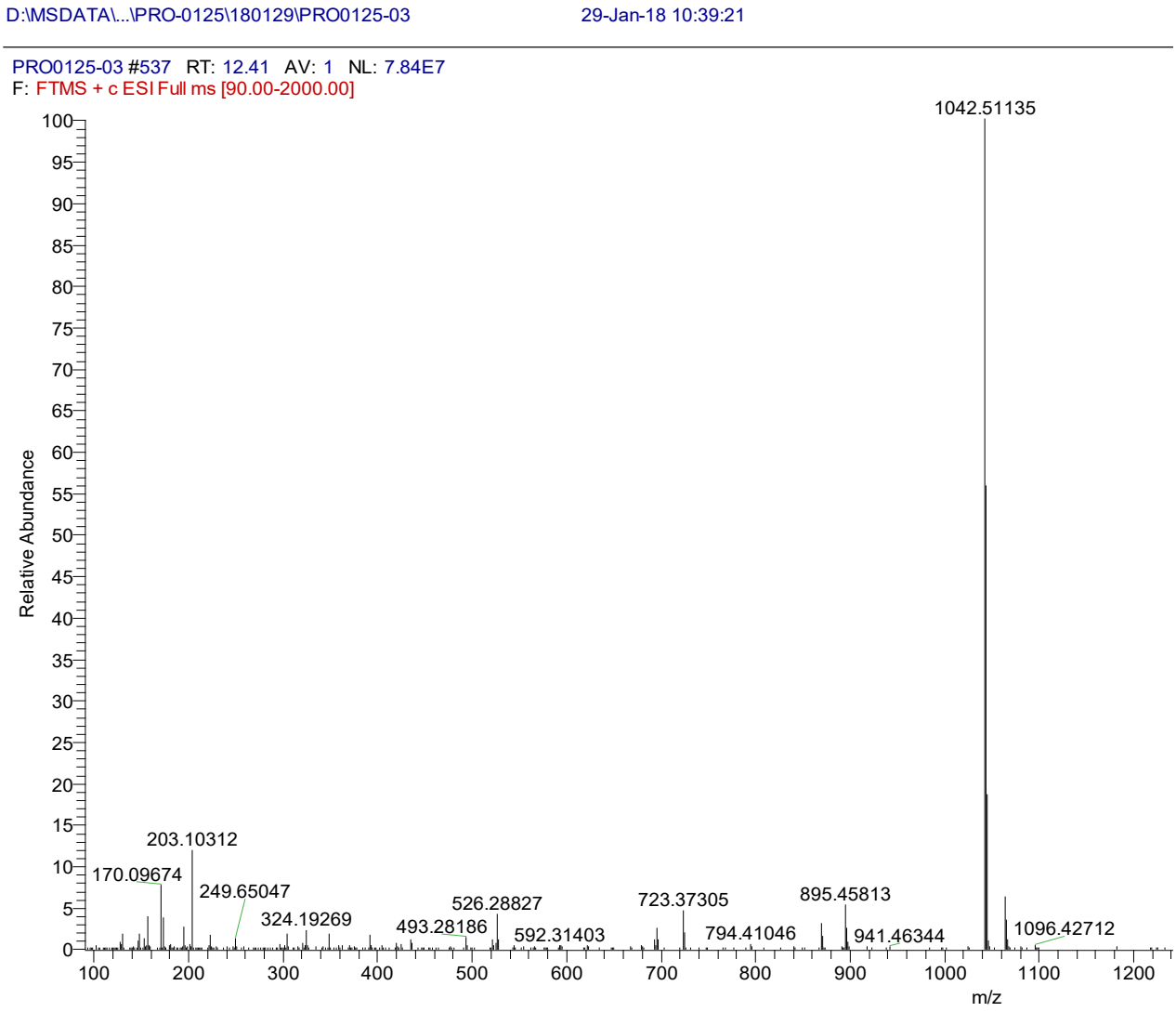

Figure 12: Mass spectrum of the time frame expected to contain PSMA-617. On the X-axis the mass of the fragments is shown (m/z), on the Y-axis the relative abundance of the fragment is shown (%).

The likelihood that PSMA-617 is present in the sample is even increased by the fact that some other quite abundant fragments in the spectrum (Figure 12), like 526.29, 723.37, and 895.46 m/z can be explained by some plausible molecular fragments of PSMA-617. The potential fragments are demonstrated in Figure 13.

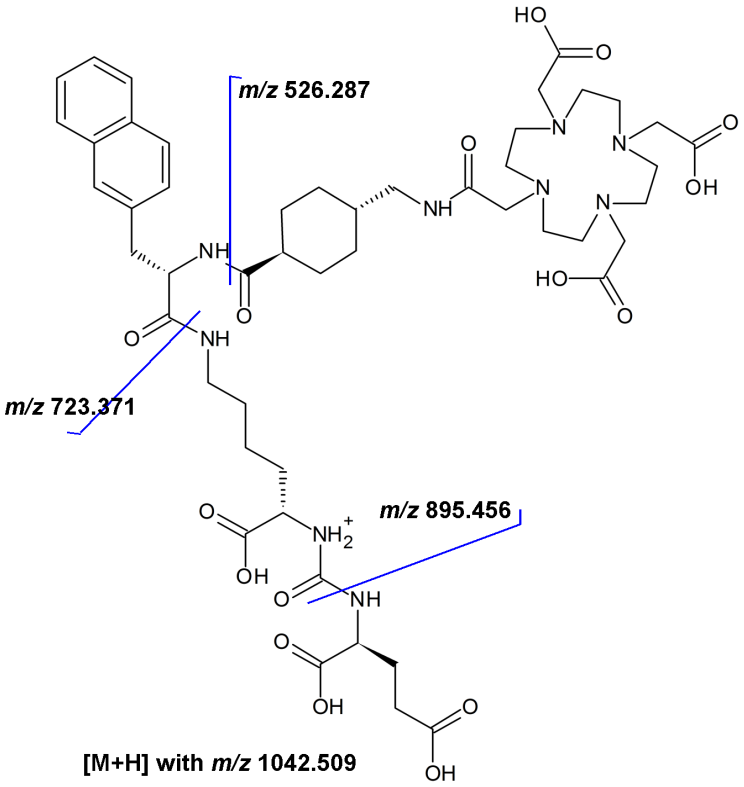

Figure 13: Some plausible fragments of PSMA-617 with their m/z values.

In the second time frame analysed, Gd-PSMA was expected to be found. As the mean theoretical molar mass of PSMA-617 is 1042.13 gram/mole and the molar mass of natural Gd is 157.25 gram/mole, the combined theoretical mass is expected to be 1199.38 gram/mole, and the monoisotopic theoretical mass is calculated to be 1199.42599 gram/mole. Yet, the Gd-ion is assumed to bind to the DOTA chelator though the amine and carboxylate groups. Of the carboxylate groups, there are three groups that three need to dissociate three times into a carboxylate anion and a hydrogen ion in order to be able to bind the metal ion. Consequently, the theoretical monoisotopic mass of Gd bound to PSMA-617 is likely to be 1199.42599-(3H) = 1196.402517 gram/mole. Accordingly, the theoretical monoisotopic $[M+H]^+$ mass is 1197.410342 m/z. The mass spectrum of the analysed time frame, as shown in Figure 14, demonstrates shows an observed $[M+H]^+$ mass of 1197.41333 m/z, which is very similar (mass error of 2.50 ppm) to the theoretical mass.

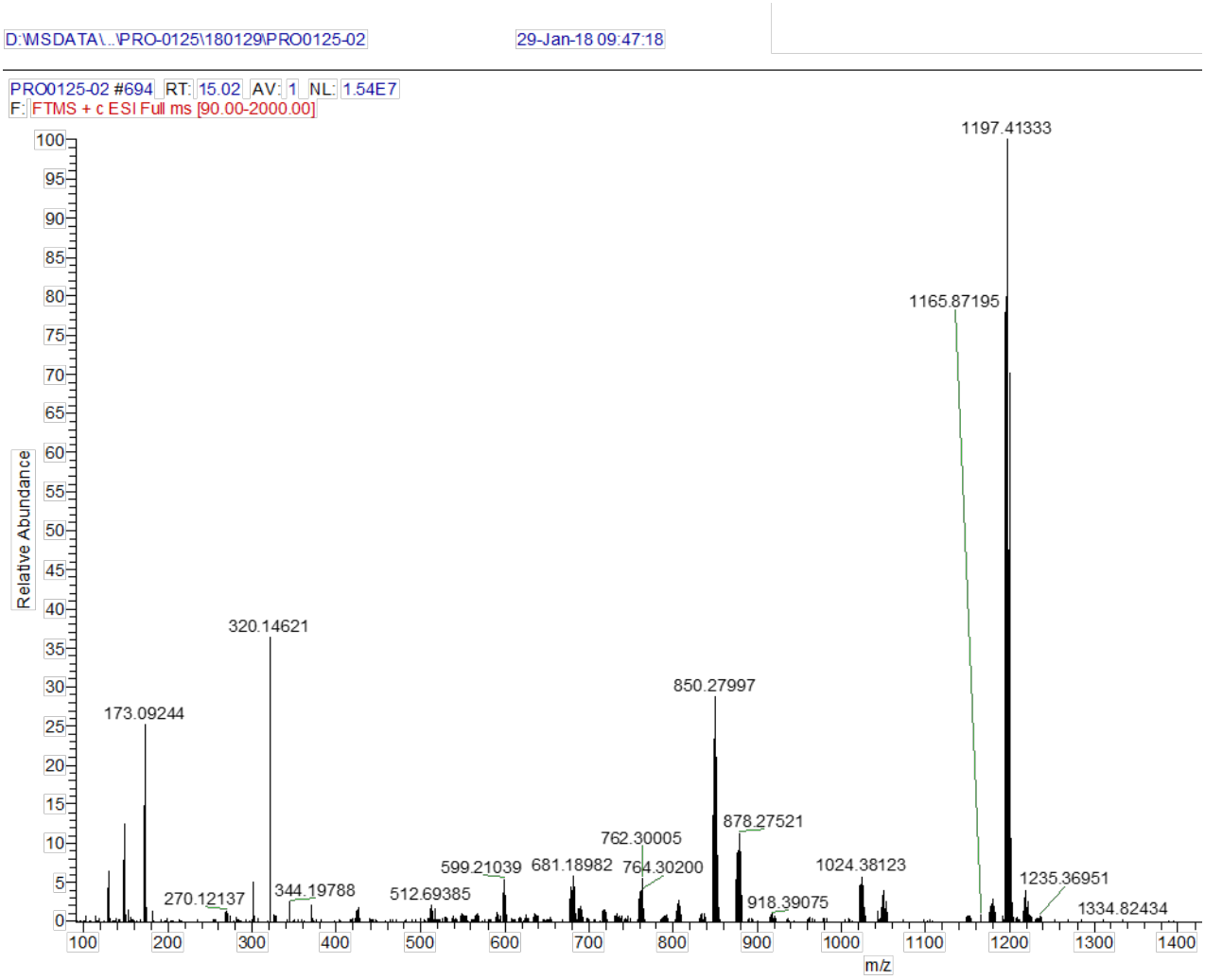

Figure 14: Mass spectrum of the time frame expected to contain Gd-PSMA-617. On the X-axis the mass of the fragments is shown (m/z), on the Y-axis the relative abundance of the fragment is displayed (%).

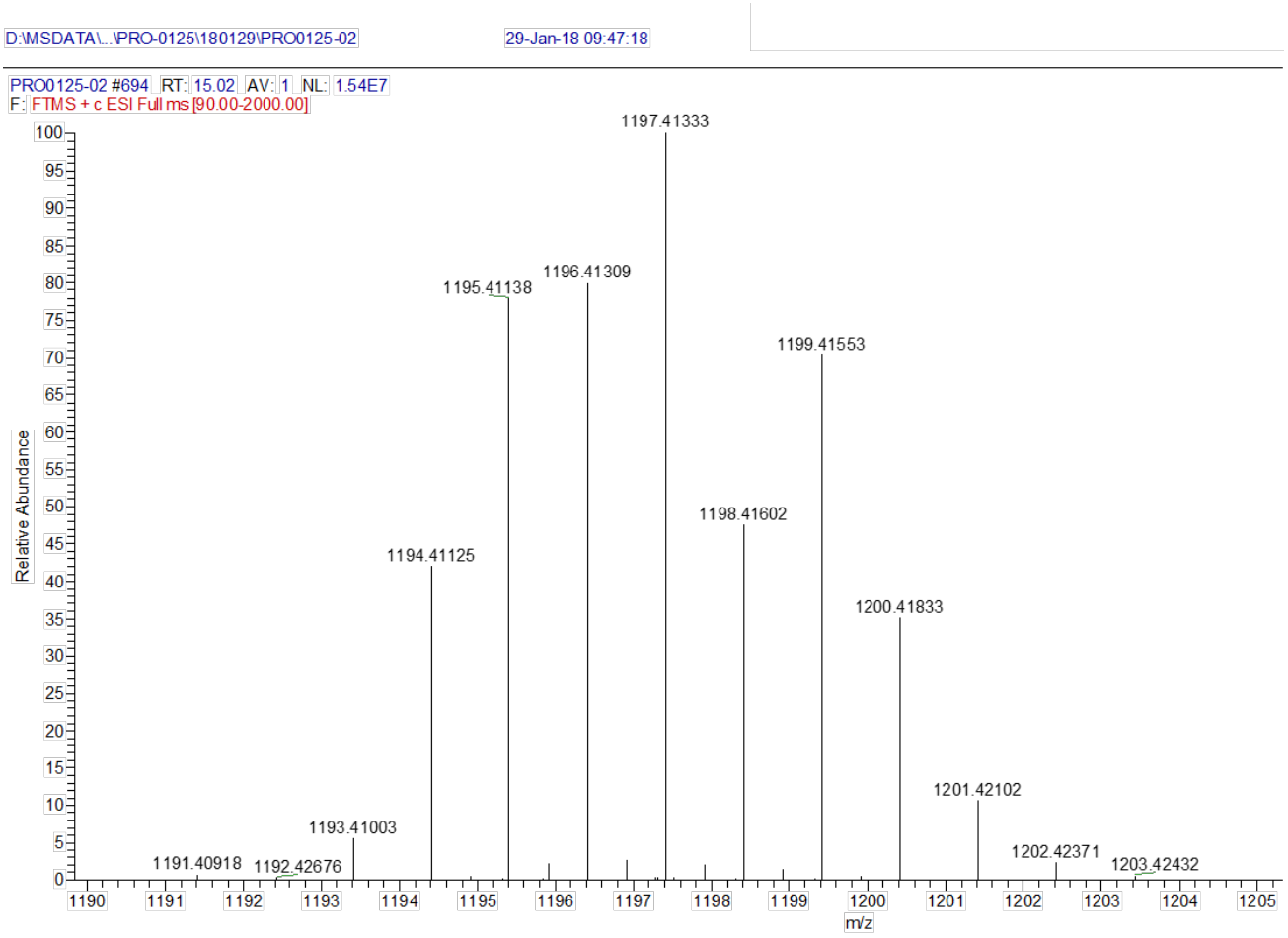

Figure 15: Mass spectrum of the time frame expected to contain Gd-PSMA-617. On the X-axis the mass of the fragments is shown (m/z), on the Y-axis the relative abundance of the fragment is shown (%). This spectrum is a magnification of the most abundant peak in the previous spectrum.

A magnification of the most abundant peak in Figure 14 demonstrates a spectrum of masses with relatively high abundancies (Figure 15). Remarkably, the distribution of the abundancies correlates very well with the natural abundance of gadolinium isotopes, as shown in Table 1 and Figure 16. Consequently, it is very likely that Gd-PSMA-617 is present in the sample. Therefore, we can conclude that the labelling of Gd to PSMA-617 has the desired result.

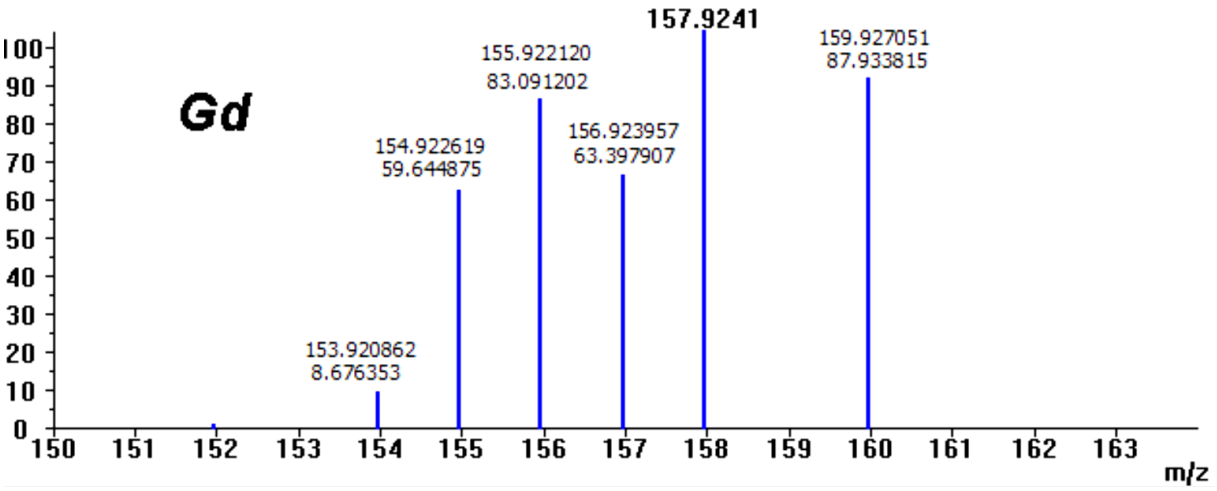

Figure 16: Theoretical mass spectrum of isotopes of natural gadolinium. On the X-axis the mass of the fragments is shown (m/z), on the Y-axis the relative abundance of the fragment is shown (%).

Concentration of Gd-ions

One aspect of the labelling of gadolinium with PSMA-617 is however not extensively investigated. This aspect concerns the amount of free gadolinium ions in solution with the labelled molecule. Although an excess of PSMA is used for the labelling in order to reduce the amount of free Gd-ions, the concentration of free ions has not been measured yet. This is because free Gd-ions cannot be detected using HPLC-UV. They can however be analysed with HPLC-MS. Theoretically, gadolinium ions are expected to behave similarly to lutetium ions with respect to solvability in the mobile phase solutions. As radioactive lutetium ions during quality control measurements are detected by a radio detector around the dead time of the chromatogram, any gadolinium ions present in the sample are likely to be detected around the dead time of the chromatogram as well. When this time frame was analysed with MS, no gadolinium was observed. This implies that either the gadolinium was not detected (for example due to the detection limit of MS) or that no gadolinium ions were present. In either case, this is a promising result for the labelling of Gd-PSMA-617.

3.2 Validation of cell lines

Demonstration of the proof-of-concept of Gd-PSMA for NCT requires subjection of PSMA-positive and PSMA-negative cells to treatment. If both PSMA-positive and PSMA-negative cells are investigated under the same conditions, any difference in for example radiation response between the cells is likely to be caused by the presence of PSMA receptors (PSMA-positive) on the cells, or the lack thereof (PSMA-negative). For that reason, it is important to select suitable cell lines, which according to the literature do either express PSMA on their membrane, of have a lack thereof. Afterwards, is was experimentally validated whether the selected cell lines did indeed express PSMA receptors on their membrane, or had a lack thereof.

3.2.1 Selection of cell lines

Optimal PSMA-positive and PSMA-negative cell lines have been selected for the experiments. Cell lines were selected based on presumed PSMA expression, availability, and ease of use. Of the selected cell lines, their culture method is described.

3.2.1.1 PSMA-positive cell line

In case of the PSMA-positive cell line the human prostate cell line LNCaP clone FGC (in short LNCaP) was selected. The cells were available in-house and were kindly provided by S. Stelloo (NKI-AvL). LNCaP cells have a population doubling time of about 34 hours (ATCC: LNCaP). The adherent cells grow in monolayers when cultured under the appropriate conditions, i.e. incubator at 37˚C and 5% CO_2. Roswell Park Memorial Institute (RPMI) 1640 medium (Gibco®), supplemented with 10% (v/v) foetal bovine serum (FBS) and 1% (v/v) Penicillin Streptomycin (Pen Strep), is used as a culture medium.

3.2.1.2 PSMA-negative cell line

As a PSMA-negative cell line PC-3 was chosen. The cells were available in-house and were kindly provided by S. Zerp (NKI-AvL). PC-3 cells have a population doubling time of about 25-28 hours (ATCC:PC-3, ExPASy). These adherent cells also grow as monolayers when cultured at 37˚C and 5% CO_2. In case of PC-3, Dulbecco's modified Eagle medium (DMEM) (Gibco®), supplemented with 10% (v/v) FBS, 1% (v/v) Pen Strep, and 0.8% (v/v) GlutaMAX (Gibco®), is used as a culture medium.

3.2.2 Analysis of PSMA expression

PSMA is a transmembrane glycoprotein (Troyer 1995). It is expressed on the membrane of prostatic epithelial cells and overexpressed on most prostate tumour cells. PSMA expression, or lack thereof, of the selected cell lines could be verified using Western blot analysis (Troyer 1995). This is because Western blot analysis can be used to separate and identify proteins. Three main steps must be performed to accomplish this task: 1) separation by size, 2) transfer to a solid support, and 3) marking target protein using a proper primary and secondary antibody to visualize (Mahmood and Yang 2012). A Western blot analysis was performed for both the PSMA-positive, LNCaP, as the PSMA-negative, PC-3, cell line.

3.2.2.1 Materials and methods

Performing a Western blot analysis includes several steps. First, in order to extract proteins, cell lysis was performed. Cell lysis was done by harvesting the cells, and subsequently adding 200 µL of RIPA buffer, containing 1% of the detergent NP-40. The solution of cells was kept on ice for about 10 minutes, after which the samples were centrifuged for 1 minute with 12000 rpm, at 4˚C, and the supernatant was used for further analysis. The concentration of extracted proteins in the LNCaP and PC3 samples was determined using Pierce™ BCA Protein Assay Kit (Thermo Fisher). A calibration curve was created, by using a concentration range of BSA standards (25 µL of the standards is used, the samples are diluted by a factor 12.5). The BSA standards and the samples were incubated for 30 minutes at 37˚C, after which the absorbance at 562 nm of each sample was read out, using a Tecan Infinite 200 plate reader.

Based on the calibration curve, it was calculated what the protein concentration of the samples was. Consequently, it could be calculated how much volume of protein extract was needed to ensure 50 µg of protein in each well. The samples were loaded in to each well, after the BlueEye prestained protein marker (Jena Bioscience GmbH) was added according to the manufacturer's instructions. NUPAGE™ Bis-Tris gel with a 4-12% gradient (Invitrogen) and MOPS buffer were used. By consecutively applying 100 V for 15 minutes and 150 V for 1 hour and 15 minutes electrophoresis was used to separate the proteins.

After the electrophoresis, the separated proteins were transferred by wet blotting to a nitrocellulose membrane for about 2 hours at 0.3 A. The membrane was blocked overnight with 5% BSA in Phosphate Buffered Saline with 0.05% Tween-20 (PBST). The next day, the PSMA Monoclonal Antibody (1H8H5) (Thermo Fisher Scientific) was added in a dilution of 2 µg/mL, and incubated overnight in 4˚C on a shaker. This was followed by three washes in TBST. The membrane was subsequently incubated with a 1:2000 diluted rabbit anti-mouse horseradish peroxidase-labelled secondary antibody. Afterwards, the membranes were again washed in TBST and developed using ECL Western Blotting Detection Reagents, according to the manufacturer's instructions. The membrane was visualized on a hyperfilm in the dark room.

Afterwards, a loading control was performed by incubating the membrane with beta actin. Subsequently, the Western blot was scanned with an Odyssey Infrared Imaging System.

3.2.2.2 Results and Discussion

The use of a range of BSA standards provided us with the following curve of absorbance (AU) against protein concentration (µg/mL), as shown in Figure 17.

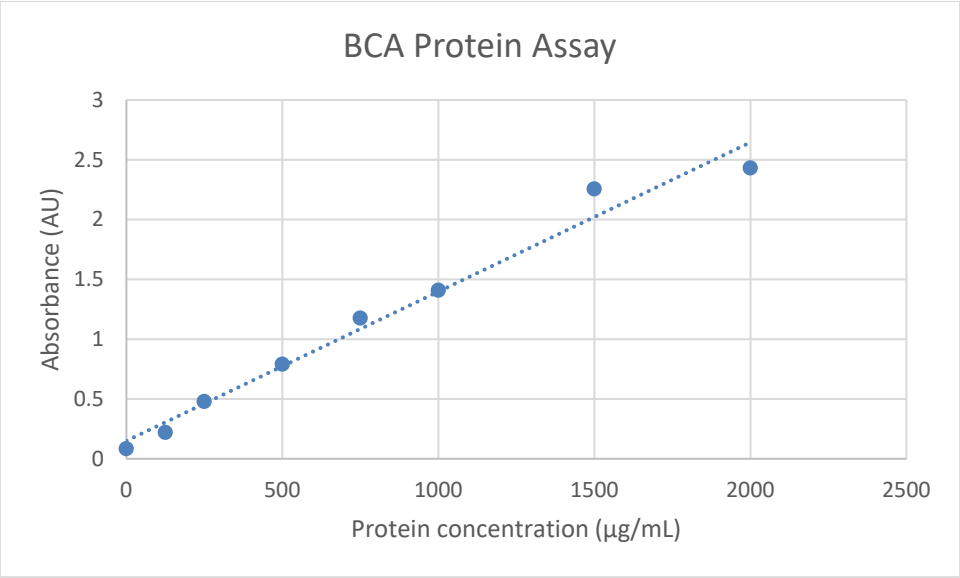

Figure 17: Plot of absorbance (AU) against protein concentration (µg/mL) for a range of BSA standards. The dotted line is the linear regression that best describes the set of points.

The dotted, straight line in Figure 17 is the linear regression that best describes the set of points (R^2=0.978) and has the following equation:

$$Y = 0.0012x + 0.1495 \quad (1.1)$$

In the equation, *Y* corresponds with absorbance, and *x* corresponds with the protein concentration. Based on the absorbance measurements of the proteins of both cell lines, and using equation (1.1) it is possible to calculate the protein concentration in the samples of the cell lines. Results of these calculations are shown in Table 2.

Table 2: For both cell lines, the protein concentration (µg/mL) is calculated, based on the absorbance (AU) measured. In the absorbance measurements, the concentration of the samples was diluted by a factor 12.5, which is corrected for.

Cell line	Absorbance (AU)	Protein Concentration according to trend line (µg/mL)	Protein Concentration corrected for 1:12.5 dilution (µg/mL)
PC-3	0.636	406	5071
LNCaP	1.03	734	9171

Having determined the protein concentration in the samples, it was possible to determine how much of the cell solution was needed in order to have 50 µg of protein per lane. For LNCaP and PC-3, respectively 5.5 µL and 9.9 µL of solution was needed.

The required amount of cell sample was injected in to the lanes; first (from the left) PC-3 was loaded, second LNCaP, and third a marker lane was added. Afterwards, the gel was run and the Western blot created in accordance with the procedure described before (paragraph 3.2.2.1). An exposure time of 10 seconds turned out to provide an optimal picture of the blot (Figure 18), while an exposure time of 1 minute showed the marker lane most clearly.

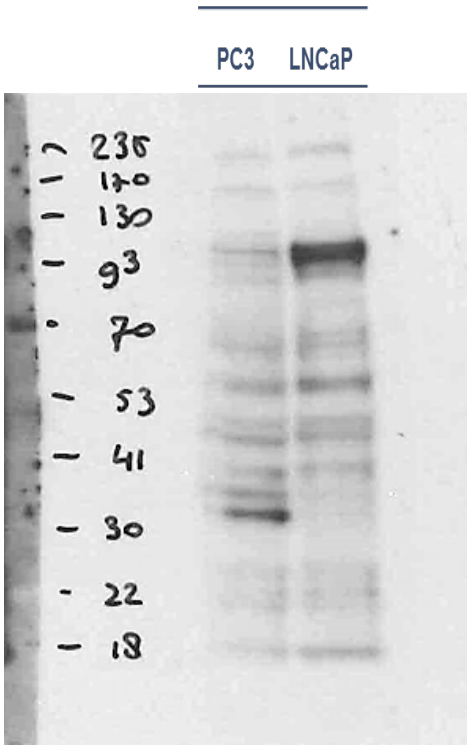

Figure 18: Image of the Western blot. An exposure time of 10 seconds is used. The left lane shows the PC-3 sample, while the right lane shows the LNCaP sample. The marker lane on the right of the LNCaP lane is hardly visible at an exposure time of 10 seconds, which is why on the far left of the figure the marker lane generated by an exposure time of 1 minute is added. The numbers next to the marker lane are inserted manually, and represent the pre-stained proteins, expressed in kDa, as provided in the manufacturer's data sheet (Jena Bioscience 2016).

According to the literature, PSMA is a 100 kDa glycoprotein (Troyer 1995). The image of our Western blot (Figure 18) shows a clear difference between the PC-3 and LNCaP sample around 93-130 kDa. Clearly, a protein band is shown in the LNCaP sample. Although it is likely that the protein band corresponds with the PSMA protein, theoretically the difference could be caused by a variance in protein loaded between the lanes. For that reason, a loading control is performed. A loading control shows whether a similar amount of protein is loaded in to each lane. Equivalent to a normal blot, the darker the protein band, the higher the concentration of protein. For our loading control, we used the 43 kDa protein ß-actin.

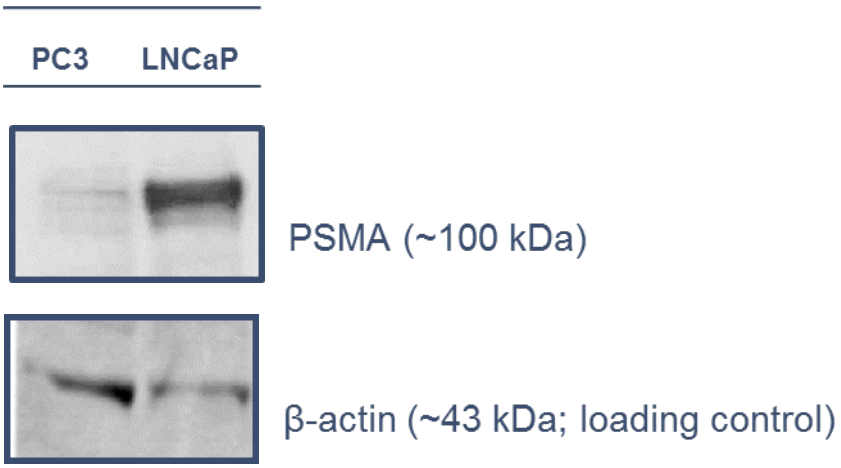

Figure 19: Comparison between the Western blot with presumed PSMA (above) and the loading control (below), which shows that more protein is loaded in to the PC-3 lane, than on the LNCaP lane.

A comparison between the Western blot with presumed PSMA and the loading control (Figure 19) shows that more protein was loaded on the PC-3 lane, than on the LNCaP lane. This implies that the difference between the lanes around the 100 kDa band cannot be explained by a higher protein load being applied to the LNCaP lane, which supports the conclusion that PSMA is expressed on LNCaP cells and is not expressed on PC-3 cells, as we intended to verify.

3.3 Uptake of PSMA

Having validated that the prostate cells used either do express the PSMA receptor (LNCaP) or have a lack thereof (PC-3), it is necessary for NCT to investigate how much PSMA can be taken up by PSMA-positive cells, and whether there is a difference in uptake in PSMA-negative cells. For NCT, simulations were performed in order to determine what concentration of Gd-PSMA is required *in vitro* for decreased cell survival due to additional dose induced by the presence of gadolinium to be observed. The requirements that follow from these simulations are discussed in this paragraph, and compared with amounts of PSMA uptake currently known from preclinical investigations and clinical practice. Afterwards, uptake experiments are described in which it was investigated whether the required amount of Gd-PSMA could be internalized in PSMA-positive cells. First, uptake experiments with equivalent radioligands were performed, followed by uptake experiments with Gd-PSMA.

3.3.1 Required uptake of PSMA

The success of NCT depends amongst others on a high difference in concentration of the target isotope between normal and neoplastic cells. In the literature on BNCT, the absolute concentration of boron-10 that must be delivered to tumour cells has been estimated to be in the range of 20-50 µg/g (Barth 1992). With a 66 times higher cross section, lower concentrations of Gd-157 might be needed, but these numbers need to be corrected for the different molar mass of the elements (i.e. 10 gram/mole for boron-10 and 157 gram/mole for gadolinium-157) and the differences in energy deposited in the cell volume after neutron capture reaction (i.e. 2.33 MeV for boron-10 (Sauerwein 2012) and 67 keV for gadolinium-157 (Kulabdullaev 2016)) as well. If we take these numbers into account, it turns out an absolute concentration of gadolinium-157 of 610 µg/g is equivalent with a boron-10 concentration of 20 µg/g. Consequently, about 30 times higher concentrations of gadolinium-157 are expected to be required to have a similar effect as with boron-10.

Paragraph 3.4.1 discusses the simulations of the relationship between the concentration of gadolinium in the cells and the additional dose expected to be induced by gadolinium. These simulations show that, in the most optimistic case and assuming 100% enrichment, a Gd-157 concentration of 17 µg/g is required *in vitro*. In a more conservative scenario, still assuming 100% enrichment of Gd-157, a concentration of 428 µg/g is required. These values respectively correspond with PSMA concentrations internalized in cells of 114 µg/g and $2.84*10^3$ µg/g. As a requirement for PSMA uptake we could say that, at a minimum, a concentration of 114 µg/g should be reached in order for Gd-PSMA to be potentially feasible.

To our knowledge, the uptake of PSMA in this range of concentrations has not been investigated thus far. Being usually labelled with a radioactive isotope, the PSMA dose is generally optimized in terms of fulfilling diagnostic or therapeutic purposes, while causing an as low level of toxicity to normal tissue as possible. A PSMA study on the biodistribution of ^{177}Lu-PSMA in mice for example, merely injected about 35 pmole of ^{177}Lu-PSMA and subsequently showed an uptake of about 2.45 pmole/gram tumour tissue (Weineisen 2015). This is equivalent with about 3 ng of PSMA/gram tumour tissue, which might be enough for therapeutic purposes with ^{177}Lu, but is much lower than the concentration required for NCT.

3.3.2 ^{68}Ga-PSMA uptake in clinical scans

In order to investigate to what extent the average ^{68}Ga-PSMA uptake in tumours with doses injected in patients in order to make PSMA-PET scans corresponds with the required uptake for NCT, we performed some measurements with PSMA-PET scans. Both the uptake of ^{68}Ga-PSMA in primary tumours and metastases was determined. It was calculated that the specific activity of ^{68}Ga at the time of administering the isotope to the patient was 40 MBq/µg PSMA-11. The average uptake of activity per tumour volume (MBq/cm^3) was determined by drawing a 3D volume around the tumour location in the PSMA-PET scans. The drawing was performed by an experienced nuclear medicine physician, using OsiriX version 9.0 (DICOM) software for image analysis. The average uptake of activity was determined in seven different patients for both primary tumours and metastases. By dividing the average uptake of activity with the specific activity, the concentration of PSMA per gram tumour was calculated.

The average PSMA concentration in primary tumour was $3.41*10^{-3} \pm 3.38*10^{-3}$ (2σ) µg/g.

The average PSMA concentration in metastases was $3.00*10^{-3} \pm 3.20*10^{-3}$ (2σ) µg/g.

Within the uncertainty ranges, the concentration of PSMA in tumour cells could thus be considered to be equal. Both concentrations however, are much lower than the concentration required for NCT. Consequently, mice studies with therapeutic dosages of ^{177}Lu-PSMA nor clinical scans with ^{68}Ga-PSMA are suitable to determine whether the required uptake of PSMA could be reached in tumour tissue. Therefore, *in vitro* experiments are needed.

3.3.3 Uptake experiments of PSMA

One of the disadvantages of Gd-PSMA being not radioactive, is that it is not as easy to quantify the amount up taken in cells as with other tracers frequently used in nuclear medicine. In the same line of reasoning, the advantage of using tracers frequently used in the nuclear medicine practice is not only that there are suitable instruments to quantify the tracers, but also that the tracers are clinically available and remainders could easily and inexpensively be used for research purposes. For those reasons, the first uptake experiments of PSMA were performed using the equivalent PSMA tracers with the radioactive gallium-68 and lutetium-177.

^{68}Ga is a radioactive isotope, with a half-life of 68 minutes, which disintegrates by β^+ (positron) emission (89%) and electron capture (11%) into zinc-68 (Bé and Schönfield 2012). In addition to the main transition (96.9%) towards stable ^{68}Zn, there are 13 gamma transitions from 5 excited levels in ^{68}Zn (see Figure 20), of which gamma photons with an energy of 1077 keV have the highest probability (2.8%) (Firestone 1998).

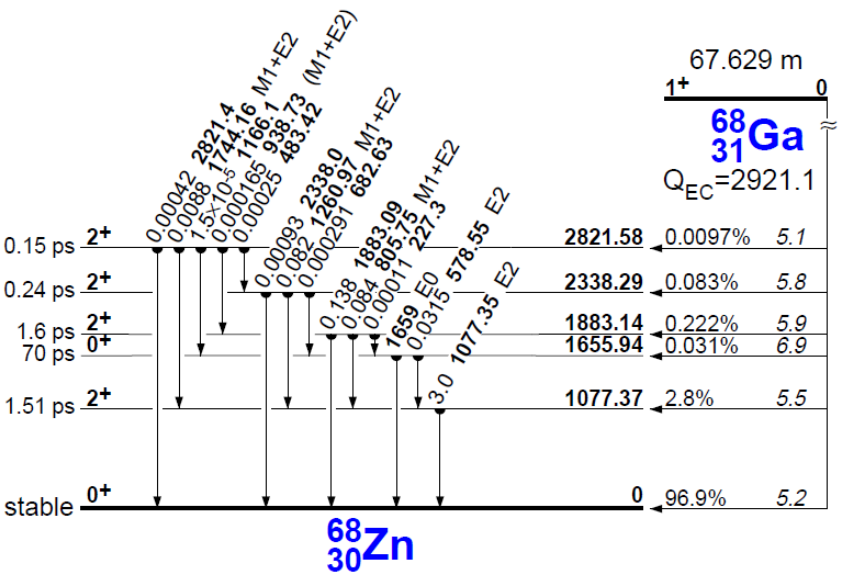

Figure 20: Decay scheme of ^{68}Ga decay into ^{68}Zn. In the third column from the right the energies of the emitted gamma photons are shown in keV. The second column from right shows the probabilities in % (Firestone 1998).

Lutetium-177 is a radioactive isotope of lutetium, a lanthanide like gadolinium. ^{177}Lu has a half-life of about 6.7 days, which disintegrates by β$^-$-emission into hafnium-177 (Firestone 1998). In addition to the main transition (~79%) towards stable ^{177}Hf, there are 3 gamma transitions from excited levels in ^{177}Hf, of which gamma photons with an energy of 113 keV and 321 keV have the highest probability (respectively 9.1% and 12.2%) (Firestone 1998).

Subsequently, the uptake of Gd-PSMA in prostate tumour cells was investigated. Ideally, amounts of PSMA orders of magnitude higher than provided by the clinic would be administered, in order to investigate whether the concentrations of accumulated tracer prescribed for NCT could be reached. Unfortunately, due to cost and availability constraints, it was not possible to use enough PSMA for this kind of investigation. The experiment with Gd-PSMA was limited to the application of amounts of PSMA just about one order of magnitude higher than in the experiments with equivalent radiotracers.

3.3.3.1 Materials and Methods

The materials and methods used for the uptake experiemtns are described in this paragraph. First, the experiments with equivalent radioligands are described, followed by the experiments with Gd-PSMA.

Uptake of equivalent radioligands

PSMA-ligand

The ^{68}Ga radioisotope was labelled in-house with a PSMA-targeting ligand and kindly provided to us by the clinic after quality control measurements had been performed. In the case of ^{68}Ga, the PSMA ligand PSMA-11 (ABX GmbH) was used. Unlike the PSMA molecules with a DOTA chelator, PSMA-11 is

conjugated with ^{68}Ga via the acyclic radiometal chelator N,N'-bis [2-hydroxy-5-(carboxyethyl)benzyl] ethylenediamine-N,N'-diacetic acid (HBED-CC), see Figure 21 (Schneirder 2016, Umbricht 2017).

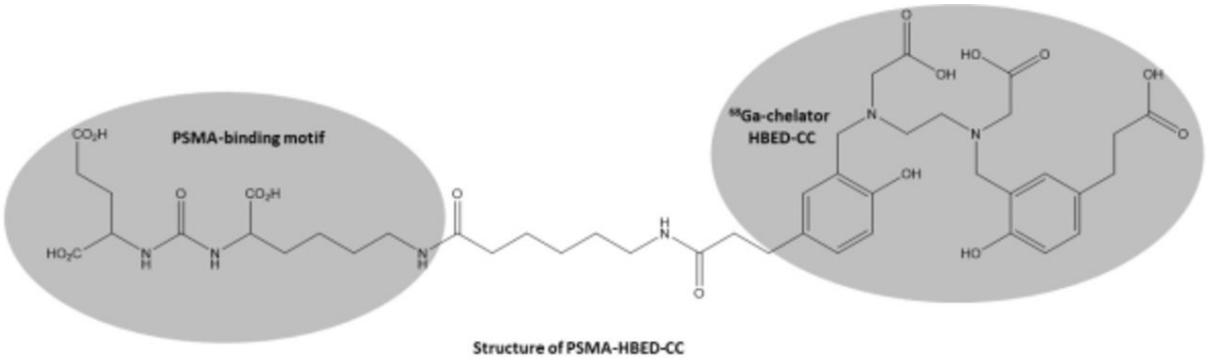

Figure 21: Molecular structure of PSMA-11, which can be labelled with the radioisotope ^{68}Ga (Scheider 2016).

Similar to the ^{68}Ga radioisotope, the ^{177}Lu isotope was labelled in-house with a PSMA-targeting ligand and kindly provided to us by the pharmacist of Nuclear Medicine after quality control measurements had been performed. In the case of ^{177}Lu, the PSMA ligand PSMA-617 (ABX GmbH) was used. This PSMA molecule has a DOTA chelator, and is also used for the labelling of Gd-PSMA (as described in paragraph 3.1).

Cell culture

The experiment with ^{68}Ga-PSMA-11 was performed with the PSMA-positive cell line only. The experiment with ^{177}Lu-PSMA-617 was performed with to both the PSMA-positive and PSMA-negative cell line.

Detection of gamma photons

The emitted gamma photons of the radioisotopes can be detected by a gamma counter. In the experiments, a Perkin Elmer Wallac 1480 WIZARD 3'' Gamma Counter was used. This gamma counter consists of well-type NaI (Tl) crystals, which collect signal from all around the sample (PerkinElmer 2005). Also, specially configured lead shielding is applied to the counter, in order to reduce crosstalk from samples on the conveyer as much as possible (PerkinElmer 2005). For the experiments, respectively the built-in gallium protocol and the built-in lutetium protocol were used for the acquisition of the data. Data is processed with RiaCalc WIZ, program 3.6, built-in software of the gamma counter. Results are expressed as counts per minute (cpm), which should be converted back to activity in Becquerel (Bq). For this reason, the detection efficiency of the gamma counter for ^{68}Ga and ^{177}Lu was determined, as discussed in Appendix 8.1. The decay time was also be corrected for. For each gamma counter experiment, the time of measurement was recorded, and the decay was corrected for using the following formula:

$$A(t) = A(0) * \left(\frac{1}{2}\right)^{\frac{t}{\tau_{1/2}}} \tag{1.2}$$

In this formula, *A(t)* is the activity in Bq at the time *t* of measurement, *A(0)* is the activity at *t*=0 (commonly the time of calibration), and $\tau_{1/2}$ is the half-life of the nuclide.

Cell experiment ^{68}Ga-PSMA-11

The day before the experiment, LNCaP cells were seeded in twenty 25-cm^2 cell culture flasks (T25, Greiner Bio-One) allowing adhesion and culture overnight at 37˚C and 5% CO_2. About 2*10^5 cells in 5 mL RPMI medium per T25 flask were seeded.

On the day of the experiment, a calibrated amount of ^{68}Ga-PSMA-11 was provided of 4mL with 183.3 MBq activity and 2.74 µg of PSMA. Of the calibrated amount, 3 mL was taken. This was diluted by taking 0.3 mL of the sample and adding it to 3.7 mL of sodium chloride 0.9%. This process was repeated six times. After the dilution series was made, three times 1 mL of each dilution was added to the 5 mL medium of a T25 flask with cells. The final concentration of PSMA in the T25 flask will be denoted as the 'administered concentration'. In addition to T25 flasks with cells, a control flask (i.e. without cells) was included in the measurement series, so as to correct the measurement for any residual activity due to the potentially imperfect washing process. The flasks were incubated at 37 °C for 0.25h, 0.5h and 1h, respectively. The cells were washed three times with PBS (made in-house) to determine the total uptake of the radioligands (PSMA-bound fraction on the surface and internalized fraction). Afterwards, the adherent cells were dissociated from the flask by administering 1 mL of Trypsin-EDTA (0.05%, Gibco^{TM}) and incubating them for 5 minutes, followed by adding 4 mL of FCS containing RPMI medium. The 5 mL of cell suspension was turned into single cells by a 70 µm cell strainer. Of the single cells, 3 mL was taken to be measured in the gamma counter. The remainder of 2 mL was incubated at 37 °C in order for the amount of cells to be counted after sufficient decay.

After about four half-lives of decay, the cells were determined to be not radioactive anymore, and the amount of cells per mL was counted using a CASY Model TT (Roche) Cell Counter and Analyzer.

The uptake of the PSMA ligand is expressed as µg PSMA per gram tumour cells, because this unit is commonly used to describe ideal conditions that should be fulfilled for NCT to be successful (Barth 1992). For this first experiment, the mass of tumour cells was estimated based on the rule of thumb that 1*10^9 cells weigh about 1 gram. This rule of thumb however, turned out to have an uncertainty margin of about one order of magnitude (Del Monte 2009). Therefore, the cell volume was determined later on with more accuracy, by performing additional cell measurements and determining cell diameter and volume with the CASY Model TT (Roche) Cell Counter and Analyzer. The details of these additional cell measurements are described in Appendix 8.2. In the data analysis of this first experiment, the estimation of the mass was later corrected for, using the more accurate numbers.

Cell experiment ^{177}Lu-PSMA-617

The day before the experiment, LNCaP and PC-3 cells were seeded in 6-wells plates, allowing adhesion and culture overnight at 37˚C and 5% CO_2. 6-wells plates were chosen, because of the smaller culture area (9 cm^2) and consequently higher potential concentration of PSMA. In case of LNCaP, about 5*10^4 cells in 2 mL RPMI medium per well, and in case of PC-3 circa 5*10^5 cells in 2 mL DMEM per well were seeded.

On the day of the experiment, a calibrated amount of ^{177}Lu-PSMA-617 was provided of about 7.8 mL with 459.7 MBq activity and 61.95 µg PSMA, which was completely used for the experiment. Initially, the tracer was diluted 1:5 (three times), subsequently dilutions of 1:4 (two times) and 1:3 (one time) were made, using sodium chloride 0.9%. The different dilutions in the dilution series were due to the use of controls. After the dilution series was made, 1 mL of each dilution was added to the medium of a well. The 6-wells plates were incubated at 37 °C for 0.5h and 1h, respectively. The cells

were washed three times with PBS (with each time removing any remainder of PBS with additional pipetting), and were kept in PBS until 0.5 mL of Trypsin-EDTA was added to dissociate the cells. The cells were incubated for 5 minutes, followed by addition of 2 mL of applicable medium. The 2.5 mL of cell suspension was turned into single cells by a 70 µm cell strainer. Of the single cells, 0.5 mL was taken to be measured in the gamma counter. The remainder of 2 mL was incubated at 37 °C in order for the amount of cells to be counted.

The samples that the gamma counter showed had radiation levels similar to the background were considered not radioactive. The amount of cells per mL in these samples was counted using a CASY Model TT (Roche) Cell Counter and Analyzer. The amount of cells per mL in the other samples was determined manually.

Uptake of Gd-PSMA

Gd-PSMA tracer

For this experiment, natural gadolinium, i.e. $GdCl_3$ solution was labelled with the PSMA ligand PSMA-617 (ABX GmbH), in a molar ratio of Gd:PSMA of 1:1.25. The labelling was performed in accordance with the method determined earlier on in our research (as described in paragraph 3.1.2), i.e. heating the solutions at 60˚C for 15 minutes. Validation of the labelling was performed with the HPLC method created during our research.

Cell culture

Similar to the ^{177}Lu-PSMA-617 experiment, both the PSMA-positive and PSMA-negative cell line were used. LNCaP cells were grown in RPMI-1640 medium, PC-3 cells were grown in DMEM.

Detection of gadolinium

The amount of gadolinium-157 in the sample was quantified using inductively coupled plasma mass spectrometry (ICP-MS). The detection limit of gadolinium-157 for ICP-MS is about 0.1 ng/mL according to the pharmacological laboratory of the AvL-NKI who performed the measurements, after calibrating for gadolinium-157. ICP-MS was performed with a Varian 810MS and a Varian SP53 autosampler, with a plasma flow of 18 L/min.

Cell experiment Gd-PSMA-617

The day before the experiment, LNCaP and PC-3 cells were seeded in 6-wells plates, allowing adhesion and culture overnight at 37˚C and 5% CO_2. In case of LNCaP, about $2*10^5$ cells in 1 mL RPMI medium per well, and in case of PC-3 circa $9*10^4$ cells in 1 mL DMEM per well were seeded.

On the day of the experiment, the Gd-PSMA was labelled and validated according to the methods described previously. In total, 3300 µL of Gd-PSMA was labelled, of which 50 µL was used for HPLC validation. The initial tracer was distributed among five wells, and the remainder was used for the dilution series. Consecutively dilutions of 1:6 (two more times), dilutions of 1:5 (two times), and 1:4 (one time) were made, using sodium chloride 0.9%. The different dilutions in the dilution series were due to the use of controls. After the dilution series was made, circa 0.5 mL of each dilution was added to the medium of a well. The 6-wells plates were incubated at 37 °C for 1h and 24h, respectively. The cells were washed three times with PBS (with each time removing any remainder of PBS with additional pipetting), and were kept in PBS until 0.5 mL of Trypsin-EDTA was added to dissociate the cells. The cells were incubated for 5 minutes, followed by addition of 1.5 mL of applicable medium.

The 2 mL of cell suspension was turned into single cells by a 70 µm cell strainer. Of the single cells, 0.1 mL was taken to count the amount of cells per mL using a CASY Model TT (Roche) Cell Counter and Analyzer. The remainder of the cells were fixed by adding 2 mL of 50% (v/v) methanol:ethanol.

Subsequently, the fixed samples were analysed by the pharmacological laboratory using ICP-MS.

3.3.3.2 Results and Discussion

In this paragraph, the results of the uptake experiments are described for ^{68}Ga-PSMA-11, ^{177}Lu-PSMA-617, and Gd-PSMA-617 respectively.

^{68}Ga-PSMA-11

The detection efficiency of the gamma counter for ^{68}Ga was determined to be 16.2 ± 0.62 (1σ) %, as discussed in Appendix 8.1.

The measurement of the amount of cells in the sample turned out to fluctuate much more than expected based on taking random samples from the flasks, seeded with a similar amount of cells. A possible cause for this large fluctuation is the cluttering of cells during incubation, after they had been turned into single cells. Such cluttering of the cells could be observed by the naked eye, and restraining of the cells did not help to solve the problem. This large fluctuation was however not supposed to have a large influence on the amount of PSMA internalized within the cells between single measurements. Therefore, it was decided to use the average cell count of the samples for further data analysis and to use the standard deviation of the cell count for the uncertainty analysis.

The amount of cells was subsequently used to determine the mass of the tumour cells. The mass of tumour cells was calculated by multiplying the amount of cells by the mass of a single cell. The mass of single PSMA-positive cells was calculated with the average volume of a single PSMA-positive cell, assuming the density of water. The average volume of single PSMA-positive cells was measured, as discussed in Appendix 8.2, to be $3.87*10^3 \pm 0.58*10^3$ (2σ) fL, which is equivalent with 3.87 ± 0.58 ng. These values were used in the data analysis of the uptake experiment with ^{68}Ga-PSMA-11, the results of which are shown in Figure 22. The residual activity found in the experiment with the control flask was subtracted from the results. This correction was in the order of 6%. Uncertainties were calculated by determining the error of the parameters involved, either by:

- estimation of the magnitude of the error (e.g. administered concentration)
- by using the error provided by the measuring device (e.g. gamma counter)
- or by taking the average of the measurement results and calculating the standard deviation (e.g. amount of cells)

Subsequently, the errors were added quadraticly, after which the square root was taken.

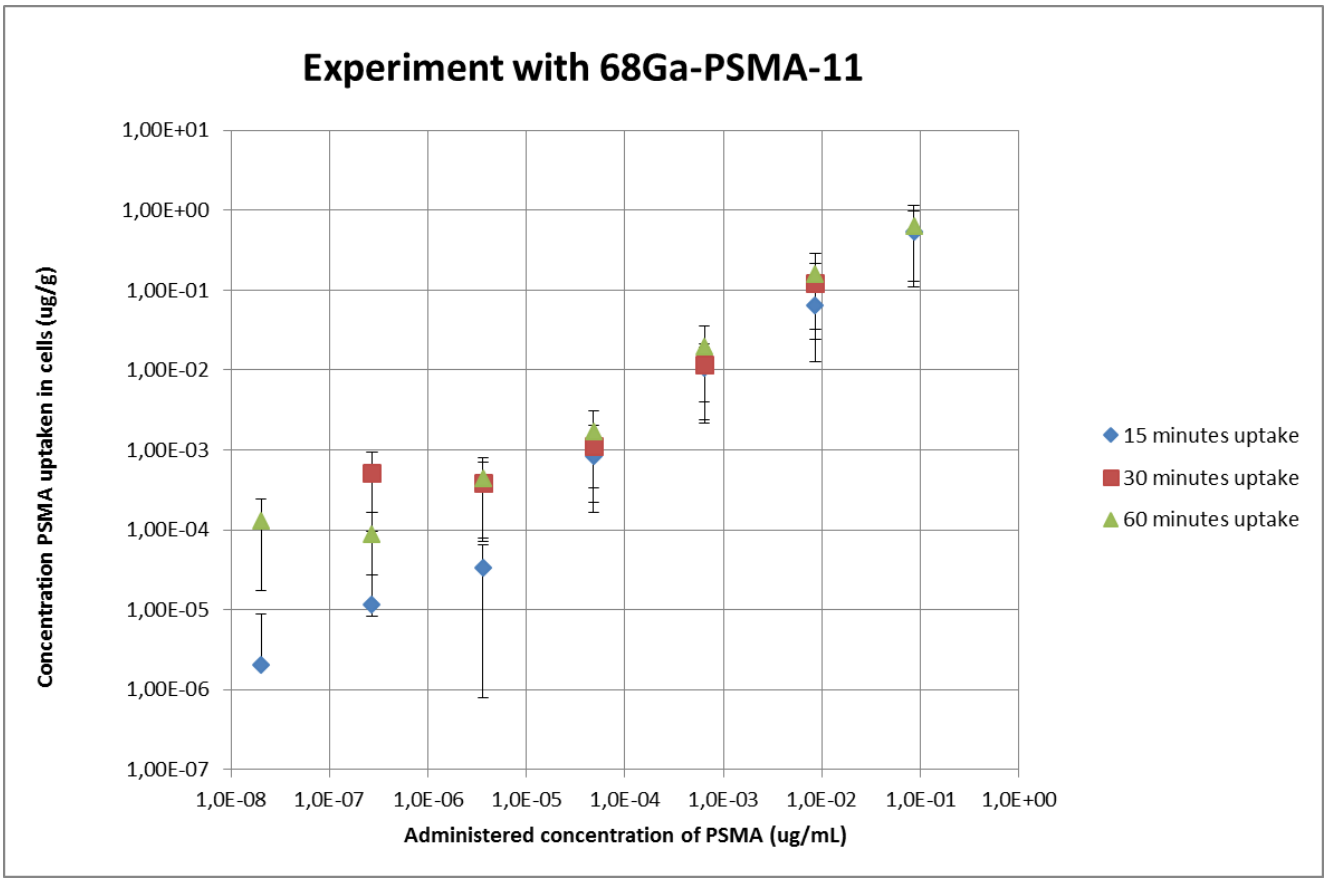

Figure 22: Log-log plot of the uptake of ^{68}Ga-PSMA-11 for a range of PSMA concentrations administered and for different time points of incubation. On the X-axis the administered concentration of PSMA is shown (µg/mL), on the Y-axis the concentration of PSMA taken up in cells is shown (µg/g). Error bars represent 2 standard deviations.

Figure 22 indicates that for concentrations above the detection limit of the gamma counter, there is no difference in uptake (within 2 sigma margins) between the different time points. This implies that the rate of uptake of PSMA is very quick and can be considered time independent. The uptake is thus merely dose dependent, and a positive correlation between the administered concentration and the concentration taken up is demonstrated. In this experiment, the highest uptake was 0.58 ± 0.47 (2σ) µg/g of PSMA-11. This highest uptake is still several orders of magnitude lower than the smallest amount required for NCT, i.e. 114 µg/g. It is therefore of interest to know the results of experiments in which higher concentrations of PSMA were administered, such as ^{177}Lu-PSMA-617.

^{177}Lu-PSMA-617

The detection efficiency of the gamma counter for ^{177}Lu was determined to be 2.1 ± 1.2 (1σ) %, as discussed in Appendix 8.1.

For consistency reasons and due to the clustering observed in some samples, it was decided to, like in the previous experiment, use the average cell count of the samples for further data analysis and to use the standard deviation of the cell count for the uncertainty analysis.

The mass of the cells was calculated in a similar manner as in the previous experiment. As discussed in Appendix 8.2, the average volume of single PSMA-positive cells was measured to be $3.87*10^3 \pm 0.58*10^3$ (2σ) fL, which is equivalent with 3.87 ± 0.58 ng. The average volume of single PSMA-negative cells was determined to be $4.36*10^3 \pm 0.69*10^3$ (2σ) fL, which is equivalent with 4.36 ± 0.69 ng. These values were used in the data analysis of the uptake experiment with ^{177}Lu-PSMA-617, the results of which are shown in Figure 23. The residual activity found in the experiment with the control wells was subtracted from the results. This correction was in the order of 3%. Uncertainties were calculated by determining the error of the parameters involved, either by:

- estimation of the magnitude of the error (e.g. administered concentration)
- by using the error provided by the measuring device (e.g. gamma counter)
- or by taking the average of the measurement results and calculating the standard deviation (e.g. amount of cells)

Subsequently, the errors were added quadraticly, after which the square root was taken.

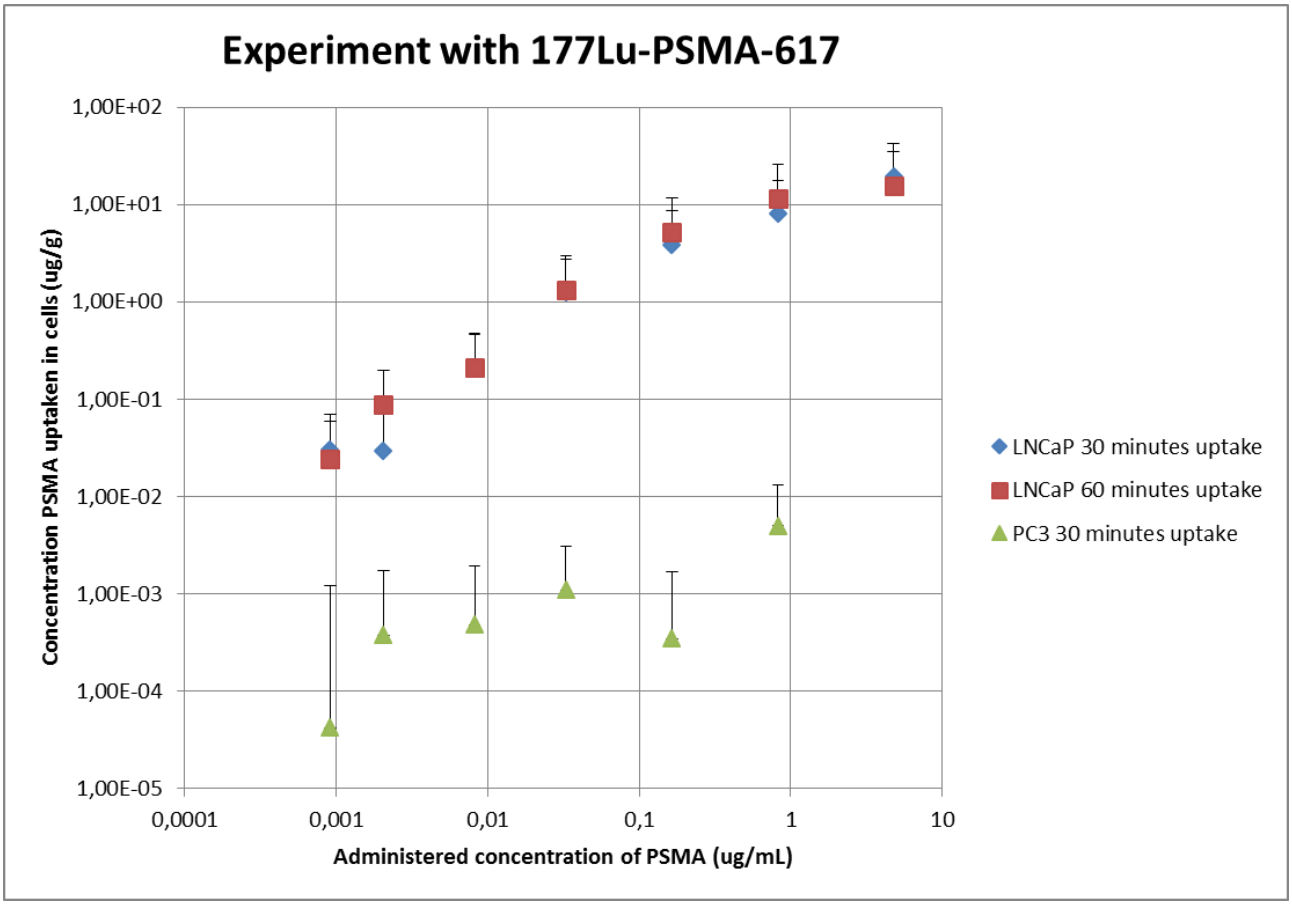

Figure 23: Log-log plot of the uptake of ^{177}Lu-PSMA-617 for a range of PSMA concentrations administered, for different time points of incubation, and for PSMA-positive and PSMA-negative cell lines. On the X-axis the administered concentration of PSMA is shown (µg/mL), on the Y-axis the concentration of PSMA taken up in cells is shown (µg/g). Error bars represent 2 standard deviations.

The plot of the uptake of ^{177}Lu-PSMA-617 shows a significant difference (> 2 standard deviations) between the uptake of PSMA-positive and PSMA-negative cell samples. Except for the highest

administered concentration, the uptake of PSMA in the PSMA-negative samples is similar to the background, which indicates that the PSMA-negative cells hardly internalize PSMA, as expected.

With regard to the uptake in PSMA-positive cells, in this experiment, the highest uptake was 17 ± 21 (2σ) µg/g of PSMA-617. This amount of uptake is still about one order of magnitude lower than the amount required for NCT.

When we combine the results of both uptake experiments, as displayed in Figure 24, the overlap in uptake of the different PSMA ligands becomes clear. Within 2 standard deviations, the uptake of PSMA-11 and PSMA-617 is quite similar. Also, a clear positive correlation is shown between the administered concentrations of both types of PSMA and the concentration taken up in the PSMA-positive cells. Yet, in case of PSMA-617, the uptake seems to saturate for higher concentrations. By investigating even higher concentrations of PSMA administered, the saturation might be confirmed.

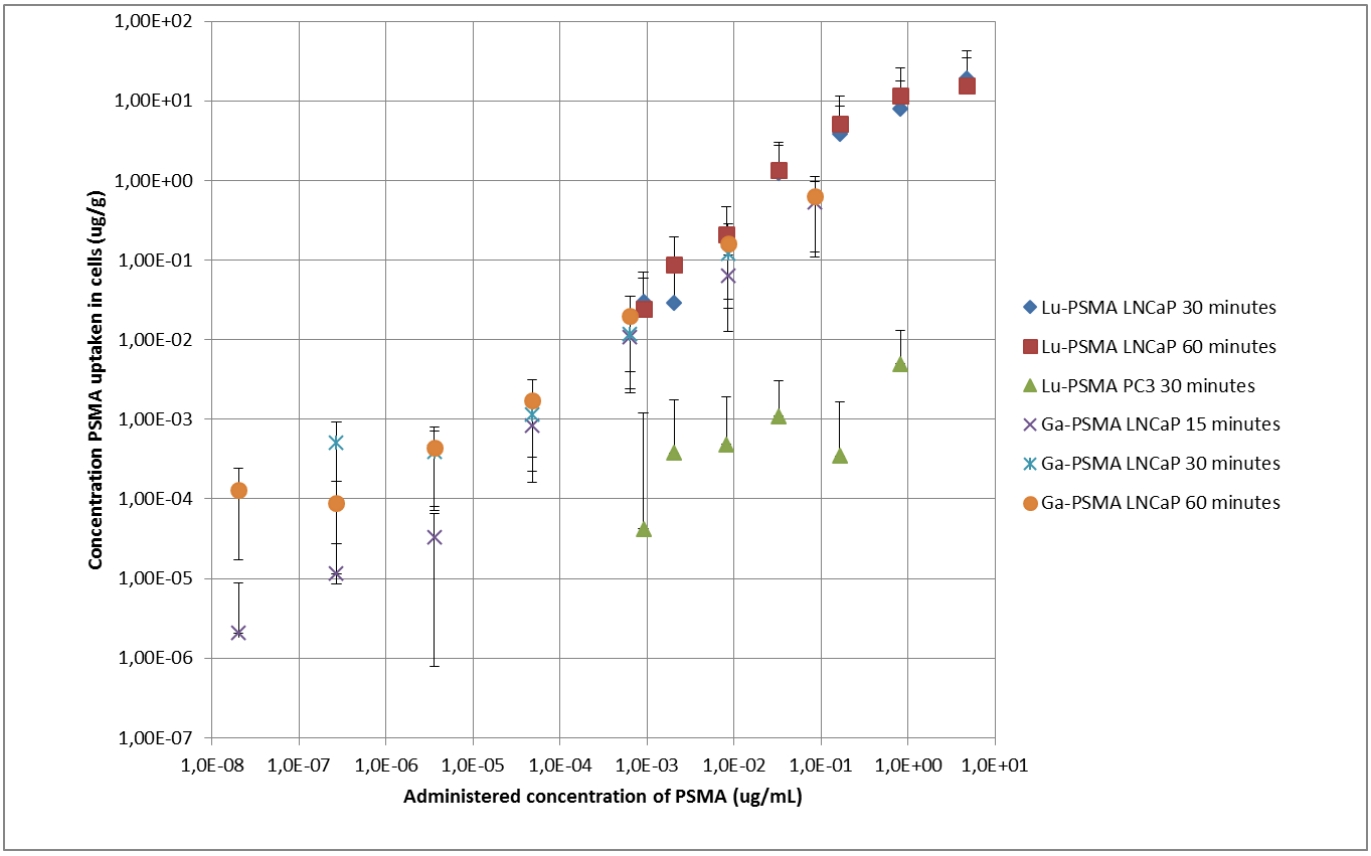

Figure 24: Log-log plot of the uptake of both ^{68}Ga-PSMA-11 and ^{177}Lu-PSMA-617 for a range of PSMA concentrations administered, for different time points of incubation, and for PSMA-positive and PSMA-negative cell lines. On the X-axis the administered concentration of PSMA is shown (µg/mL), on the Y-axis the concentration of PSMA taken up in cells is shown (µg/g). Error bars represent 2 standard deviations.

Gd-PSMA-617

The results of the Gd-PSMA uptake experiment are shown in Figure 26. For consistency reasons, the average cell count of the samples was used for further data analysis and the standard deviation of the cell count was used for the uncertainty analysis.

The mass of the cells was calculated in a similar manner as in the previous experiments. As discussed in Appendix 8.2, the average volume of single PSMA-positive cells was measured to be $3.87*10^3 \pm 0.58*10^3$ (2σ) fL, which is equivalent with 3.87 ± 0.58 ng. The average volume of single PSMA-negative cells was determined to be $4.36*10^3 \pm 0.69*10^3$ (2σ) fL, which is equivalent with 4.36 ± 0.69 ng. These values were used in the data analysis of the uptake experiment.

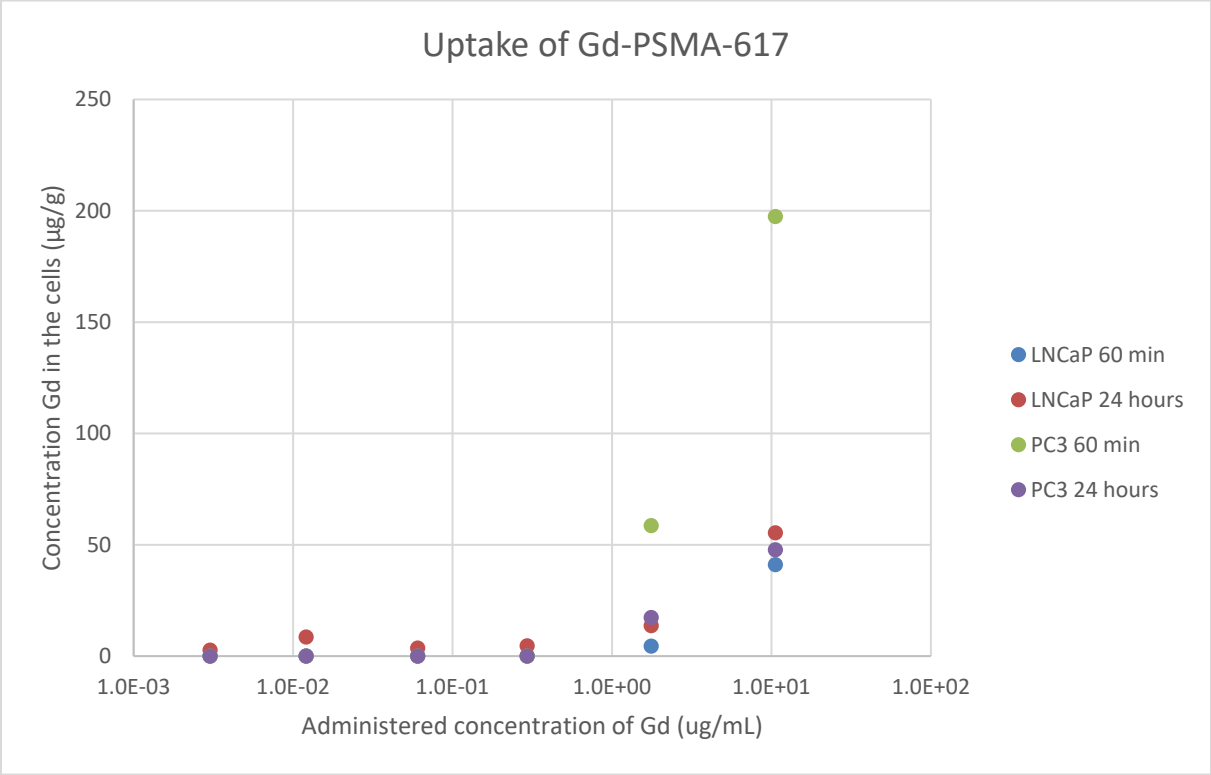

Figure 25: Plot of the uptake of Gd-PSMA for a range of PSMA concentrations administered, for different time points of incubation, and for PSMA-positive and PSMA-negative cell lines. On the (logarithmic) X-axis the administered concentration of PSMA is shown (µg/mL), on the (linear) Y-axis the concentration of PSMA taken up in cells is shown (µg/g).

Although about half of the results were below the detection limit of ICP-MS, Figure 25 indicates some positive correlation between the concentration of Gd-PSMA administered and the concentration taken up in the cells. Noticeably, the highest concentrations of Gd-PSMA were measured in PSMA-negative samples. In addition, a control sample with largest concentration of Gd-PSMA administered, showed an uptake similar to the uptake of the PSMA-negative sample with the highest concentration. These findings are remarkable, because they are inconsistent with the difference between PSMA-positive and PSMA-negative and background samples demonstrated in previous experiments. A straightforward explanation for the difference would be the washing procedure, but this procedure has been performed similarly to the ^{177}Lu-PSMA-617 experiment. Actually, it is likely the washing procedure was performed more stringent, as due to the lack of radiation, one did not need to consider exposure nor decay, so more time could be spend upon it. Due to time and availability constraints, the experiment could not be repeated, and unfortunately remains inconclusive.

3.4 Towards *in vitro* experiments of the radiation response

In paragraph 3.3.3.2 we discussed that the maximum experimental uptake of PSMA is still about a factor of ~10 lower than the minimum PSMA concentration requirement derived in paragraph 3.3.1. Nevertheless, the results of the uptake experiments so far do not exclude the possibility that the internalization of the required amount of PSMA can be achieved in future experiments. This would, however, require further investigations with relatively large amounts of PSMA and enriched gadolinium. Given the current prices of enriched gadolinium and PSMA, this implies rather costly future experiments.

In this paragraph, we will first discuss the simulations that provide us with the minimum requirements for the gadolinium and PSMA concentrations. Afterwards, several preliminary experiments will be discussed, which were performed in order to ensure that useful *in vitro* irradiation experiments can be executed if the required concentrations are indeed achieved in future. These preliminary experiments included:

- Determination of required thermal neutron fluence rate;
- Assessment and selection of currently available neutron sources;
- Assessment of the effect on cell viability of transport of cells from the hospital-side to the reactor-side and back;
- Determination of the level of neutron activation of the irradiated samples.

3.4.1 Minimum required gadolinium concentration

Before *in vitro* irradiation experiments are performed, it is of interest to investigate what concentration of Gd-PSMA should be taken up in the PSMA-positive cells, in order to observe significant effect due to additional dose induced by the presence of gadolinium.

In order to understand what a significant effect due to additional dose entails, an important measure to express the radiobiological effect needs to be introduced first. This measure is the Relative Biological Effectiveness (RBE).

Radiobiological effect

The Relative Biological Effectiveness (RBE) expresses the difference in biological effect for the same absorbed dose of different kinds of radiation. The RBE is the ratio between a reference absorbed dose of radiation of a standard type (usually X-rays of a 200-300 kV tube), and the absorbed dose of radiation of interest that causes the same amount of biological damage under equal circumstances [Bos 2007]. Thus, RBE is expressed by the following formula:

$$RBE_{radiationtype,i;effect,j} = \frac{D_{reference;effect,j}}{D_{radiationtype,i;effect,j}} \tag{1.3}$$

Different types of radiation have different biological effectiveness mainly because they transfer their energy to the tissue in different ways. Consequently, particles with a high linear energy transfer (LET)

tend to have a higher RBE than particles with a low LET. Table 3 provides an overview of the RBE of common types of radiation [Bos 2007].

Table 3: Overview of the RBE of common radiation types [Bos 2007].

Radiation type	Energy level	RBE
Photons	All energies	1
Electrons, except for Auger electrons emitted by atoms bound to DNA	All energies	1
Neutrons	< 10 keV	5
	10-100 keV	10
	> 100 keV – 2 MeV	20
	> 2 MeV – 20 MeV	10
	> 20 MeV	5
Protons	> 2 MeV	5
α-particles, heavy ions		20

As Table 3 indicates, RBE values of 20 are considered to be the highest among common radiation types. In case of gadolinium neutron capture, the dose delivering particles are mainly Auger electrons and internal conversion elections. Internal conversion electrons are expected to have a RBE of 1. Auger electrons are likely to have a RBE value of 1 as well, because, although the distribution of PSMA is not very well known [Meneghetti 2012, Banerjee 2015], it is not expected to be bound to the DNA (see paragraph 2.4.2.4). Yet, in an optimistic scenario of estimating the biological effect due to the gadolinium in the cells, we could take higher RBE values. Such an optimistic scenario would entail Gd-157 being directly bound to DNA molecules. In the most optimistic case, we could calculate with a RBE value of 25.

Requirements for *in vitro* experiments

In order to observe a significant difference in cell survival due to additional dose induced by the presence of gadolinium, one might assume a dose enhancement of 20%. Since the background dose of the *in vitro* irradiation experiments mainly consists of thermal neutrons, we could assume a RBE of 5 for the background. In the most optimistic case of a RBE value of 25 for the dose effect of gadolinium, an enhancement of the physical dose relative to the physical background dose (both in Gy) of merely 4% is required. On the other hand, in the more conservative case of a RBE of 1, a physical dose enhancement of 100% is required.

The gadolinium concentrations required to achieve such dose enhancements, could be determined with Monte Carlo simulations.

Monte Carlo simulations on dose effect of gadolinium

Monte Carlo simulations can be used to calculate the (average) additional physical dose delivered to cells containing gadolinium, due to the irradiation with a thermal neutron beam. The Monte Carlo simulations were performed by Diederik Feilzer, a fellow master student who works at TU Delft on the computational aspect of this Gd-NCT project [Feilzer 2018]. The setup and details of the simulations are discussed in Appendix Monte Carlo simulations on dose effect of gadolinium8.3. In this paragraph, the results of the simulations will be discussed and the required concentrations of Gd and PSMA that follow from them.

Simple interpolation model

The simulations showed that the concentration of gadolinium in the cell layer, its level of enrichment and the thickness of the cell layer have negligible influence on the physical dose deposited by the simulated thermal neutron beam ("neutron dose"), and by the photons in the beam ("photon dose"). These parameters do however influence the dose induced by the presence of gadolinium ("Gd-dose"). The concentration of gadolinium in the cells has a positive effect on the dose due to gadolinium and is, at least up to 100 µg/g of gadolinium, linear. A linear influence of the enrichment level on the deposited Gd-dose has been found as well, and is assumed to be independent of the concentration of gadolinium administered. In addition, thicker cell layers have a relative higher dose, independent of the gadolinium concentration. A simple interpolation model that captures the effects of the different parameters on the gadolinium dose has been formulated by Diederik Feilzer as follows:

$$[\mathrm{Gd}]\cdot(1+4.2094\cdot \mathrm{F})\cdot(1+0.0748\cdot \mathrm{d})\cdot 4.34148\cdot 10^{-16}[Gy\cdot cm^2] \quad (1.4)$$

In this equation, *[Gd]* is the concentration of gadolinium in µg Gd/g tumour cells and *F* is the enrichment fraction. The enrichment fraction is the relative quantity of 100% enriched Gd to natural Gd. Finally, *d* represents the thickness of the cell layer in µm (Feilzer 2018).

The physical dose deposited by the neutrons and photons in the simulated thermal neutron beam turn out to be respectively:

Neutron dose: $6.5*10^{-13}$ [Gy cm^2]

Photon dose: $1.7*10^{-12}$ [Gy cm^2]

Adding these two values together, provides the deposited background dose, which is $2.4*10^{-12}$ [Gy cm^2]. A dose enhancement of 4% gives a corresponding Gd-dose of $9.4*10^{-14}$ [Gy cm^2], and a dose enhancement of 100% requires a Gd-dose of $2.4*10^{-12}$ [Gy cm^2].

Using equation (1.4), it is possible to calculate the concentrations of gadolinium required to achieve the desired effective dose enhancements. The diameter of PSMA-positive cells was measured to be 19.1 ± 0.73 (2σ) µm, so this number is taken as input for *d*, the thickness of the cell layer. As we reason from the most optimistic case and want to calculate the minimum concentration of Gd required to achieve an observable effect, it is assumed that 100% enriched gadolinium-157 is used. Consequently, *F* is taken to be 1.

This provides the following Gd-157 concentrations required for the different dose enhancements:

- 17 µg/g Gd-157 for 4% dose enhancement
- 428 µg/g Gd-157 for 100% dose enhancement

It should be noted that the concentration required in case of 100% dose enhancement needed to be extrapolated outside the range for which the interpolation model was specified to be valid (i.e. up to 100 µg/g of Gd-157). Due to self-shielding effects, it might be that the model is not behaving linearly anymore for concentrations higher than 100 µg/g (although this is unlikely in a single cell layer). In that case, higher concentrations of Gd-157 are expected to be needed in order to have the same percentage of dose enhancement.

Having determined the required concentrations of Gd-157, it is possible to calculate what PSMA concentrations would be required to be internalized in cells. Table 4 demonstrates the conversion of [Gd] to PSMA concentration.

Table 4: Conversion of the required Gd concentrations to the equivalent concentrations of PSMA needed to be taken up in cells

Gd-157 concentration in cells (µg/g)	Gd-157 concentration in cells (µmol/g)	PSMA-617 concentration in cells (µmol/g)	PSMA-617 concentration in cells (µg/g)
17	0.11	0.11	114
428	2.7	2.7	$2.84*10^3$

So, the minimum concentration of PSMA-617 that needs to be internalized in PSMA-positive cells in the most optimistic scenario is 114 µg/g. In a more conservative case, still assuming 100% enrichment of gadolinium, a concentration of $2.84*10^3$ µg/g of PSMA is required.

3.4.2 Required thermal neutron fluence rate

Having determined the minimum gadolinium concentration required to expect any additional dose effects induced by the presence of gadolinium to be observed, it is of interest to investigate what neutron fluence rates are required to actually observe any dose effects.

According to the literature, in order to perform NCT, a neutron source is required which produces neutrons with (epi)thermal neutrons, with as little contaminants (e.g. gamma photons and fast neutrons) as possible, and with a high fluence rate (Moss 2014). For clinical purposes, epithermal neutron fluence rates higher than $5*10^{12}$ $m^{-2}s^{-1}$ were required (Bakker 2018). For *in vitro* experiments, similar fluence rates might be required, but in these cases, thermal neutrons are needed.

Assuming that dose-survival experiments commonly investigate ranges of 0-20 Gy, a dose enhancement of 20% would imply a dose range of 0-24 Gy. This indicates a background dose of 20 Gy, and an additional dose induced by Gd of 4 Gy. Assuming that the background dose of the thermal neutron beam mostly consists of neutrons, a RBE value of 5 could be taken into account. Consequently, an effective dose of 20 Sv could be achieved by a neutron background dose of 4 Gy. If we assume that for logistic and radiobiological reasons the maximum irradiation time is about 4 hours, the dose rate of the thermal neutron beam should be about 1 Gy/h. This corresponds with a thermal neutron fluence rate of ~$4.3*10^{12}$ $m^{-2}s^{-1}$.

3.4.3 Characteristics of available neutron beams

As described in the literature review (paragraph 2.4.6) the availability of neutron sources worldwide is limited nowadays. For example, the neutron beam at the High Flux Reactor (HFR) in Petten used for BNCT treatments years ago, is not operational anymore. This former BNCT beam had a thermal fluence rate of about $2.6*10^{12}$ $m^{-2}s^{-1}$ and an epithermal fluence rate of about 3.3 $m^{-2}s^{-1}$ (Nievaart 2007). At the moment, in the Netherlands, two nuclear reactor sides would be able to provide a beam with

(epi)thermal neutrons, though of lesser fluence rates than the former BNCT beam: the research reactor at TU Delft and the HFR in Petten (which has two out of eleven beams still in use).

3.4.3.1 Characteristics of neutron beam at HFR

For logistic reasons, in Petten merely one beam was available for irradiation experiments, i.e. the HB5. Before any irradiation experiments could be performed, the characteristics of the beam (i.e. thermal neutron fluence rate, homogeneity of the beam, the fluence rate of fast neutrons and the gamma flux) had to be determined again, as the latest measurement dates from 1995 (before a major conversion of the reactor core took place) [(Bakker 2018)]. The homogeneity of the beam is determined with a neutron radiography technique. In this technique an image is made of the beam using a neutron converter plate which visualizes the distribution of the neutrons in the beam. On the neutron converter plate, in the centre of the neutron beam, dosimetry monitors will be positioned, in order to measure the fluence rates of thermal (assuming 2200 m/s), intermediate and fast neutrons in the beam. The gamma flux was measured with films made of red Perspex.

The results of the visualization of the neutron distribution were demonstrated to us in real-life. Pictures of the radiography images are expected after this report is due. Images shown to us demonstrated that the beam is rather homogeneous. Merely in one corner the neutron fluence rate is lower compared to the average value over the beam profile.

The results of the measurements of the neutron fluence rates are shown in Table 5.

Table 5: Thermal, epithermal, and fast fluence rates ($m^{-2}s^{-1}$) of the HFR-HB5 neutron beam.

Thermal fluence rate ($m^{-2}s^{-1}$)	Epithermal fluence rate ($m^{-2}s^{-1}$)	Fast fluence rate ($m^{-2}s^{-1}$)
$3.92*10^{10}$	$2.02*10^{8}$	$9.09*10^{7}$

As Table 5 indicates, the fluence rate of higher-than-thermal neutrons in the beam is about 1% of the thermal fluence rate, which is considered to be acceptable.

The results of the gamma flux of the HB5 beam are also expected after this report is due.

3.4.3.2 Characteristics of neutron beam at TU Delft reactor

The beam available at the research reactor in Delft has a fluence rate of thermal neutrons previously determined to be $2*10^{11}$ $m^{-2}s^{-1}$. So, the fluence rate is about 4 times higher than the fluence rate of the currently available neutron beam at Petten.

For this project, the gamma dose of the beam at the TU Delft reactor was measured. Measurements were performed with red Perspex film, positioned perpendicular and parallel (1.5 cm distance) to the beam.

After 6 hours and 48 minutes of irradiation, the total dose in the film placed perpendicular to the beam was 7.27 Gy. The film positioned parallel to the beam received a dose of 0.36 Gy. So, we can conclude that apparently the neutrons interact with the film, which cause a much higher dose in the film placed perpendicular to the beam. Besides, we can conclude that the neutron dose rate is about

1 Gy/h, which is equal to the dose rate required for *in vitro* irradiation experiments. It should however be noted, that this dose rate represents all the neutrons in the beam, not merely the thermal neutrons. The thermal neutron dose rate might consequently be lower. Finally, we can conclude that the gamma dose rate is approximately 0.05 Gy/h, which is considered to be an acceptable dose rate for contamination in the beam.

3.4.3.3 Simulated background doses of neutron beams

Having determined the thermal neutron fluence rates of the different beams, with Monte Carlo simulations it is possible to calculate the dose deposited by the beam. By multiplying the simulated neutron dose and photon dose of the beam with the thermal neutron fluence rate, dose rates could be calculated. Table 6 provides an overview of the simulated neutron and photon dose rate and dose deposited after 4 hours of irradiation. The results for both the beam in Delft and the operational HB5 beam and the former BNCT beam in Petten are provided. It is assumed that the neutron and photon spectrum of the beams in Petten are similar to the beam in Delft. The photon fluence rates are expected to be lower than the neutron fluence rates, but as no data is available on the photon fluence rates yet, fluence rates are assumed to be similar. For the former BNCT beam, it is assumed that both thermal and epithermal neutrons in the beam are moderated such that only thermal neutrons are delivered to the cells. Furthermore, due to its former clinical applications and the presence of a filter, it is assumed that there is hardly any photon contamination in the beam, so the photon dose is considered to be zero.

Table 6: Overview of the simulated Gd dose after irradiation, and relative physical dose enhancement compared to the background dose. Results are provided for both the beam in Delft and the operational HB5 and former BNCT beam in Petten.

	Delft	**Petten HB5**	**Petten former BNCT beam**
Neutron dose rate (Gy/s)	$1.3*10^{-5}$	$2.6*10^{-6}$	$3.3*10^{-4}$
Photon dose rate (Gy/s)	$3.4*10^{-5}$	$6.7*10^{-6}$	0
Neutron dose after 4 hours of irradiation (Gy)	$1.9*10^{-1}$	$3.7*10^{-2}$	$4.7*10^{0}$
Photon dose after 4 hours of irradiation (Gy)	$4.9*10^{-1}$	$9.6*10^{-2}$	0
Total background dose after 4 hours of irradiation (Gy)	$6.8*10^{-1}$	$1.3*10^{-1}$	$4.7*10^{0}$

It should be noted that the background dose (i.e. photon + neutron dose) of the simulations is lower than the dose measured at the beam in Delft (as described in paragraph 3.4.3.2). According to Feilzer, this might be due to:

- the fact that the dose of faster-than-thermal neutrons is not taken into account and should be added to the total background dose,
- potentially different geometries used for calibrating the dose in the foil and for simulating the dose in the adherent cell layer, and
- the use of a potentially inaccurate thermal neutron spectrum.

Based on Table 6, we can conclude that merely the former BNCT beam is expected to have a thermal neutron fluence rate in accordance with the dose rate required for additional dose effects induced by gadolinium to be observed. It is therefore recommendable to commence the process of reoperating

the beam again. If this turns out to be impossible, the beam in Delft might be, based on experimental measurements, a suitable alternative, especially if longer irradiation times are feasible.

3.4.4 Irradiation experiments

Due to the limited uptake of PSMA in the cells, the simulations showing that higher uptake and higher neutron fluence rates are needed for effect due to gadolinium to be expected, and due to the practical circumstance that no PSMA-617 was in stock anymore, it was decided to not perform any irradiation experiments with Gd-PSMA yet. It was however recommendable to already perform a first irradiation experiment to investigate logistics and other practical matters, neutron activation, background radiation and source contamination, and the effect on the viability of the cells.

3.4.4.1 First irradiation experiment

Materials and methods

Cell culture

For the experiment both PSMA-positive and PSMA-negative cancer cells were used. To ensure proper controls, LNCaP was both grown in RPMI-1640 medium (Gibco®), supplemented with 10% (v/v) FBS and 1% (v/v) Pen Strep and in DMEM (Gibco®), supplemented with 10% (v/v) FBS, 1% (v/v) Pen Strep, and 0.8% (v/v) GlutaMAX (Gibco®). Growing LNCaP cells in DMEM is possible, but generally less recommended than growing them in RPMI medium, which is why in the previous experiments RPMI medium was used. PC-3 cells were grown in DMEM (Gibco®), supplemented with 10% (v/v) FBS, 1% (v/v) Pen Strep, and 0.8% (v/v) GlutaMAX (Gibco®).

Neutron source

As a neutron source, the neutron beam HB5 of the HFR in Petten was used. Despite the worse conditions compared to the neutron beam in Delft, this beam was chosen, because a lot of effort was put in to make the beam operational for the experiments, and because these first experiments might be a stepping stone for re-operating the former BNCT beam. According to the latest measurements (see paragraph 3.4.3), the neutron fluence rate of thermal neutrons in the HB5 is $3.92*10^{10}$ $m^{-2}s^{-1}$.

Cell experiment

About two days before the experiment, LNCaP and PC-3 cells were seeded in T25 flasks to allow them to adhere and grow and become as confluent as possible at 37˚C and 5% CO_2. T25 flasks were chosen, because, although they do not completely cover the irradiation aperture, they are less leaky than smaller sample holders, such as 35-mm dishes.

Merely one sample could be irradiated, which was T25 flask with LNCaP cells cultured in RPMI medium. Other samples were used as a control, to investigate the effect of the uncommon conditions the cells were exposed to on the viability of the cells. These uncommon conditions include the topping off of the T25 flask with medium (to ensure cells have enough nutrients, also when irradiated in a vertical position, and neutrons are not scattered due to air bubbles in the sample), no CO_2 exchange due to a closed cap, residing for several hours at room temperature, and significant movement due to being transported by car. For those reasons, several controls were taken into account, which include:

- T25 flasks in the incubator, with a normal amount of medium and an open cap
- T25 flasks in the incubator, with a normal amount of medium and a closed cap
- T25 flasks in the incubator, filled up with medium (and a closed cap)
- T25 flasks on a lab table outside the incubator, filled up with medium (and a closed cap)
- T25 flasks taken with us in the car, filled up with medium (and a closed cap), tested in duplo

The different conditions were tested for both LNCaP in RPMI medium, LNCaP in DMEM, and PC-3 in DMEM.

On the day of the irradiation, the samples were prepared by filling them up with 60 mL of medium heated in a water bath to 37˚C, and subsequently positioning them on the location assigned.

The samples transported in the car were packed in a Styrofoam box, which also contained two 500 mL flasks filled up with water of 37˚C. During transport, the box was kept on the lap of one of the passengers and the temperature in the car was set as high as acceptable for the passengers. Having arrived at the reactor side in Petten, the samples were transported as quickly as possible to the irradiation area. The sample to be irradiated was positioned at the beam exit, and the control samples were positioned in the neighbouring area. The sample was irradiated for 4 hours.

After the irradiation, the samples were tested for activation by the hand-held contamination monitor COMO 170, and transported back by car to the NKI-AvL. At the NKI-AvL, all the samples (including controls left at the NKI-AvL) were prepared to be analysed for cell viability by consecutively removing the culture medium, by washing the cells with PBS, by trypsinizing them with 0.5 mL of Trypsin-EDTA and by adding 2 mL of fresh medium to the suspended cells. As this could not be done with all the samples at once, batches were prepared at the same time, and other samples were kept in the incubator at 37˚C and 5% CO_2 (with cap open).

Cell viability analysis

Cell viability was assessed using a quick first-order approach: by performing the dye exclusion test with Tryphan Blue Solution 0.4% (Thermo Fisher Scientific) as a cell stain. The dye exclusion test is based upon the concept that viable cells do not take up impermeable dyes (like Trypan Blue), but dead cells are permeable and take up the dye. Consequently, the amount of dark blue cells is a rough estimation of the percentage of dead cells in the sample.

10 µL of Tryphan Blue was added in a 1:1 ratio to a sample of suspended cells, and consequently observed under a (light) microscope. A comparison was made with a sample taken from cells before sub culturing, which we expected to have non-viable as well as viable cells. The irradiated and control samples were randomized and tested in duplo.

Results and Discussion

In the reference sample taken from cells before sub culturing, 2-3 non-viable cells were observed, and the remainder of the cells were considered to be viable. In the case of a 10 µL sample, let's assume a maximum of 10% of the cells were non-viable.

With regard to the irradiated sample and the controls, the following cell viability was observed (Table 7):

Table 7: Overview of the percentage of non-viable cells for the irradiated sample and the different controls investigated.

Sample	Average percentage non-viable cells (%)
Incubator, normal medium, open cap	0-1%
Incubator, normal medium, closed cap	0-1%
Incubator, filled with medium, closed cap	0-2.5%
Lab table, filled with medium, closed cap	0-5%
Car, filled with medium, closed cap	0-5%
Irradiation, filled with medium, closed cap	5-10%

As Table 7 indicates, the cell viability in all the controls is in a similar range. The controls outside the incubator might have a slightly lower viability, but this is not significant. Also the irradiated sample has a very high level of cell viability. It is doubtful whether the slight increase in non-viable cells is significant. If it is, the level of non-viability is still lower than the reference sample, which mostly can be considered to contain viable cells.

The low level of non-viable cells is good news for future irradiations with Gd-PSMA, as logistics and background dose turned out to not be a bottleneck. It should be noted however, that the viability assays were performed several hours after the irradiation. It might be that in the meantime, membrane damage may have been repaired.

Therefore, it is recommendable to repeat the irradiation experiments and perform clonogenic assays afterwards, as cell survival assays are considered the golden standard in radiobiology, providing the best indication of the amount of viable cells. Due to time and practical constraints, it was not possible to perform clonogenic assays after this irradiation experiment. During our research, we did however gain some experience with performing clonogenic assays with PSMA-positive and PSMA-negative cell lines, the results of which are discussed in Appendix 8.4.

3.4.4.2 Neutron activation experiments

In addition to measuring the viability of the cells after irradiation, the potential activation of the sample due to neutron irradiation was investigated. After the irradiation, the sample and the controls taken to Petten were tested for activation by the hand-held contamination monitor COMO 170.

While the controls did not show any activation above background level, about 100 counts per second were measured on the irradiated sample. As this was considered to be an acceptable level of radiation, the sample was taken back to the NKI-AvL, where it was measured again using the gamma counter with a broad wipe protocol. About 60 cps were measured circa two hours after the first measurement.

Over the weekend, the sample was measured again and did not show more counts than the background anymore.

Irradiations were repeated at the reactor side in Petten with either an empty T25 flask, a T25 flask filled with RPMI, or a T25 flask filled with DMEM. Samples were irradiated for 4 hours each. The empty T25 flask did not show significantly more counts than the background. Both flasks filled with medium showed increased amounts of activity, about 100 cps for RPMI, and about 160 cps for DMEM,

measured directly after irradiation. After about 40 hours, the amount of counts was similar to the background again. Based on these observations, it is assumed that sodium and potassium were activated by the neutrons, as these elements are frequently present in organic material, and their decay pattern fits the observations.

The level of activation in the first irradiation measurements was deemed acceptable. If future irradiations would use even longer irradiation times and/or a beam with a higher neutron fluence rate, the level of activation might increase beyond acceptable limits. This may be something to take into account for future research.

4 Discussion

To investigate the feasibility of using Gd-PSMA for NCT, we estimated the minimum concentration of PSMA required in PSMA-positive cells, and studied if this concentration could be achieved *in vitro*. The uptake in cells was shown to increase with administered concentration, but the concentrations in the cells achieved thus far are at least ~10 times too low to expect any significant dose enhancement induced by the presence of gadolinium.

As the current experiments have been performed with natural gadolinium, there appear to be two straightforward future options to increase the dose effect due to gadolinium. First, the administered concentration of PSMA must be increased, in order to increase the uptake in cells. As our experiments indicate that there might be saturation in the uptake, it is worthwhile to investigate some higher orders of magnitude of administered PSMA concentrations.

With respect to the saturation of PSMA uptake, one might expect saturation to occur when, for example, all receptors are bound. Although the literature provides different values for the amount of PSMA receptors on LNCaP cells (ranging from $45*10^3$ (Lückerath 2018) to $1.1*10^6$ (Taylor 2012) receptors/cell), both values are lower than the amount of PSMA molecules calculated to be taken up per cell during our ^{177}Lu-PSMA uptake experiments. In these experiments, for the highest concentration of PSMA, the amount of PSMA molecules per cell is in the order of $1*10^{7.}$ This amount is about one order of magnitude higher than the largest literature values on the number of receptors. Consequently, the amount of receptors does not seem to be the reason for saturation in the uptake, if this occurs at all.

There is however a bottleneck foreseen with regard to uptake experiments with administered concentrations orders of magnitude higher than currently applied. This bottleneck not only entails the costs of PSMA-617, which was the reason for the limited use during our experiments, but also the current availability of the molecule. Since the PSMA-617 ligand has been bought by a commercial party, the molecule is no longer supplied to health clinics, as they first want to perform a large clinical Phase III trial with PSMA-617. After the trial, one can expect the price of PSMA-617 to increase even further. Therefore, it is worthwhile to search for alternative PSMA molecules with a similar DOTA-chelator, but a different linker part. One alternative PSMA molecule that fulfils these requirements and has already been used in patients (Weineisen 2015), is the molecule PSMA I&T, synthesized by Weineisen et al (Weineisen 2014). It is, however, unclear whether this molecule will be supplied to other clinics. If it is, that would be helpful for the progress of PSMA related treatments, although a new molecule also implies that labelling, validation, and dosing have to be performed all over again.

With regard to the costs of the PSMA-molecules, it is clear that the costs increase with the amount of PSMA used. In that sense, using Gd-PSMA for NCT is not only expected to be an expensive treatment due to a neutron beam being used, but also due to much larger amounts of PSMA required compared to alternative PSMA-targeted radioligand therapies (RLT), such as ^{177}Lu- and ^{225}Ac-labelled PSMA treatments. The main advantage of Gd-PSMA over alternative PSMA RLT is that Gd-PSMA is assumed to cause less systemic toxicity due to non-irradiation of PSMA-binding organs, like the salivary glands, and due to the therapeutic potential of NCT with highly selective tumour damage, while sparing normal tissues. Due to the cost aspect, it is nevertheless essential that the clinical case for Gd-PSMA is proven to be (very) convincing and that the therapeutic potential is higher than that of alternative PSMA RLT, before it becomes likely that the treatment will be applied in the clinic.

The second option to increase the dose effect due to gadolinium, is the use of enriched gadolinium-157 rather than natural gadolinium. In the most optimistic scenario, the use of 100% enriched gadolinium-157 was assumed. The use of natural gadolinium instead would increase the concentration required with about a factor five, to 89 μg/g Gd. Currently, enriched gadolinium-157 is only supplied by Oak Ridge National Laboratory, USA. Rather than the cost aspect is the molecule supplied a bottleneck for future use. Enriched gadolinium-157 is supplied as Gadolinium(III) oxide, which hitherto turned out to be insolvable. Both acidic (30% HCl), neutral and basic (50% NaOH) solvents have been tried to solve natural Gadolinium(III) oxide, as well as the ammonium chloride route (although not at the prescribed temperature of 230˚C yet) (Meyer 1989), thus far without success. Some improvement is desired in this regard, before enriched gadolinium can be used for irradiation experiments.

Another requirement for the clinical application of Gd-NCT is the use of neutron beams with higher neutron fluence rates. It was concluded that the former BNCT beam would be suitable for *in vitro* experiments as well. Because of the successful first irradiations at the HFR during this project, NRG has initiated the process of reopening the BNCT beam. As the beam has not been operational for several years, however, it is not clear how much time re-operating the beam would take.

Higher dose rates also imply higher rates of activation due to neutron irradiation. The first irradiation experiments were shown to activate, but at an acceptable level of ~100 cps. Higher dose rates might cause activation levels beyond acceptable limits. In that case, additional radiation safety precautions will be required.

Finally, a major cause of uncertainty in the expected biological effect of the gadolinium dose is the intracellular distribution of internalized PSMA being unknown. Fluorescence imaging indicates that PSMA is internalized near the cell membrane and near the nucleus, but not internalized in the nucleus (Meneghetti 2012, Banerjee 2015). For high RBE values with regard to Auger electrons, emission of these particles from atoms bound to a radiosensitive target, such as DNA, but probably also the cell membrane, is required. As fluorescence imaging might influence pharmacokinetics, it is worthwhile to investigate the intracellular distribution of PSMA with other techniques, such as subcellular fractionation and organelle isolation. If the distribution of PSMA turns out to be such that the biological effect due to gadolinium is not expected to be optimal, one might consider investigating the possibility of changing the linker part of the PSMA molecule to optimize the intracellular distribution. If this turns out to be difficult, one might also consider investigating the labelling of PSMA to other target isotopes with large cross sections and more favourable particles emitted, such as boron-10 and xenon-135.

5 Conclusion

Despite its strong technical and radiobiological characteristics, the superiority of NCT relative to current standard treatment options could not be demonstrated to date.

Nevertheless, recent developments regarding new, highly targeted delivery agents, dose optimization using a theranostic approach, advanced treatment planning, and the availability of in-hospital accelerators for neutron production, together may allow for a next generation of NCT. In particular with respect to the new tracer molecules, due to their highly specific uptake, broad new applications and potential for personalized treatment are foreseen. In this research, we have investigated one of these new tracers, the Prostate Specific Membrane Antigen (PSMA) which binds specifically to prostate tumour cells. When labelled with gadolinium-157, NCT dose could be delivered selectively to this cellular target.

This research has investigated *in vitro* whether NCT with Gd-PSMA tracer molecules is feasible as a new treatment modality for prostate cancer. With respect to the four specific aims listed in the Introduction (Chapter 1), the following conclusions can be drawn.

The labelling of gadolinium to PSMA has been realized. A ratio of Gd:PSMA of 1:1.25 for 15 minutes at 60˚C is investigated to provide optimal labelling of Gd-PSMA. LNCaP was selected as a PSMA-positive cell line and PC-3 was selected as a PSMA-negative cell line.

PSMA expression was validated, after which the cells could be used as an experimental model to determine the optimal dose of Gd-PSMA in the cells.

A concentration of 17 ± 11 (1σ) µg/g of PSMA could be achieved in PSMA-positive cells. Monte Carlo simulations with equivalent gadolinium concentrations indicated, however, that at least a ~10 times higher concentration of PSMA internalized in PSMA-positive cells will be required for a significant dose enhancement induced by the presence of gadolinium to be observed.

Preliminary *in vitro* irradiation experiments without gadolinium have indicated that the current neutron background dose and the neutron activation level are acceptable with regard to cell viability, and that transport of cells from the hospital-side to the reactor-side and back is not deemed to be a bottleneck. These irradiations form a successful starting point for future irradiations with Gd-PSMA.

In conclusion, meaningful *in vitro* studies of Gd-PSMA for NCT will become feasible when (1) the uptake of Gd-PSMA in cells can be increased by at least another factor of ten, (2) a beam with a thermal neutron fluence rate of > $4*10^{12}$ $m^{-2}s^{-1}$ can be made available (e.g. by re-opening the former BNCT beam in Petten), and (3) the level of activation due to irradiation by this beam remains acceptable. Further research requires multidisciplinary input from all partners involved.

6 Acknowledgements

I owe many people thanks for helping me with this project. First of all, I would like to thank Olaf van Tellingen for providing me with so much opportunity to measure on his HPLC system and giving me additional support when needed. Also, I would like to thank Ellen Wientjes for providing all materials required to perform a proper Western blot, and for giving additional guidance as well.

Of course, I would like to thank all partners involved in this project. In particular, I want to thank Shuraila Zerp for reading concepts of this thesis and providing useful feedback. Also, I would like to thank all people of B5 for valuable and lively discussions. In addition, I would like to thank NRG for their efforts to provide us with a suitable neutron beam, the pharmacy of NKI-AvL for performing several pharmacological measurements, the RNC for providing materials and useful guidance and Diederik Feilzer and Zoltán Perkó for performing useful simulations on Gd-NCT.

Thanks as well to the people from Nuclear Medicine and Radiology, especially in the Tuinhuis, for having me and providing a nice work atmosphere. Special thanks should be given to Martine Jonker-Geluk for her valuable guidance with regard to the pharmacological aspects of this project, and to Else Aalbersberg for providing me with lab skills and valuable knowledge about myself. And most importantly, I would like to thank my supervisors, Wouter Vogel and Antonia Denkova, for their endless support, time, and valuable discussions.

This project would not have been successful without the support of my family and friends. Thank you all for your support, especially when times were though. I would like to thank my parents for their financial support of my long graduation journey and their trust that I would make it till the end. And last but definitely not least, I would like to thank Dennis, my dearest, for helping me getting my work-life-balance straight ;).

7 Bibliography

1. Moss RL. Critical review, with an optimistic outlook, on Boron Neutron Capture Therapy (BNCT). Appl Radiat Isot. 2014 Jun; 88:2-11.
2. Nedunchezhian K, Aswath N, Thiruppathy M, Thirugnanamurthy S. Boron Neutron Capture Therapy - A Literature Review. J Clin Diagn Res. 2016 Dec; 10(12): ZE01-ZE04.
3. Sauerwein WAG, Moss RL, Wittig, A, Nakagawa, Y (eds), Neutron Capture Therapy; Principles and applications. Springer-Verlag. 2012; Heidelberg.
4. Hawthorne MF. The Role of Chemistry in the Development of Boron Neutron Capture Therapy of Cancer. Angew. Chem. Int. Ed. Engl. 1993; 32: 950-984.
5. Lückerath K, Stuparu AD, Wei L, Kim W, Radu CG, Mona CE, Calais J, Rettig M, Reiter RE, Czernin J, Slavik, R, Herrmann K, Eiber M, Fendler WP. Detection threshold and reproducibility of ^{68}Ga-PSMA-11 PET/CT in a mouse model of prostate cancer. J Nucl Med. 2018 March 30 (Epub ahead of print): 1-29.
6. Ahuja S, Dong M. Handbook of Pharmaceutical Analysis by HPLC. Academic Press. 2005; Volume 6; 1st Edition.
7. Snyder LR, Kirkland JJ, Dolan JW. Introduction to Modern Liquid Chromatography. John Wiley & Sons, Inc. 2009 Dec; 3rd Edition.
8. Mellon FA. Mass Spectrometry. Principles and Instrumentation. Encyclopedia of Food Sciences and Nutrition. Academic Press. 2003; Second edition: 3739-3749.
9. Banerjee SR, Ngen EJ, Rotz MW, Kakkad S, Lisok A, Pracitto R, Pullambhatla M, Chen Z, Shan T, Artemov D, Meade TJ, Bhujwalla ZM, Pomper MG. Synthesis and Evaluation of GdIII-Based Magnetic Resonance Contrast Agents for Molecular Imaging of Prostate-Specific Membrane Antigen; Supporting Information. Angew. Chem. Int. Ed. 2015; 54: 10778-10782.
10. ATCC, in partnership with LGC Standards. LNCaP clone FGC (ATCC CRL-1740^{TM}). URL: https://www.lgcstandards-atcc.org/en/Products/All/CRL-1740.aspx#generalinformation. Retrieved on 26 April 2018.
11. ATCC, in partnership with LGC Standards. PC-3 (ATCC CRL-1435^{TM}). URL: https://www.lgcstandards-atcc.org/Products/All/CRL-1435.aspx?geo_country=nl. Retrieved on 26 April 2018.
12. ExPASy. PC-3 (CVCL_0035). Cellosaurus, Bioinformatics Resource Portal. Swiss Institute of Bioinformatics (SIB). URL: https://web.expasy.org/cellosaurus/CVCL_0035. Version 25 March 2018. Retrieved on 26 April 2018.
13. Troyer JK, Becketi ML, Wright, Jr. GL. Detection and characterization of the prostate-specific membrane antigen (PSMA) in tissue extracts and body fluids. Int. J. Cancer. 1995; 62:552-558.
14. Mahmood T and Yang P-C. Western Blot: Technique, Theory, and Trouble Shooting. N Am J Med Sci. 2012 Sep; 4(9): 429-434.
15. Jena Bioscience. BlueEye Prestained Protein Marker; 10-245 kDa. Data Sheet. Jena Bioscience GmbH. 2016, Jul; Jena, Germany.
16. Kulabdullaev GA, Abdullaeva GA, Kim AA, Rakhmonov TT, Kurmantaev A. About Radiation in ^{nat}Gd for Neutron Capture Therapy. Journal of Health Science. 2016; 4:35-44.
17. Bé M-M, Schönfield E. ^{68}Ga. Table de Radionuléides. LNE-LNHB/CEA. 2012/7/4.
18. Del Monte U. Does the cell number 10^9 still really fit one gram of tumour tissue? Cell cycle. 2009; 8 (3): 505-506.
19. Firestone RB. Table of Isotopes CD-ROM. Baglin CM (editor). Wiley Interscience. 1998; Eighth Edition.
20. PerkinElmer Life and Analytical Sciences. WIZARD Automatic Gamma Counters. PerkinElmer, Inc. 2005; Shelton, USA.
21. Umbricht CA, Benešová M, Schmid RM, Türler A, Schibli R, van der Meulen NP, Müller C. 44Sc-PSMA-617 for radiotheragnostics in tandem with 177Lu-PSMA-617—preclinical investigations in comparison with 68Ga-PSMA-11 and 68Ga-PSMA-617. EJNMMI Research. 2017; 7:9.

22. Scheider B, Zhu H, Cheng Z, Iagaru A, Kopka K, Chin F. Preparation and chemical analysis of clinical grade 68Ga-PSMA-HBED-CC, an emerging tracer for imaging of prostate cancers. J Nulc Med. 2016 May 1; 57 (2): 1117.
23. Barth RF, Soloway AH, Fairchild RG, Brugger RM. Boron neutron capture therapy for cancer. Realities and prospects. Cancer. 1992 Dec 15; 70(12): 2995-3007.
24. Skelly Frame EM, Uzgiris EE. Gadolinium determination in tissue samples by inductively coupled plasma mass spectrometry and inductively coupled plasma atomic emission spectrometry in evaluation of the action of magnetic resonance imaging contrast agents. Analyst. 1998; 123: 675-679.
25. Bakker K and Bobeldijk I. Werkdocument bestralingsvoorstel Gd-NCT in HB 4/5/8. Confidential. NRG, 2018; 24013/18.146431.
26. Nievaart VA. Special Tailoring for Boron Neutron Capture Therapy. PhD thesis. TU Delft, 2007 June 26; Delft.
27. Feilzer D. Interpolation Model for GdNCT cell culture experiment in MCNP6. 2018 Feb; 1-7.
28. Bos AJJ, Draaisma FS, Okx WJC. Inleiding tot de stralingshygiëne. Sdu Uitgevers bv. 2007; Den Haag.
29. Meneghetti M, Scarsi A, Litti L, Colombatti M. Serrs: Plasmonic Nanostructures for SERRS Multiplexed Identification of Tumour-Associated Antigens. Small. 2012 December; 8 (24).
30. Weineisen M, Simecek J, Schottelius M, Schwaiger M, Wester HJ. Synthesis and preclinical evaluation of DOTAGA-conjugated PSMA ligands for functional imaging and endoradiotherapy of prostate cancer. EJNIMMI Res. 2014 Dec; 4(1):63.
31. Meyer, G. The Ammonium Chloride Route to Anhydrous Rare Earth Chlorides-The Example of YCl3. Inorganic Syntheses. 1989; 25: 146–150.

8 Appendices

8.1 Detection efficiency gamma counter

The gamma counter used (Perkin Elmer Wallac 1480 WIZARD 3''), provides results in terms of counts measured per unit of time. In order to ensure a proper conversion from activity in Becquerel to counts per unit of time, the detection efficiency of the gamma counter was determined for each of the radioisotopes used. i.e. both for ^{68}Ga and ^{177}Lu.

The detector efficiency was determined using a dose calibrator, which is validated according to clinical standards, as the radioactive isotopes used for this experiment are validated by this calibrator before they are used in the clinic. Because measurements in the dose calibrator are geometry dependent, the activity of the radioactive sample was determined before and after emptying the syringe with activity into an Eppendorf tube. Consequently the difference in activity was the activity to be used for the experiment to determine the detection efficiency of the gamma counter. The mass of the empty Eppendorf tube and the filled Eppendorf tube was measured with an analytical balance (MC1 Analytic AC 210 s, Sartorius) with 0.1 mg readability, in order to determine the volume of the sample.

Afterwards dilution series was made with the radioactive sample in the tube. In the case of ^{68}Ga, the sample was diluted 1:10 for four times, and subsequently diluted 1:5, 1:2, and 1:2. In the case of ^{177}Lu, the sample was diluted 1:10 for four times, 1:2, 2:5, 1;2 for two times, 1:5, and 1:10. The smaller than 1:10 dilutions in the series were chosen because of the expected range of interest for the uptake experiments. Of each dilution, the activity of the concentration was calculated and 1 mL was measured in the gamma counter. For each gamma counter experiment, the time of measurement was recorded, and the decay was corrected for using formula (1.2).

Figure 26 shows a plot of the measured count rate (cps) of the gamma counter against the administered activity (Bq) for the isotope ^{68}Ga, and Figure 27 shows the results for ^{177}Lu.

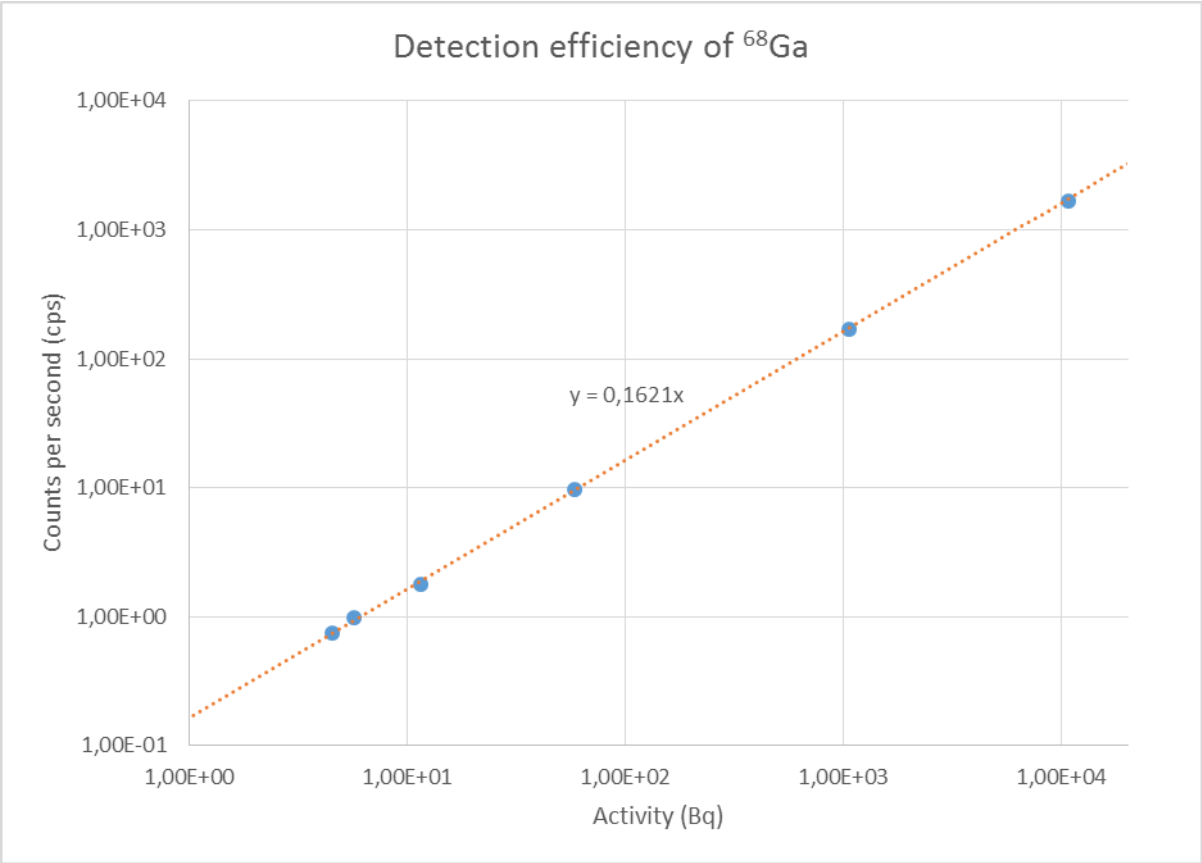

Figure 26: Plot of the measured count rate (cps) of the gamma counter against the administered activity (Bq) for the isotope ^{68}Ga. The dotted line is the linear regression that best describes the set of points. The corresponding equation provides the detection efficiency of ^{68}Ga in the gamma counter.

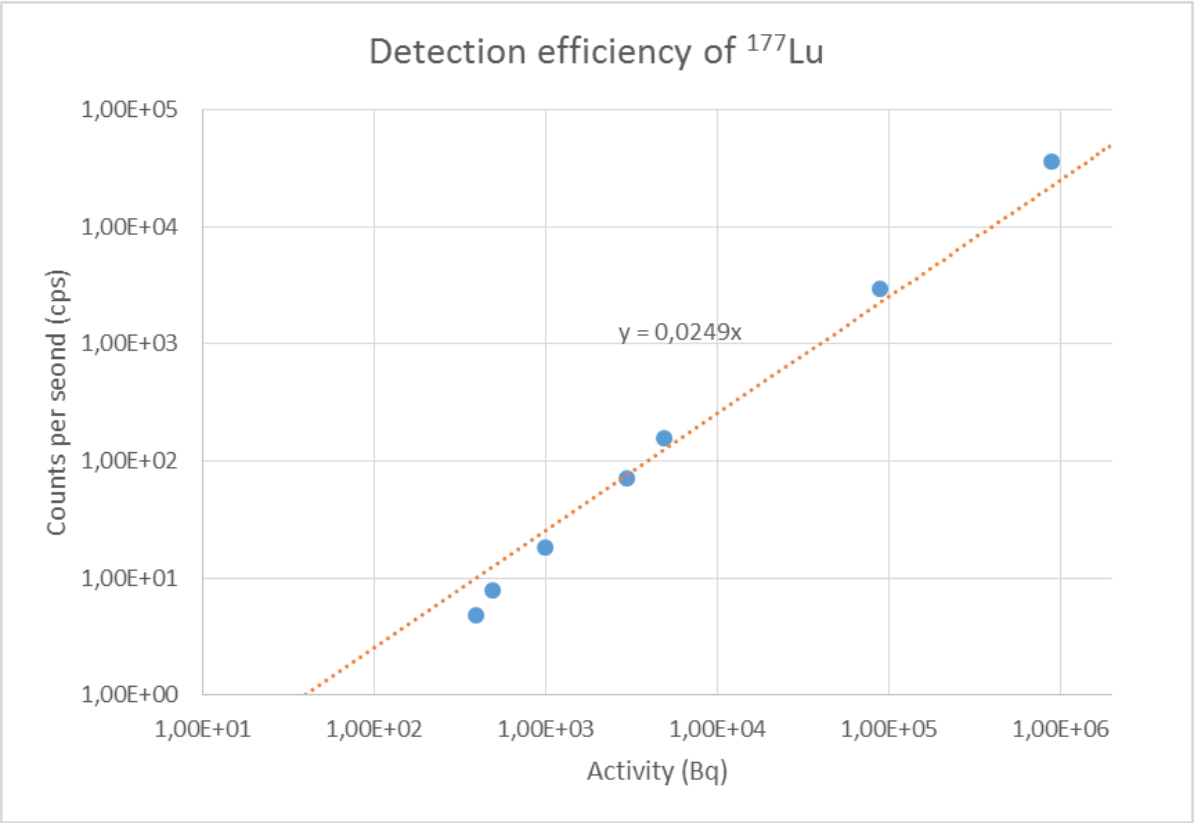

Figure 27: Plot of the measured count rate (cps) of the gamma counter against the administered activity (Bq) for the isotope ^{177}Lu. The dotted line is the linear regression that best describes the set of points. The corresponding equation provides the detection efficiency of ^{177}Lu in the gamma counter.

The dotted lines in Figure 26 and Figure 27 show the linear regression that best describes the set of points. The corresponding equation provides the detection efficiency of the gamma counter for each of the isotopes.

In case of ^{68}Ga, the equation is: y=0.1621x, so the detection efficiency is about 16%.

In case of ^{177}Lu, the equation is: y=0.0249x, so the detection efficiency is about 2.5%.

These efficiencies have been applied in the data analysis of the uptake experiments with equivalent radioligands, as described in paragraph 3.3.3.2.

8.2 Determination of cell volumes

Cell volumes were determined by performing some additional cell experiments.

8.2.1 Materials and methods

The day before the experiment, LNCaP and PC-3 cells were seeded in 6-wells plates, allowing adhesion and culture overnight at 37˚C and 5% CO_2. In case of LNCaP, about 5*10^4 cells in 2 mL RPMI medium per well, and in case of PC-3 circa 5*10^5 cells in 2 mL DMEM per well were seeded.

On the day of the experiment, the cells were washed three times with PBS (with each time removing any remainder of PBS with additional pipetting), and were kept in PBS until 0.5 mL of Trypsin-EDTA was added to dissociate the cells. The cells were incubated for 5 minutes, followed by addition of 1.5 mL of applicable medium. The 2 mL of cell suspension was turned into single cells by a 70 µm cell strainer. The single cells were incubated for about 90 minutes. Of the single cells, 0.1 mL was taken to count the amount of cells per mL, and to determine the cell diameter and the cell volume using a CASY Model TT (Roche) Cell Counter and Analyzer.

8.2.2 Cell volumes

PSMA-positive cells

The average cell diameter of single PSMA-positive cells was measured to be 19.1 ± 0.7 (2σ) µm. The average volume of single PSMA-positive cells was measured to be $3.87*10^3 \pm 0.58*10^3$ (2σ) fL, which is equivalent with 3.87 ± 0.58 ng.

PSMA-negative cells

The average cell diameter of single PSMA-positive cells was measured to be 19.8 ± 1.1 (2σ) µm. The average volume of single PSMA-negative cells was determined to be $4.36*10^3 \pm 0.69*10^3$ (2σ) fL, which is equivalent with 4.36 ± 0.69 ng.

8.3 Monte Carlo simulations on dose effect of gadolinium

The following paragraph provides an overview of the setup of the Monte Carlo simulations, as performed by Diederik Feilzer.

As the setup for the Monte Carlo simulations, a Polystyrene petri dish with an area of about 12.5 cm^2 and a wall thickness of 1.3 mm was used. In the petri dish, an adherent cell layer with a single cell thickness of 10 µm-20 µm was modelled on the bottom of the dish. The dish was assumed to be filled with culture medium (modelled as Tissue, Soft material). The incidence of the irradiation beam was assumed to be perpendicular to the area of the adherent cell layer, and the dish was assumed to be positioned such that the cell layer would be irradiated first (and the culture medium afterwards). A sketch of the setup is shown in Figure 28.

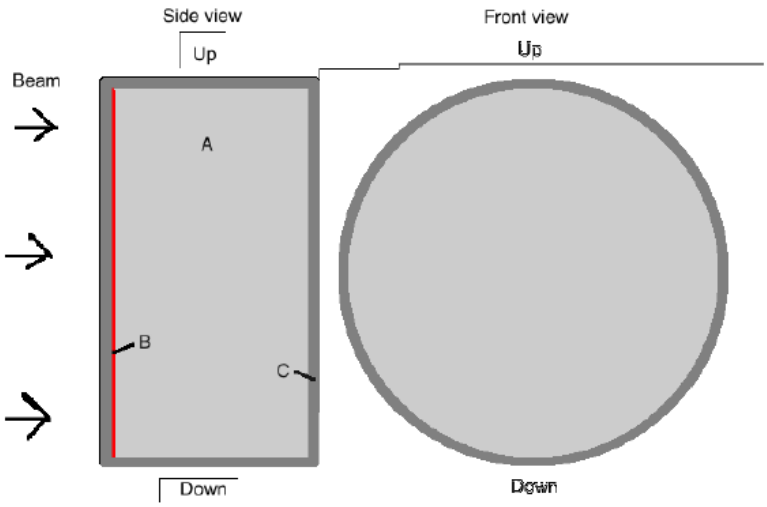

Figure 28: Sketch of the simulated setup, with the side view on the left and the front view on the right. A) is the culture medium, B) the adherent cell layer, and C) the Polystyrene wall of the dish. The irradiation beam is sketched on the left, and has an incidence perpendicular to the area of the adherent cell layer [(Feilzer 2018)].

Gadolinium administered to the cells is assumed to be merely present in the cell layer. Simulations are performed for both natural gadolinium (of which the isotopes Gd-155 and Gd-157 are assumed to contribute to the energy deposition after neutron irradiation) and for 58% and 100% enriched Gd-157, respectively. A range of gadolinium concentrations in the cell layer were investigated, from 0.01 µg/g to 100 µg/g of gadolinium.

The Monte Carlo simulations were performed with MCNP6 in coupled neutron-photon-electron (NPE) mode. For each experimental setting, the calculation was executed for a neutron source and a contaminating gamma source separately [(Feilzer 2018)]. A uniform thermal neutron spectrum and the photon spectrum of the Delft beam were used [(Feilzer 2018)].

The outcomes of the simulations are expressed in MeV per gram per source particle. These values were converted to Gy cm^2, by multiplying them with the factor $2.0742*10^{-9}$ [Gy cm^2 g MeV^{-1}]. This factor was determined as follows:

As 1 eV is equal to $1.6021766*10^{-19}$ J, 1MeV is equal to $1.6021766*10^{-13}$J. The unit Gray is equal to J/kg. This is equal to $1*10^{-3}$ J/g.

So, 1 MeV/gram=$1.6021766*10^{-13}$ J/g=$1.6021766*10^{-10}$·$1*10^{-3}$ J/g=$1.6021766*10^{-10}$ Gy.

All source particles are spread out over the whole petri dish area. The petri dish has a radius *r* of *r* = 2.03 cm, so the area *A* of the dish is: *A* = pi**r*^2 = 12.946 cm^2

The expression of the outcome in MeV per gram per source particle really means per (source particle per total area, i.e. per 12.946 cm^2).

So, 1 MeV/gram per src.neutron/12.946 cm^2 = 12.946 cm^2/src.neutron * MeV/gram = 12.946 * 1.60217662e-10 Gy cm^2/src.neutron = 2.074e-9 Gy cm^2/src.neutron

Since src.neutron is a dimension less unit, it could be omitted, which results in the conversion factor of **2.074e-9 Gy cm^2**

The converted outcomes of the simulations [Gy cm^2] can be expressed as dose rates [Gy s^{-1}], by multiplying them with the neutron fluence rate [$cm^{-2}s^{-1}$] of the beam.

8.4 Clonogenic assay

As clonogenic assays are considered to be the golden standard to assess cell survival, some first steps were performed in order to set-up future clonogenic assays with PSMA-positive and PSMA-negative cells. The clonogenic assays were performed in accordance with Protocol C.004.GP.V1, kindly provided by B5.

The first clonogenic assay with PSMA-postive LNCaP cells did not succeed, because hardly any colonies were formed. It turned out that using so-called conditioned medium (i.e. old cultured medium of the cells) rather than fresh culture medium, caused the cells to grow. Another reason why the first clonogenic assay with LNCaP did not succeed, was that the cells were washed away before staining. A solution to this problem was to use PBS with Ca^{2+} and with Mg^{2+}, rather than normal PBS without these ions.

A second clonogenic assay was performed with PSMA-positive and PSMA-negative cells, according to the previously mentioned protocol, in combination with the additional remarks.

Cells were seeded in 6-wells plates. Three times 500 single cells were seeded, and three times 1000 single cells of both cell lines. After more than two weeks of incubation, the assays were stained, and the colonies counted.

The plating efficiency of LNCaP turned out to be 32 ± 10 (1σ)%

The plating efficiency of PC-3 turned out to be 7.9 ± 1.7 (1σ)%.

It is not clear what caused the difference in plating efficiency between the cell lines. The PC-3 were however cultured in a different medium (DMEM versus RPMI), and were not incubated with conditioned medium. Future investigations are needed to show whether this explains the difference.